



Review

Alpha-Synuclein PET Tracer Development—An Overview about Current Efforts

Špela Korat ¹, Natasha Shalina Rajani Bidesi ², Federica Bonanno ³, Adriana Di Nanni ³, Anh Nguyễn Nhật Hoàng ^{4,5}, Kristina Herfert ³, Andreas Maurer ³ , Umberto Maria Battisti ², Gregory David Bowden ³ , David Thonon ⁴, Daniëlle Vugts ¹, Albert Dirk Windhorst ¹ and Matthias Manfred Herth ^{2,6,*}

¹ Department of Radiology and Nuclear Medicine, Amsterdam UMC, Vrije Universiteit Amsterdam, De Boelelaan 1085c, 1081 HV Amsterdam, The Netherlands; s.korat@amsterdamumc.nl (Š.K.); d.vugts@amsterdamumc.nl (D.V.); ad.windhorst@amsterdamumc.nl (A.D.W.)

² Department of Drug Design and Pharmacology, University of Copenhagen, Jagtvej 160, 2100 Copenhagen, Denmark; natasha.bidesi@sund.ku.dk (N.S.R.B.); umberto.battisti@sund.ku.dk (U.M.B.)

³ Werner Siemens Imaging Center, Department of Preclinical Imaging and Radiopharmacy, Eberhard Karls University Tübingen, Röntgenweg 15, 72076 Tübingen, Germany; Federica.Bonanno@med.uni-tuebingen.de (F.B.); Adriana.Di-Nanni@med.uni-tuebingen.de (A.D.N.); Kristina.Herfert@med.uni-tuebingen.de (K.H.); Andreas.Maurer@med.uni-tuebingen.de (A.M.); Gregory.Bowden@med.uni-tuebingen.de (G.D.B.)

⁴ Elysia Raytest, Rue du Sart-Tilman 375, 4031 Liège, Belgium; hoangnguyennhatanh@doct.uliege.be (A.N.N.H.); david.thonon@elysia-raytest.com (D.T.)

⁵ GIGA Cyclotron Research Centre In Vivo Imaging, Department of Chemistry, University of Liège, Allée du 6 Août 8, 4000 Liège, Belgium

⁶ Department of Clinical Physiology, Nuclear Medicine and PET, Rigshospitalet, Blegdamsvej 9, 2100 Copenhagen, Denmark

* Correspondence: matthias.herth@sund.ku.dk



Citation: Korat, Š.; Bidesi, N.S.R.; Bonanno, F.; Di Nanni, A.; Hoàng, A.N.N.; Herfert, K.; Maurer, A.; Battisti, U.M.; Bowden, G.D.; Thonon, D.; et al. Alpha-Synuclein PET Tracer Development—An Overview about Current Efforts. *Pharmaceuticals* **2021**, *14*, 847. <https://doi.org/10.3390/ph14090847>

Academic Editor: Irina Velikyan

Received: 6 July 2021

Accepted: 17 August 2021

Published: 26 August 2021

Publisher's Note: MDPI stays neutral with regard to jurisdictional claims in published maps and institutional affiliations.



Copyright: © 2021 by the authors. Licensee MDPI, Basel, Switzerland. This article is an open access article distributed under the terms and conditions of the Creative Commons Attribution (CC BY) license (<https://creativecommons.org/licenses/by/4.0/>).

Abstract: Neurodegenerative diseases such as Parkinson's disease (PD) are manifested by inclusion bodies of alpha-synuclein (α -syn) also called α -synucleinopathies. Detection of these inclusions is thus far only possible by histological examination of postmortem brain tissue. The possibility of non-invasively detecting α -syn will therefore provide valuable insights into the disease progression of α -synucleinopathies. In particular, α -syn imaging can quantify changes in monomeric, oligomeric, and fibrillic α -syn over time and improve early diagnosis of various α -synucleinopathies or monitor treatment progress. Positron emission tomography (PET) is a non-invasive in vivo imaging technique that can quantify target expression and drug occupancies when a suitable tracer exists. As such, novel α -syn PET tracers are highly sought after. The development of an α -syn PET tracer faces several challenges. For example, the low abundance of α -syn within the brain necessitates the development of a high-affinity ligand. Moreover, α -syn depositions are, in contrast to amyloid proteins, predominantly localized intracellularly, limiting their accessibility. Furthermore, another challenge is the ligand selectivity over structurally similar amyloids such as amyloid-beta or tau, which are often co-localized with α -syn pathology. The lack of a defined crystal structure of α -syn has also hindered rational drug and tracer design efforts. Our objective for this review is to provide a comprehensive overview of current efforts in the development of selective α -syn PET tracers.

Keywords: alpha-synuclein; imaging; synucleinopathies; positron emission tomography

1. Introduction

Abnormal alpha-synuclein (α -syn) depositions (α -synucleinopathies) in neurons, nerve fibers, or glia cells are the hallmark for many neurodegenerative diseases such as Parkinson's disease (PD), dementia with Lewy bodies (DLB), and multiple system atrophy (MSA) [1]. PD, for example, is the most common progressive neurodegenerative movement disorder. Today, approximately 7–10 million patients worldwide are affected. In Europe,

the proportion of the people suffering from PD is 1.6% for those aged 65+ and up to 3% for those aged 80+. As the average age of the population in the EU continues to rise, the overall number of PD patients also increases, placing a significant burden on society due to associated healthcare costs [2–4]. Currently, the combined direct and indirect cost of PD, including treatment, social security payments, and lost income from an inability to work, is estimated to be nearly EUR 42 billion in the United States of America (USA) alone. Although symptoms can, to a certain extent, be medically remediated, there is currently no cure for PD. Medication costs for an individual with PD average approximately EUR 2100 per year [5].

The underlying biochemical mechanism of PD is not fully understood, and it is difficult to ascertain possible causes of the disease from its effects. More importantly, the clinical diagnosis of PD is not straightforward in the early phases of the illness. This seriously complicates the identification of targets for novel therapies and the interpretation of treatment outcomes. It is imperative to correctly diagnose the illness as early as possible since early intervention is key to limiting the neurodegenerative process. The pathological hallmark of PD is deposition of α -syn protein in the brain followed by dopaminergic neuronal loss [6–8]. Currently, α -syn deposition cannot be assessed accurately in vivo. The inability to quantify these abnormal aggregates limits the accurate clinical diagnosis of PD as well as DLB and MSA, and also hinders research into the understanding of these diseases; thus, impeding the development of new treatments. Positron emission tomography (PET) molecular imaging has the potential to reveal the pathogenesis of brain disorders when suitable tracers are available. PET can localize and quantify drug targets, monitor treatment effect, or image disease pathophysiology on a molecular basis. Various studies have indicated toward the importance of imaging with respect to patient inclusion in clinical trials, especially for PD [9]. Currently, imaging of dopaminergic neurons has been used to monitor the effects of investigational disease-modifying drugs in PD, but dopamine cell loss is a downstream effect of α -syn deposition and thus, there is great interest in imaging this specific protein in PD therapies for monitoring progression as well as for early diagnosis. Cerebrospinal fluid biomarkers, skin tissue biopsies, and other imaging techniques will likely be developed in the future as well. However, a PET tracer in the central nervous system (CNS) has the potential to provide evidence for central target engagement, following disease progression and drug treatment efficacy. By developing a tracer that selectively identifies α -syn deposition, the correct cohort of patients may be included in clinical trials and the readout of these trials may be correlated with the underlying disease pathology. Thus, the ability to image α -syn deposition will be a game-changing achievement [7] and will facilitate the development of effective treatments. Presently, there are no tracers available for the detection of α -syn deposition in patients. The main obstacles are difficulties in identifying selective α -syn deposition binding ligands (to be used as tracers) that are suitable for PET measurements. Considering this, the Michael J. Fox Foundation for Parkinson's Research (MJFF) announced a challenge to develop such a tracer sponsoring a USD 2 million prize to the first successful team.

In this review, we aim to give a detailed summary of the potential radiotracers targeting α -syn developed thus far. For this reason, a bibliographic search was performed from various sources, including PubChem, ChEMBL, Reaxys, World Intellectual Property Organization (WIPO), PubMed and other online resources (in Table S1, Supporting Information). We describe the rationality in their design, highlight lessons to be learned from these efforts, and give suggestions on how to move forward.

2. Alpha-Synuclein and PET Imaging

2.1. Alpha-Synuclein within the Central Nervous System

α -Syn is an abundant protein throughout the CNS. It represents approximately 1% of cytosolic proteins in the brain and is predominantly found in the neocortex, hippocampus, substantia nigra, thalamus, and cerebellum [10]. Although α -syn has been localized within the nucleus of mammalian neurons [11,12], the vast majority of α -syn has been found in

presynaptic termini in a free or membrane-bound form [13]. The normal functional role of α -syn is still not completely understood, nor is its involvement in CNS diseases [14]. However, α -syn has been suggested to play a specific role in synaptic plasticity. For example, a sustained reduction in α -syn expression levels was detected in specific zebra finch brain regions, which were implicated during song acquisition [15]. α -Syn has also been shown to be an inhibitor of phospholipase D2 (PLD2), which indicates that it has a specific function in membrane trafficking [14,16]. Furthermore, there is evidence that α -syn is involved in neurotransmitter release [14] and more importantly in the formation of toxic radical species [17]. Finally, α -syn has also been suggested to be involved in DNA repair processes, including the repair of double-strand breaks [18].

Alpha-Synucleinopathies in PD, DLB and MSA

PD patients show abnormal intraneuronal inclusions named Lewy bodies (LB) and Lewy neurites (LN), which are predominantly present in the substantia nigra. Both filament types contain α -syn as a major component. DLB patients also possess LB and LN filaments. In contrast to PD, these filaments are mainly distributed in the cerebral cortex [19]. The major filamentous component of glial and neuronal cytoplasmic inclusions in MSA patients is also α -syn [20]. Contrary to inclusions found in PD and DLB, in MSA, filamentous components are not only found in neurons but also within oligodendrocytes and in the cytoplasm of nerve cells [19,21–23] (Figure 1). Patient-derived α -syn fibrils from different α -synucleinopathies, namely PD, DLB, and MSA, possess structural differences. Specifically, PD and MSA fibrils exhibit flat and twisted polymorphs, while, in contrast, DLB fibrils are cylindrical with no twist [24]. The precise role of α -syn in PD, DLB, and MSA is still not understood [25]. However, early α -syn aggregates (protofibrils) and oligomer species that are formed during the aggregation process are believed to mediate neurotoxicity through the disruption of cellular homeostasis and other effects on various intracellular targets leading to mitochondrial toxicity, enhancement of inflammatory responses, and synaptic and endoplasmic dysfunction [26–31]. Furthermore, α -syn leads to the release of radical species, which is suggested to trigger neurodegeneration. Finally, DNA repair function also appears to be compromised in LB inclusion bearing neurons [17]. Several overview reviews about the toxic effect of α -syn have been published and summarize the current state-of-the-art knowledge [28,32,33].

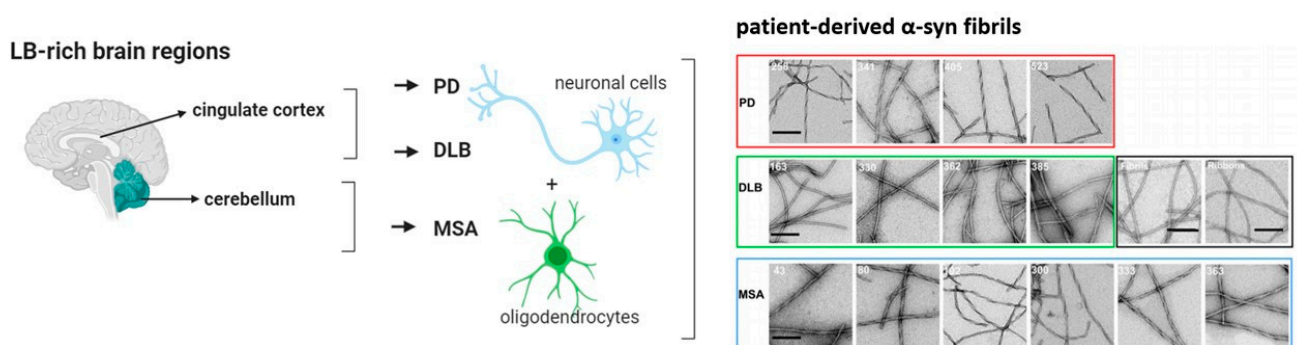


Figure 1. Simplified illustration of the differences of α -syn deposition and structure in PD, DLB, and MSA neurodegenerative diseases. In particular, LB-rich brain regions deposited in the cingulate cortex are thought to be specific for PD and DLB, while depositions within the cerebellum are specific for MSA. Additionally, inclusions of α -syn are found in neuronal cells in PD and DLB. Conversely, in MSA these inclusions are found in oligodendrocytes ((left), visualized with BioRender). Structural differences of α -syn have been reported in patient-derived α -syn fibrils (right). (Adapted from [24] and visualized with BioRender).

2.2. The Structure of α -Syn

The native form: Considerable effort has been made to reveal the native state of α -syn. However, it is still debated if native α -syn exists as an unfolded monomer [34],

as a helically folded tetramer [35], as multimer conformations [36], or as a mixture of all these forms [36]. In contrast, the primary structure of α -syn is well described. It is encoded by the SNCA gene and encompasses 140 amino acids (Figure 2A). The protein is divided into three domains: the N-terminal amphipathic region (1–60 residues), the non-amyloid- β component (NAC) hydrophobic region (61–95 residues), and the C-terminal acidic region (96–140 residues) [37]. Several isoforms of α -syn exist and are formed through alternative splicing [38,39]. The synuclein protein family is reported to undergo extensive post-translational modifications (PTMs) in vivo including phosphorylation, truncation, acetylation, or nitration [40].

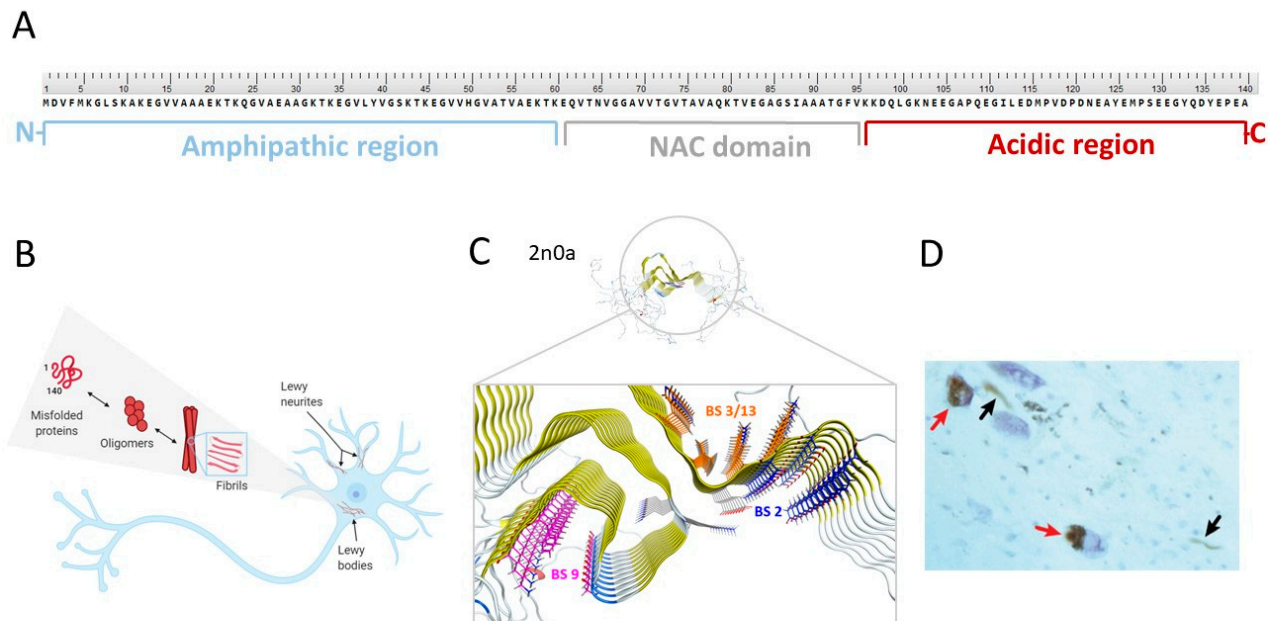


Figure 2. (A) Primary structure of α -syn with highlighted regions: N-terminal (in blue), NAC (in grey), and C-terminal (in red). (B) Conformational states of α -syn (adapted from [41] and visualized with BioRender). (C) Solid-state NMR atomic-resolution (4.8 Å) of α -syn fibrils (PDB ID: 2n0a, adapted from Twohig et al. [42]) with putative binding sites: binding site 2 (BS2; in blue), binding site 9 (BS9; in pink), binding site 3/13 (BS3/13; in orange) on α -syn fibrils (reprinted with permission from [43]). Copyright 2018 American Chemical Society. Structure of α -syn was imported from PDB and visualized with MOE 2018). (D) The α -syn pathology of PD with two pigmented nerve cells containing LB (red arrows) and LN (black arrows). (Adapted from [19]).

α -Syn fibril formation: Under certain physiological conditions, native α -syn can aggregate. Thus far, it is unclear if a specific conformation of α -syn or other processes trigger aggregation and ultimately, convert soluble native α -syn into β -sheet rich, tightly stacked fibrils. However, aggregation is thought to occur via a highly dynamic equilibrium between numerous conformations, various oligomeric states and (proto)fibrils (Figure 2B) [36]. Understanding the aggregation process is difficult since it is highly complex and can be affected by a broad set of parameters. For instance, various environmental factors appear to have an influence on an increased risk for PD, such as exposure to pesticides, herbicides, exposure to heavy metals, organic solvents, and various sources of oxidative stress [44]. Conversely, it has also been shown that certain mutations within the α -syn encoding SNCA gene enhance or reduce the formation of protofibrils [45]. Changes within the α -syn NAC domain appear pivotal for α -syn fibrillation, especially within the amino acid sequences 71 VTGVTAVAQKTV 82 or 66 VGGAVVTGV 74 . Removal of either of these sequences abrogated the fibril formation completely [46,47]. PTMs have also been shown to influence the aggregation process. For example, phosphorylation on residue S129 leads to extensive aggregation (Figure 2D) [48]. This PTM appears to be pathologically relevant since it is

present in >90% of all α -syn derived from PD patients, but only seen in 4% of native soluble α -syn [49].

Three-dimensional (3D) structure and possible binding sites for small molecules: To date, no high-resolution and detailed 3D structure of α -syn fibrils has been reported. The highly repetitive nature of the respective secondary structure and the residue-type degeneracy pose significant challenges to this endeavor [50]. The lack of knowledge of the function of α -syn, its binding partners, their binding mechanism, and the broad set of possible PTMs have been found to be additional complications [37]. Nevertheless, certain structural secrets of α -syn fibrils have been revealed [50–52]. For example, Tuttle et al. could have elucidated the structure of a single filament fibril of α -syn using solid-state nuclear magnetic resonance (ssNMR) (Figure 2C) [50]. Years later, Li and colleagues were the first to distinguish between two structurally different forms of fibril species, termed protofilaments, using cryogenic electron microscopy [53]. In 2018, Hsieh et al. conducted a molecular blind docking study using the structural data obtained from the ssNMR study by Tuttle et al. This study aimed to identify possible binding regions of small molecules toward α -syn fibrils [43]. Three putative binding sites, namely binding site 2 (Y39-S42-T44; BS2), 9 (G86-F94-K96; BS9), and 3/13 (K45-V48-H50 and K43-K45-V48-H50; BS3/13) were identified (Figure 2C). To test these virtual hits, chemically diverse putative binders were synthesized, and their binding profile was examined using photoaffinity labeling and radioligand binding studies. Results strongly indicated that there are several binding sites [43]. How this knowledge can be used to design selective and high-affinity α -syn ligands has to be further investigated.

2.3. Challenges—Why Is It Difficult to Develop an α -Syn PET Tracer?

Challenge 1. The target

The development of an α -syn PET tracer is more challenging in comparison to the development of tracers for other amyloids such as A β or tau. A key reason for this is that the absolute concentration of α -syn aggregates within the brain is thought to be 10- to 50-fold lower than that of A β or tau (Figure 3A) [7,54,55]. Consequently, high affinity of a putative tracer, most likely in the subnanomolar range, is required. Next, co-existence and co-localization of α -syn with A β and tau fibrils requires a PET tracer with high selectivity over A β and tau in order to be able to image α -syn at all (Figure 3C) [56]. For instance, A β pathology can be found in more than 80% of all synucleinopathies. In DLB, A β deposits are detected in approximately 85% of all cases and tau pathology is observed in approximately 30% [7,54,57,58]. Unfortunately, A β or tau fibrils form structurally similar β -pleated sheets (Figure 3B), complicating the development of selective α -syn binding ligands. Furthermore, and in contrast to A β , the highest concentration of α -syn inclusions can be found intracellularly (Figure 3D). Therefore, any successful α -syn PET tracer has to be able to cross cell membranes, in addition to the blood-brain-barrier (BBB) [54,56]. Usually, this is not considered the biggest hurdle, but it may lead to issues, e.g., the D_{2/3} PET tracer [¹¹C]raclopride can pass the BBB, but it cannot pass cell membranes [59]. It might also be that extensive in vivo PTMs possibly result in a variety of substructures that might not be recognized by the tracer developed for the unmodified structure (Figure 3E) [54,56].

Challenge 2. The design

Another aspect that in general challenges the development of tracers for amyloids is the standard development strategies that have been established over the last decades for more traditional targets such as receptors and enzymes that cannot be applied to these protein-based structures without precisely defined binding pockets. The underlying binding mechanism is poorly understood and studies identifying for example binding sites, or to reveal kinetic and thermodynamic ligand-binding parameter using computational or other strategies are in its infancy [43,60,61]. Conversely, structure-based drug design of these ligands is hampered by the limited availability of high-resolution X-ray crystal structures of α -syn fibrils. Moreover, it is questionable if these structures are able to mimic the aggregates and conditions of the fibrils in vivo. For this reason, the only option available

to develop an α -syn PET tracer is a ligand-based approach. However, this strategy has several limitations mainly related to the small number of ligands and data available for the binding. Furthermore, the extensive literature and structures available on A β or tau tracers cannot be exploited to design new compounds in order to avoid selectivity issues.

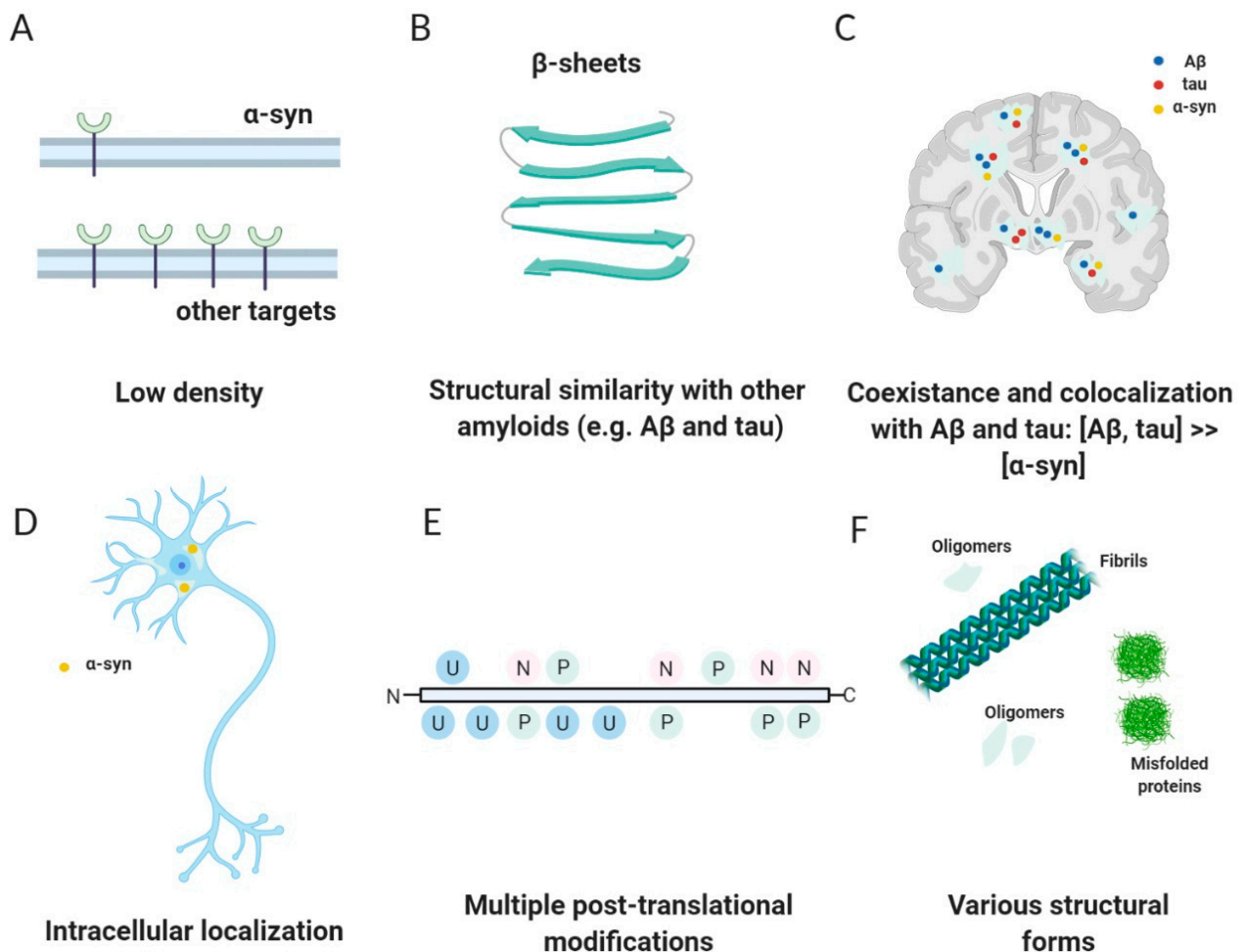


Figure 3. Challenges and characteristics of an ideal α -syn tracer. (Reprinted with permission from [56]. Copyright 2014 the Society of Nuclear Medicine and Molecular Imaging, Inc.) (A) Low density and concentration of α -syn in comparison with other targets. (B) Structural similarity with other proteins such as A β and tau. (C) Coexistence and colocalization with structural similar amyloids such as A β and tau. (D) Intracellular localization. (E) Multiple post-translational modifications such as phosphorylation (P), ubiquitination (U), and nitration (N). (F) Various structural forms such as fibrils, oligomers, and misfolded proteins. (Visualized with BioRender).

Challenge 3. The evaluation

The reliability and predictability of *in vitro* binding assays is crucial in any PET tracer development and is a big challenge for α -syn tracer development. It has been postulated that structural variation of α -syn between patient brain-derived *in vivo* aggregates and *in vitro* α -syn fibrils can explain the difficulties in translating new α -syn PET tracers to clinical research [62]. Structural heterogeneity between *in vivo* brain-derived material from PD and MSA patients have been reported and support this hypothesis [62,63]. Do these conformational differences have an influence on the binding pattern of potential ligands that have still to be elucidated, i.e., are binding motifs in different conformational α -syn fibrils changed in such a way that prevent ligands to bind universally to all forms (Figure 3F)?

Similar considerations also apply to α -syn depositions formed in animal models [7]. Are these forms structurally related to those formed in humans and can they be used for screening purposes to identify selective ligands? In this context the selection of the animal model plays a crucial role in the outcome of these experiments. In general, in vivo animal testing for tracers targeting brain aggregates is currently performed in wild-type healthy animals such as mice, rats, and non-human primates (NHP). However, recent studies are moving toward the use of disease models since they are able to mimic intracellular inclusion bodies that are as similar to those found in humans. Currently, several genetically modified rodent models are available. These are usually robust, but the long time required for the development of the pathology (several months) and the high costs limit the use of these animals. For these reasons, the most employed rodent models are the seeding model with pre-formed fibrils (PFF), viral vector model, and the combination of viral vectors and PFF [64–66]. The combination of a viral vector and PFFs have shown all the important hallmarks of α -synucleinopathies and was reported to accelerate the induction of α -syn aggregates as rapid as within 10 days after PFF injection [65]. Another quick, robust, and easy to implement model was developed by Verdurand et al. by injecting fibrils into striatum of rats and conducting in vivo imaging 7 days after inoculation [67]. Rodents may not provide all the data (safety, P-gP efflux, metabolites, etc.) for the tracer, and they need to be tested in larger animals. NHP models with α -syn inclusion have been created with inoculation of fibrils, LB, and viral vectors but all the models require months to form the pathology, making them expensive [68–70]. The optimum would be to develop a rodent model of α -synucleinopathy that is suitable for in vivo PET imaging of α -syn pathological forms. The model must fulfil the criteria of rapid, abundant, and progressive pathology development over time. Another animal that has gained popularity in brain imaging is the domestic pig [71,72]. Creating an α -syn pig model that is appropriate, fast, and inexpensive will drastically reduce the cost of developing such tracers.

It is doubtful if in vitro assays or in vivo models based on fibrils are predictive and clinically relevant; models to study specific uptake in vivo are lacking. For this reason, exclusively patient-derived material should be used for screening new α -syn tracers. However, access to human tissue that is well characterized in respect to its pathology is limited and application of high-throughput screening methods to this material is currently not available. This obviously slows down the development process.

2.4. Success Criteria for a Small Molecule α -Syn PET Tracer

A successful PET tracer for neuroimaging is dependent on several key parameters (Figure 4) [73]. First, the ligand must be labeled in sufficient amounts (activity yield >500 MBq). Usually, carbon-11 (^{11}C) or fluorine-18 (^{18}F) are the nuclides of choice for small molecule-based PET neuroimaging tracers. These nuclides display excellent decay characteristics for PET imaging (short half-life, good branching ratio, and short positron range) [74] and radiotracers labeled using these radionuclides can also be produced in good radiochemical yields (RCY) in most well-equipped radiopharmacies (activity yield >500 MBq) [75]. Additionally, potential ligands can be radiolabeled with these isotopes without introducing bulk and charge, which often prevents sufficient blood-brain barrier (BBB) penetrance. BBB permeability should be high with an early standard uptake value (SUV) >1.0 [54] (within several minutes, for example 5–10 min). Brain uptake for amyloid tracers is recommended to be $\geq 0.4\%$ ID/g in rat brain or $\geq 4.0\%$ ID/g in mouse brain [54]. Additionally, the plasma clearance half-time should be fast (less than 30 min) [54] to reduce background signal from blood. Ideally, the tracer binds reversibly to its target and no metabolites exist within the brain. These characteristics greatly simplify kinetic modeling and allow for appropriate quantification and reproducibility [56]. The tracer should show a low non-displaceable binding component to increase signal-to-noise ratio within the brain [54] and has to be accessible in high molar activity (A_m) (>50 GBq/ μmol , we believe) to avoid target saturation or non-negligible self-blocking [76,77]. An additional key parameter for any successful neuro PET tracer is its selectivity toward off-targets

expressed or deposited in same brain regions. A recommended selectivity over these off-targets is thought to be > 30–100 [78]. For a successful α -syn PET tracer, the MJFF has published a criteria list, which has to be fulfilled to receive the MJFF Alpha-synuclein Imaging Prize [79]. We have adapted this list and will use it to assess the ability of published structures to image α -syn via PET (Figure 4).

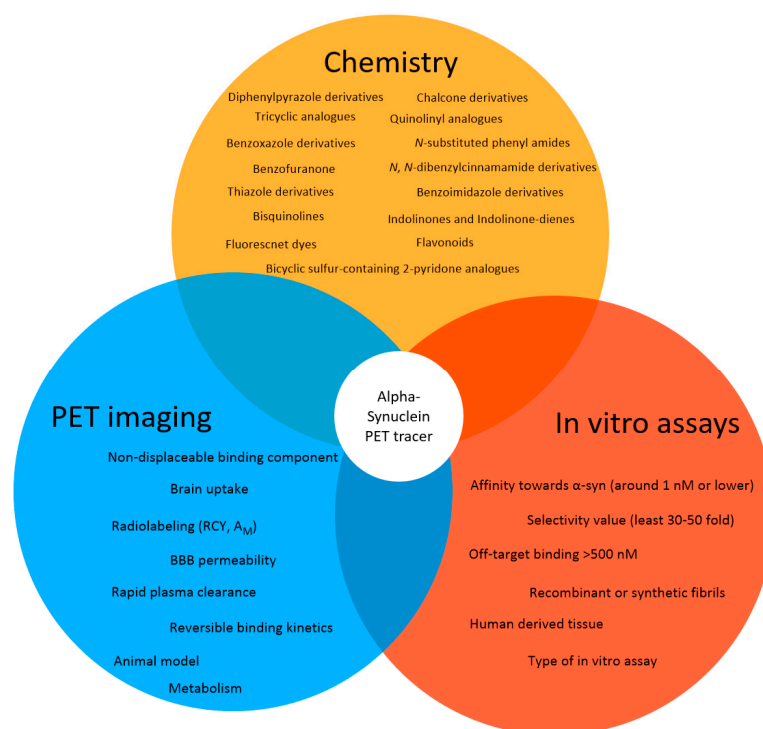


Figure 4. The approach for the development of α -syn selective PET tracers. The initial search was conducted from various sources (in Table S1, Supporting Information) in order to create an overview of compounds that have been designed and developed to image α -syn. The identified structures should be screened using criteria similar to the structures proposed by the MJFF for a successful α -syn PET tracer and are based on in vitro assays and PET imaging technique.

Suggested Success Criteria for a α -Syn PET Ligand in the Preclinic Setting

- Radiolabeling with ^{11}C or ^{18}F should be achievable in a RCY of >10% (activity yield >500 MBq) and in a high molar activity (>50 GBq/ μmol);
- Affinity toward α -syn around 1 nM or lower;
- The radioligand enables quantification of lower density α -syn targets in the presence of higher density A β or tau proteins;
- The binding affinity or density selectivity for α -syn over A β or tau should be at least 30–50 fold (\sim 1 nM vs. 50 nM);
- Off-target binding >500 nM;
- Selective binding to α -synuclein-rich brain homogenates from PD patients (versus A β , tau rich homogenates);
- Binds to LBs/LNs in human tissue;
- BBB permeability, with early peak uptake of SUV >1.5;
- \geq 0.4% ID/g in rat brain or \geq 4.0% ID/g in mouse brain;
- No or minimal radiometabolites within the brain;
- Low non-displaceable binding component (rule of thumb: $\log D_{7.4} < 3$ [80]);
- Reversible binding kinetics with rapid plasma clearance (<30 min).

3. Alpha-Synuclein PET Tracer Development—From a Molecular Development Point of View

Over the past decades, a set of chemically diverse compounds have been developed that target α -syn. The development was based on various strategies including rational drug design and high-throughput screening approaches. In this section, we will present a selection of these structures and highlight their potential to be used as α -syn selective PET tracers. Additionally, we will critically reflect their in vitro and in vivo biological evaluation results.

Historically, the first investigated α -syn binders were based on fluorescent dyes such as Thioflavin-T (**ThT**) or Thioflavin-S (**ThS**) (Figure 5A,B) [81]. These structures, however, were not selective and consequently, numerous attempts to develop fluorescent dyes with an improved binding affinity have been made over the years. For example, Celej and colleagues studied the effect of N-arylaminoanthracene sulfonate derivatives upon interaction with conjugated α -syn fibrils. **2,6-ANS** and **2,6-TN** (Figure 5A) showed little fluorescence in the presence of non-aggregated α -syn, but much more fluorescence, occasionally with spectral shifts, when applied to fibrils [82]. Affinities were, however, only in the low micromolar range. In the same year, Volkova et al. conducted a similar study with monomethine cyanines. **T-284** and **SH-516** were shown to associate with fibrillar α -syn with affinities of 560 nM and 650 nM, respectively (Figure 5A) [81,83]. To better understand the interaction of these structures, especially **SH-516** was studied in a model proposed by Krebs et al. that describes the binding of dyes to amyloids [84]. It was suggested that monomethine cyanines bind in a long channel that run parallel to the length of the fibril axis (Figure 5C) [85]. This information was used to develop second generation dyes. The resulting tri- and pentamethine cyanines displayed selectivity toward fibrillar or oligomeric α -syn over monomeric α -syn [83]. Interestingly, the pentamethine cyanine dye **SL-631** (Figure 5A) also bound better to less dense and structured oligomers compared to beta-sheet containing fibrils. In contrast, the trimethine cyanine **SH-299** (Figure 5A) was able to bind to β -sheets. This distinct binding pattern was attributed to the distinct steric characteristics of both compounds. The more sterically hindered structure **SL-631** is supposed to be incapable of entering and binding in the groove formed by β -sheets, whereas the less bulky structure **SH-299** is thought to be capable. **SH-299** may serve as an imaging agent for both oligomeric and fibrillar α -syn species whereas **SL-631** is better suited for oligomeric forms [86]. In 2013, Neal et al. developed three heterogeneous structures to image α -syn selectively. **LDS-798** and the phenoxazine dyes **Nile Red** and **Nile Blue** (Figure 5A) were able to selectively bind to LB in postmortem human tissue of DLB or PD patients. Selectivity over amyloid or tau pathology in human AD tissue was detected. Surprisingly, to date no further attempts concerning radiolabeling and binding affinity measurements have been conducted [87].

From a broader point of view, the studies mentioned above show that it is possible to selectively bind and image α -syn in postmortem human tissue. However, most probes displayed low affinity and poor selectivity toward α -syn and are, as such, not suitable for development as PET tracers. Conversely, these ligands were considered excellent lead structures and were consequently employed as a starting point to develop other α -syn selective ligands in many of the studies discussed below.

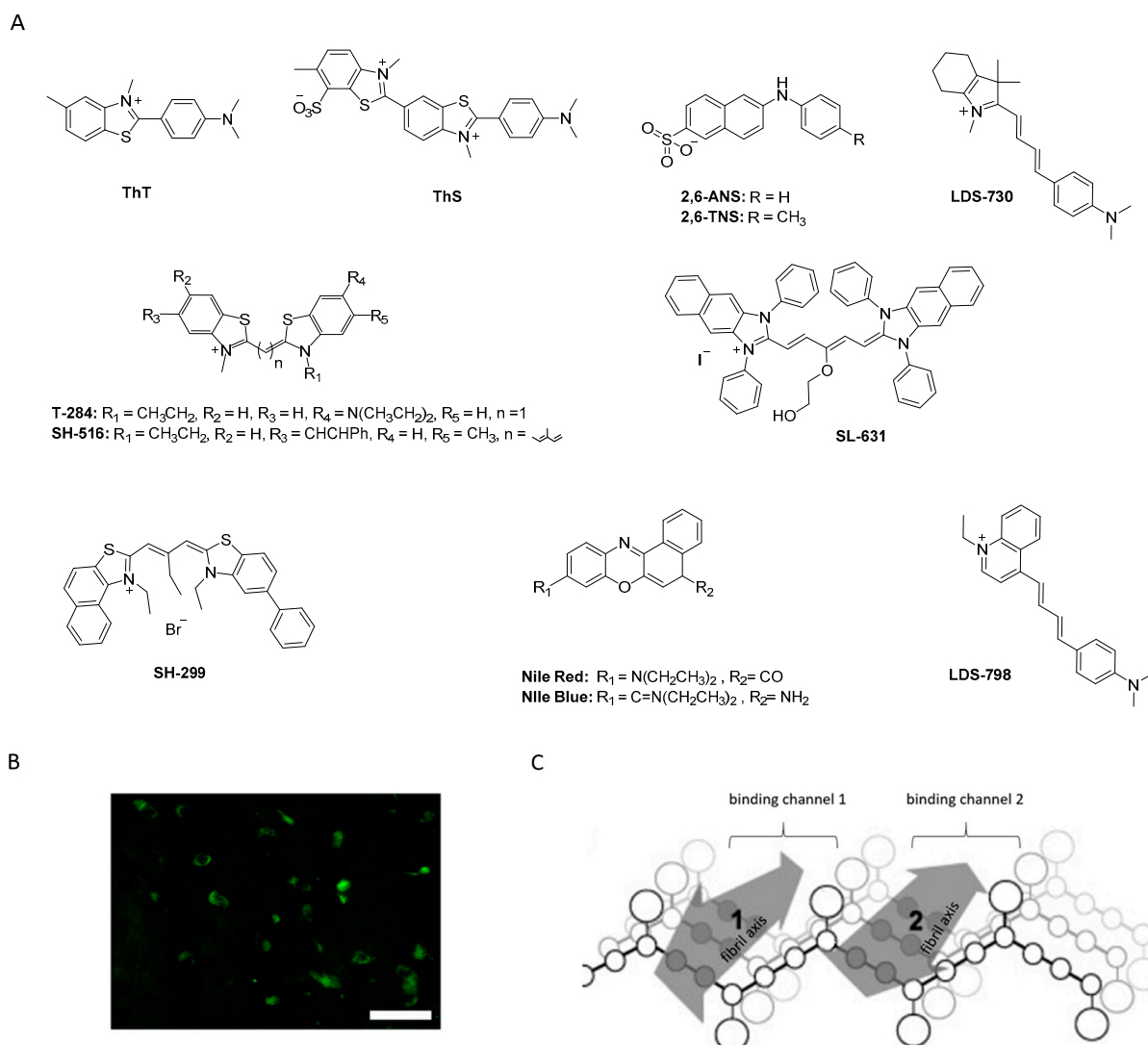


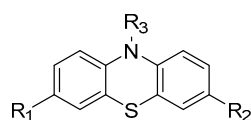
Figure 5. (A) Chemical structures of fluorescent probes and cyanine dyes. (B) ThS positive neurons confirming α -syn pathology (adapted from Patterson et al.) [88]. (C) Hypothetical presentation of how mono- and trimethine cyanine dyes interact with α -syn fibrils (reprinted with permission from [83]. Copyright 2008 Elsevier).

3.1. Tricyclic Analogues (TCAs)

3.1.1. Phenothiazine Analogues

Phenothiazine analogues (SILs) have widely been studied as potentially selective α -syn PET ligands. They were developed based on rational drug design considerations. For example, structurally related bisarylimines have been proven to show neuroprotective effects in PD related models, most likely due to their antioxidant properties [89]. Within this structural class, several phenothiazines were found to inhibit insoluble α -syn filament aggregation at low micromolar IC₅₀ concentrations [89–91]. Encouraged by these findings, several phenothiazines analogues were synthesized and their binding properties evaluated based on a fluorescent ThT competition assay. Several ligands with affinities between 30 and 80 nM were identified (Figure 6). The first promising structure identified within this study was a dimethoxy substituted phenothiazine analogue with an affinity of approximately 120 nM. Replacement of one of the methoxy group with a cyano-group or an amine decreased the affinity more than 3 to 5-fold. In contrast, replacement with a nitro-group increased affinity approximately 4-fold (SIL5, Figure 6) [92]. Further attempts to improve the affinity by altering this position with other substituents failed in a follow-up study [93]. Structure activity relationship (SAR) studies around the methoxy group of SIL5 (K_i between

32.1 nM and 83.3 nM, Figure 6) revealed that the binding affinity toward α -syn decreased in the following order: $-\text{OCH}_3 > -\text{Br} > -\text{I} > -\text{H}$. However, the fluoroethoxy (**SIL26**) and the (3-iodoallyl)oxy (**SIL23**) derivatives showed only slightly reduced affinity in the order of 50 nM [92]. Furthermore, *N*-substitution of phenothiazines greatly reduced affinity against α -syn fibrils [92,94]. In 2018, binding of SILs toward α -syn fibrils was studied. In particular, **SIL23** and **SIL26** preferentially bind to BS 3/13 of α -syn fibrils [43].



General structure 1

| General structure 1 | | | | | | | | | | |
|---------------------|------------------------------------|------------------|-----------------|----------------------------------|---------------|----------------------------------|-------|----------------------------------|---------------------|------------------------------------|
| # | R ₁ | R ₂ | R ₃ | Fibrils | | | | Human PD brain homogenates | | |
| | | | | K _i [nM] ^a | | K _i [nM] ^b | | K _i [nM] ^c | clogP ^{d*} | cLogD _{7.4} ^{**} |
| | | | | α -syn | α -syn | A β ₁₋₄₂ | tau | | | |
| | | | | | | | | | | |
| 1 | OCH ₃ | OCH ₃ | H | 122 ± 5.1 | n.d. | n.d. | n.d. | n.d. | 4.01 | 4.7 |
| 2 | OCH ₃ | CN | H | 346 ± 37 | n.d. | n.d. | n.d. | n.d. | 4.07 | 4.1 |
| 3 | OCH ₃ | NH ₂ | H | >500 | n.d. | n.d. | n.d. | n.d. | 2.79 | 3.4 |
| SIL5 | OCH ₃ | NO ₂ | H | 32.1 ± 1.3 | 66.2 | 110 | 136 | 83.1 | 4.32 | 4.2 |
| SIL22 | Br | NO ₂ | H | 75.3 ± 8.4 | 31.9 | 102 | 173 | 57.1 | 5.31 | 4.5 |
| SIL23 | OCH ₂ CHCHI | NO ₂ | H | 57.9 ± 2.7 | 148 * | 635 * | 230 * | 119–168 * | 5.87 | 5.3 |
| SIL26 | OCH ₂ CH ₂ F | NO ₂ | H | 49.0 ± 4.9 | 15.5 | 103 | 125 | 33.5 | 4.57 | 4.3 |
| 4 | OCH ₃ | NO ₂ | CH ₃ | >500 | n.d. | n.d. | n.d. | n.d. | 4.44 | 4.3 |
| SIL3B | H | NO ₂ | H | n.d. | 19.9 | 71.5 | 52.3 | 49.4 | 4.02 | 4.3 |

Figure 6. Phenothiazine analogues with binding properties determined from two different assays. ^a Affinity toward α -syn fibrils determined by ThT fluorescence assay [92]. ^b Affinity toward recombinant α -syn and tau and synthetic A β ₁₋₄₂ fibrils determined by [¹²⁵I]SIL23 competition assay [55]. ^c Affinity toward human PD brain homogenate determined by [¹²⁵I]SIL23 competition assay [55]. * K_d value determined with the radioligand [¹²⁵I]SIL23 on fibrils or human PD brain homogenate. ^d clogP computed from BioByte software. ^{**} clogD_{7.4} computed from ACD/Percepta. n.d.: not determined.

Inspired by these findings, Bagchi et al. radiolabeled **SIL23** with iodine-125 and evaluated its selectivity profile against A β ₁₋₄₂ and tau fibrils as well as its binding properties at LBs and LNs present in human PD brains. In this study, **SIL23** showed a K_d value of 148 nM on α -syn fibrils and comparable affinity in human tissue. These values are, however, a 2-fold lower than the affinity determined by the fluorescent ThT competition assay, highlighting the variations between both assays. Its selectivity toward A β ₁₋₄₂ and tau fibrils is low and as such **SIL23** is not suitable for the development of a PET α -syn tracer. However, [¹²⁵I]**SIL23** is, nonetheless, an excellent tool to evaluate the binding profile of other phenothiazine analogues. **SIL26** showed the best selectivity profile in this assay. A 6-fold and 8-fold selectivity for α -syn over A β ₁₋₄₂ and tau fibrils was detected, respectively. In general, K_i values obtained from PD brain homogenate assay were comparable with those obtained from α -syn fibrils. This indicated that not only can the [¹²⁵I]**SIL23** competition assay accurately predict binding in human tissue, but also that the fibrillar α -syn binding site is conserved between recombinant α -syn fibrils and the in vivo formed species in PD patients [55]. Although **SIL5** and **SIL26** did not show particularly high binding affinity and selectivity, they showed most promising results among the tested phenothiazines and were therefore radiolabeled for in vivo PET studies (Figure 7A). [¹¹C]**SIL5** was isolated in a RCY

of 35–45% (decay-corrected to EOB) and an A_m of >363 GBq/ μmol and [^{18}F]SIL26 in a RCY of 55–65% (decay-corrected to EOB) and an A_m of >200 GBq/ μmol [95]. Both tracers were able to pass the BBB and had homogeneous distribution throughout the brain in male Sprague-Dawley rats. Total brain uptake for [^{11}C]SIL5 was 0.953%ID/g at 5 min p.i. and 0.287%ID/g at 30 min p.i. In contrast, [^{18}F]SIL26 showed a lower total brain uptake of 0.758%ID/g at 5 min p.i. but a higher uptake than [^{11}C]SIL5 (0.359%ID/g) at 120 min p.i. The decreased washout may be a result of the increased lipophilicity of [^{18}F]SIL26 in comparison with [^{11}C]SIL5. Faster washout kinetics are generally preferred in PET studies, [96] and consequently, [^{11}C]SIL5 was selected for in vivo PET imaging studies in healthy NHP (Figure 7B). Expected homogenous uptake within the brain was observed (since no target should be present in healthy subjects) [95]. Standardized uptake value (SUV) peak uptake was >3 at approximately 7 min and slowly decreased and flattened over 70 min to values around 1 SUV. This value is a good indicator for the non-displaceable binding component of the tracer and may be too high, taking into account the low amount of α -syn fibrils that should be present in diseased animals. As such, a further study should be performed in α -syn positive animals, e.g. transgenic mice expressing α -syn fibrils, to see if [^{11}C]SIL5 can selectively image α -syn. It has been shown that, at least for SIL23, the binding site in mice expressing the human α -syn transgene containing the A53T mutation (M83 line) is present in this transgenic mouse model for PD, whereas mice expressing the WT human α -syn transgene (M7 line) did not show any specific SIL23 in brain tissue homogenates. Since SIL5 is a close analogue of SIL23 and can therefore be displaced by SIL23, it is likely that both compounds bind at the same binding site. As such, the A53T transgenic mouse model appears to be a suitable in vivo model to test the in vivo binding characteristics of [^{11}C]SIL5 or related compounds [95].

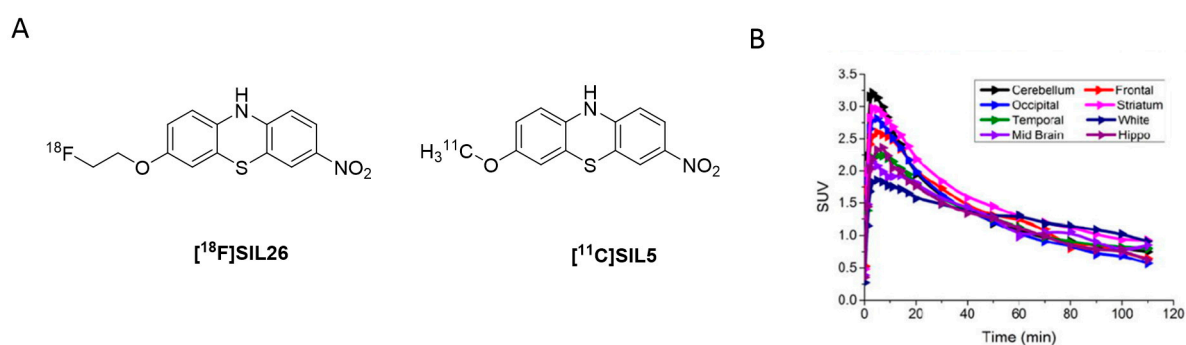


Figure 7. Radiolabeled phenothiazine analogues. (A) Chemical structures of [^{18}F]SIL26 and [^{11}C]SIL5. (B) TACs from in vivo evaluation of [^{11}C]SIL5 in healthy NHP (adapted from) [95].

3.1.2. Phenoxazine and Phenazine Analogues

In parallel to the phenothiazines, their isosteres, the phenoxazines and the phenazines, were also evaluated as potential α -syn PET tracers. Tu et al. synthesized a small compound library consisting of 8 compounds and determined their binding affinity toward recombinant α -syn fibrils by a ThT-based fluorescence assay. Several ligands showed affinity in the nanomolar range (Figure 8A) and among them TZ-2-39 with the lowest K_i value of 9.5 nM [97]. In comparison with the phenothiazines, the phenoxazines showed better affinity toward α -syn fibrils. For example, SIL5 showed a K_i of 32.1 nM while TZ-2-33 a K_i of 25.7 nM. Values were determined using the same binding assay set-up. No further attempts have been made thus far to improve the binding profile of this structural class. TZ-2-48 showed displaceable binding and was shown to bind preferentially to the BS 3/13 position of α -syn fibrils [43]. Interestingly, the phenazines (Figure 8B) did not show any significant affinity toward α -syn, highlighting the importance of oxygen or sulfur in the bridge between the aromatic rings [97].

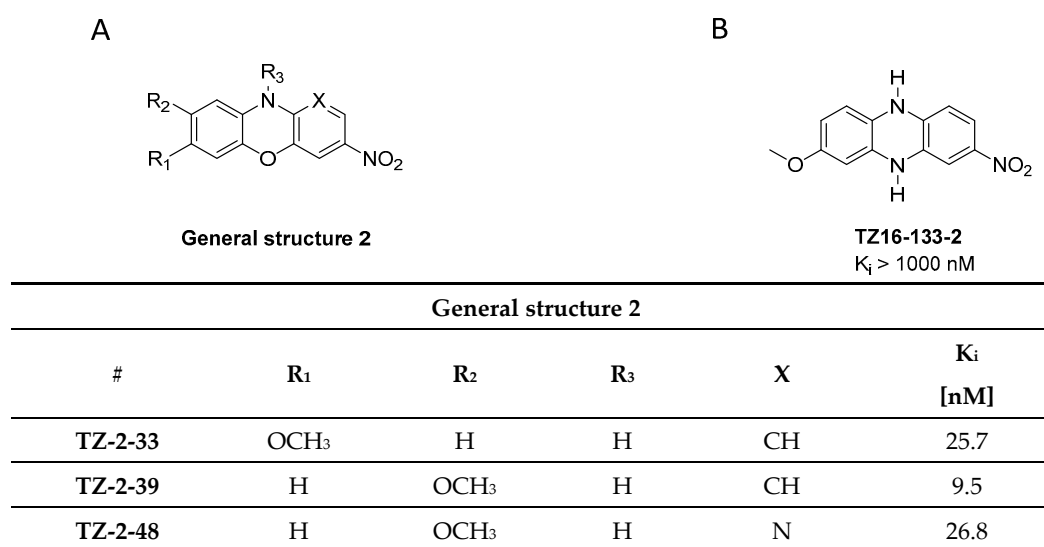


Figure 8. General structure of phenoxazine and phenazine analogues. (A) Chemical structure of phenoxazine analogues with binding properties utilized from ThT fluorescence assay using α -syn fibrils [97]. (B) Chemical structure of phenazine analogues **TZ16-133-2** with binding affinity K_i > 1000 nM [97].

3.2. Benzoxazole Derivatives

3.2.1. BF-227

BF-227 was initially developed as a PET ligand to image amyloid plaques in AD patients (Figure 9A) [98]. However, during its biological evaluation **BF-227** was found to bind also to α -syn fibrils with an affinity of K_d 9.63 nM, 10-fold lower than its affinity to A β _{1–42} fibrils (K_d 1.31 nM). Inspired by these results, **BF-227** was evaluated in human brain tissue. Contradictory results with respect to the ability of **BF-227** to detect α -syn in human brain tissue have been reported [99–102]. For example, Fodero-Tavoletti and colleagues reported that **BF-227** binds to α -syn in PD, but not in DLB patients [99]. A follow-up study analyzing the binding properties of **BF-227** in human postmortem tissue using brain specimens from PD and DLB patients showed that **BF-227** can detect α -syn fibrils in all cases [99]. A PET study in MSA patients confirmed that [¹¹C]**BF-227** (Figure 9A,B) is suitable for imaging α -syn deposition in these patients [100], but a recent publication by Verdurand et al. questioned the binding of **BF-227** to pathological forms of α -syn. Autoradiography (ARG) on MSA and control brain sections without α -syn pathology were investigated. In contrast to previous studies, Verdurand and colleagues selected the medulla oblongata as their target region to study the binding of **BF-227**. The reason for this is that the medulla oblongata is systematically affected during disease progression in MSA without developing A β co-pathology. [¹⁸F]**BF-227** (which is chemically identical to [¹¹C]**BF-227**) could not detect any α -syn inclusions when compared to healthy controls [101]. This study concluded that **BF-227** cannot be used as an α -syn PET ligand [99,100]. The discrepancy between results was explained with concentration differences of **BF-227** used in ARG and fluorescent measurements. In contrast to fluorescence measurements, where micromolar concentrations are required, only nanomolar concentrations are needed in ARG. The concentration differences stem from the sensitivity of fluorescence compared radioactivity detection. Authors exemplified the latter by conducting fluorescence study and exposing MSA patient at 100 μ M of unlabeled **BF-227** without corresponding ARG detection at 1 nM (Figure 9C) [101]. However, the given explanation cannot explain the positive results gained within the PET study of [¹¹C]**BF-227** [100]. Verdurand and colleagues suggest that PET differences in this study are unlikely related to α -syn binding. More importantly, they showed that **BF-227** can selectively bind to A β and as such suggesting that mixed A β or α -syn pathologies, which often coexist, could have been imaged in the aforementioned PET study [101].

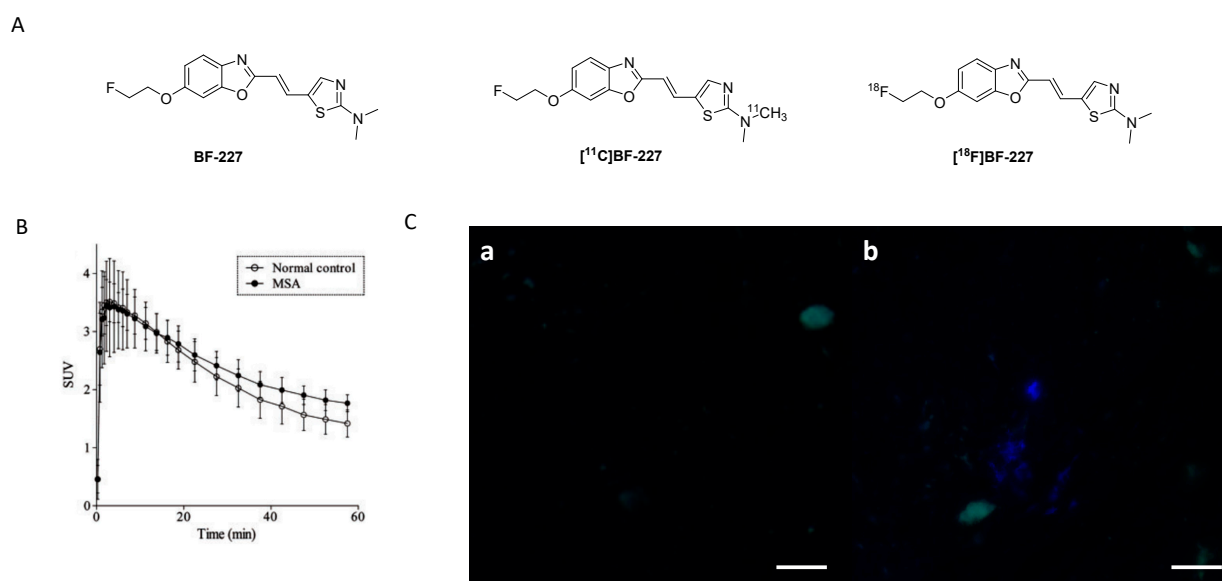
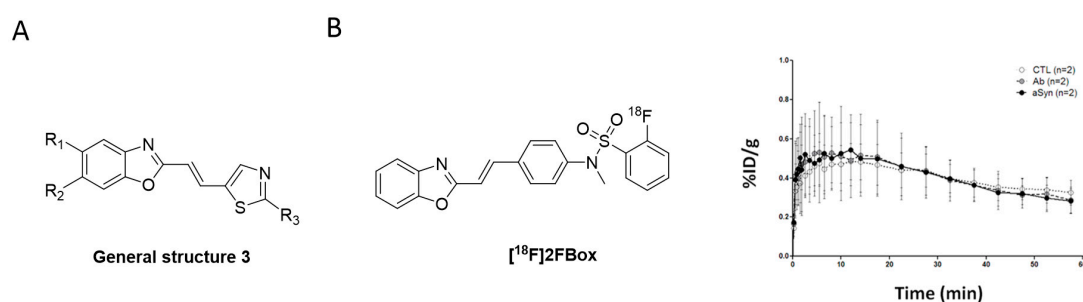


Figure 9. (A) Chemical structures of **BF-227**, [^{11}C]BF-227 and [^{18}F]BF-227. (B) TACs of [^{11}C]BF-227 in putamen in normal controls and MSA patients (Reprinted with permission from [100]. Copyright 2010 Oxford University Press). (C) Fluorescence detection of BF-227 (at 100 μM) using MSA brain sections. (a) Tissue autofluorescence (in green) that is imaged prior to BF-227. (b) BF-227 labeling (in blue) of few inclusions. Microscopic examination under DAPI (blue, exposure 500 ms) and FITC (green, exposure 100 ms) filters (adapted from [101]).

These findings highlight the difficulties of validating the binding properties of a given chemical structure for its suitability for imaging α -syn fibrils. Control experiments are of crucial importance to rule out binding to other fibrillar structures such as $\text{A}\beta_{1-42}$, especially in human tissue. Evaluation assays should be carefully validated with respect to their ability to predict whether a chemical structure is able to image α -syn fibrils in human tissue. Different conformational forms and densities of α -syn in MSA, DLB, and PD tissue can also influence the outcome of a study and lead to false conclusions. In summary, further experiments are required to validate the usefulness of **BF-227** as an α -syn PET ligand. Current results suggest that **BF-227** is not capable of imaging α -syn fibrils in vivo.

3.2.2. SAR Studies of BF-227

A series of BF-227-like compounds were designed in order to increase the affinity and selectivity profile of **BF-227** (Figure 10A) toward α -syn. Various oxyethylene groups (5–7) as well as hydrogen, iodine (8) and fluorine (9) were introduced to study the substitution pattern of the 6-position of the benzo[*d*]oxazole. Introduction of these oxyethylene groups did not alter the affinity or the selectivity profile of the compound at all. Substitution of the fluoroethoxy group with an iodine increased the selectivity approximately 10-fold, whereas substitution with fluorine or hydrogen lowered the affinity toward α -syn fibrils from 53 nM to 286 nM (Figure 10) [103]. Interestingly, this research suggested that the binding affinity of **BF-227** toward α -syn fibrils was significantly different when compared to the affinity initially reported by Fodero-Tavoletti et al. [99] (Figure 10). A possible explanation for this discrepancy may be that different in vitro assays as well as different fibril preparations were used in these studies.



| # | R ₁ | R ₂ | R ₃ | K _i [nM] | | clogP * | cLogD _{7.4} ** |
|-------------------------|----------------|---|----------------------------------|--|---|---------|-------------------------|
| | | | | α -syn | A β ₁₋₄₂ | | |
| BF-227 | H | OCH ₂ CH ₂ F | N(CH ₃) ₂ | 9.63 ^a ; 53 ^b ; 14.03 ± 43.52 ^c | 1.31 and 80 ^a ; 12 ^b ; 4.3 ± 1.5 ^d | - | - |
| [¹⁸ F]2FBox | - | - | - | 3.3 ± 2.8 ^c | 145 ± 114.5 ^c | 4.76 | 4.0 |
| General structure 3 | | | | | | | |
| 5 | H | OCH ₂ CH ₂ OCH ₂ F | N(CH ₃) ₂ | 83 | 11 | - | - |
| 6 | H | O(CH ₂ CH ₂ O) ₂ CH ₂ F | N(CH ₃) ₂ | 52 | 13 | - | - |
| 7 | H | O(CH ₂ CH ₂ O) ₄ CH ₂ F | N(CH ₃) ₂ | 75 | 18 | - | - |
| 8 | H | I | N(CH ₃) ₂ | 74 | 223 | - | - |
| 9 | H | F | H | 286 | 1446 | - | - |

Figure 10. (A) General structure of BF-227-like compounds with binding properties specified in table. Affinities were determined for α -syn and A β ₁₋₄₂ fibrils. Binding affinities were determined by several techniques: ^a K_d values identified with Scatchard analysis [99,103]. ^b In vitro saturation assay using synthetic α -syn and A β ₁₋₄₂ fibrils [67]. ^c In vitro saturation binding assay [67]. ^d In vitro binding assays (K_i) determined for A β ₁₋₄₂ fibril in competitive binding assay using [¹²⁵I]BF-180 [98]. * clogP values were calculated by BioByte. ** clogD_{7.4} values calculated by ACD/Percepta. (B) The chemical structure of [¹⁸F]2FBox with the TAC from small-animal PET imaging of fibril-injected rats (controls were taken from the striata regions) (reprinted with permission from [67]. Copyright 2018 American Chemical Society).

3.2.3. Rational Drug Design around BF-227

In 2018, Verdurand et al. applied a rational drug design approach to two other lead structure scaffolds (benzimidazoles and TCAs) based on benzoxazoles. Computational modeling was applied, and various combinations of lead structure motifs were docked into an α -syn fibril model [67]. Among the 10 virtually designed compounds, two ligands (2FBox and 4FBox) were considered worthwhile to be synthesized and in vitro tested. ¹⁸F-Radiolabeling of these molecules succeeded with a RCY of 10–19% and an A_m = 68–543 GBq/ μ mol. Affinity and selectivity were determined with an in vitro saturation assay using synthetic α -syn and A β ₁₋₄₂ fibrils. [¹⁸F]2FBox (Figure 10B) showed the best binding characteristics with an affinity of K_d = 3.3 ± 2.8 nM against α -syn fibrils and a roughly 50-fold selectivity over A β ₁₋₄₂ fibrils. In vitro ARG of rat brains showed that [¹⁸F]2FBox was able to detect α -syn fibrils previously injected. Interestingly, preclinical imaging using the same animal model showed that [¹⁸F]2FBox was not able to image these α -syn fibrils in vivo, although [¹⁸F]2FBox showed sufficient brain uptake and an acceptable, but slow clearance profile. Peak brain uptake was 0.47% ID/g at 12 min p.i. (SUV = 1.6), and the tracer was washed out slowly, lowering its peak uptake only 20% within 50 min. The authors suggested that the discrepancy between the in vitro to in vivo results might be due to the low spatial resolution of PET imaging in comparison to in vitro ARG. The high non-displaceable binding component of [¹⁸F]2FBox could also possibly prevent selective imaging. However, [¹⁸F]2FBox also failed to detect selective binding on postmortem brain tissue (medulla oblongata) from PD and MSA patients using ARG [67].

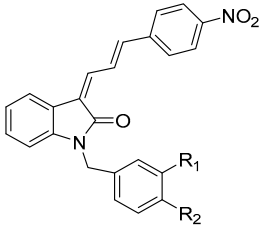
The discrepancy between results obtained from computational modeling, postmortem human tissue, and recombinant human fibrils are concerning, but support the hypothesis that fibrils formed in vitro (and virtual models thereof), may not sufficiently represent in vivo forms in all cases. Further validation of this hypothesis is urgently needed. Since **2FBox** did not show selective binding to α -syn in postmortem tissue, we believe that **2FBox** is not a promising starting point for the development of suitable α -syn PET radioligands.

3.3. Indolinones and Indolinone-Dienes

In 2007, Honson et al. reported that indolinone structures confer moderate affinity, but poor selectivity toward α -syn over $A\beta_{1-42}$ and tau fibrils [104]. Neal et al. later demonstrated that the two fluorescent dyes **LDS 798** and **LDS 730** (Figure 5A) were capable of detecting LB in postmortem PD tissue [87]. This inspired Chu et al. to combine the key features, namely the double bond fragment of the dyes and the indolinone structure, into one new lead. With these modifications, they hoped to increase the selectivity toward α -syn [105]. A series of over 40 compounds was synthesized, and the novel indolinone-diene derivatives displayed higher selectivity toward α -syn. Single double bonds only showed moderate affinity and no selectivity while diene analogues showed improved affinity and selectivity. We speculate that the increased length of these diene analogues is responsible for this and allow for a stronger interaction between the ligand and the binding site. The *Z*, *E* configuration was shown to be more active (Figure 11A,B). Five indolinone-diene analogues showed an affinity of $K_i < 25$ nM toward α -syn fibrils and > 5 -fold selectivity over $A\beta_{1-42}$ and tau fibrils. Compound **15a** appeared to be most promising with the highest observed affinity for α -syn (K_i of 2.08 nM) and an approximately 68-fold and 40-fold lower affinity for $A\beta$ and tau fibrils, respectively. Affinities were measured using a ThT based competitive binding assay. These promising data prompted Chu et al. to ^{18}F -radiolabel **15a** (Figure 11B) resulting in an isolated activity of 0.71 ± 0.23 GBq (decay corrected) and an A_m ranging from 29.6 to 185 GBq/ μmol . K_d measurements of [^{18}F]**15a** confirmed the affinity and selectivity profile measured by aforementioned competition binding assay, i.e., **15a** can selectively be displaced from its binding site [43]. Binding affinities toward α -syn, $A\beta$ and tau fibrils were determined to be 8.9, 271 and 50 nM, respectively and **15a** was identified to preferential bind to BS 3/13 of α -syn fibrils [43].

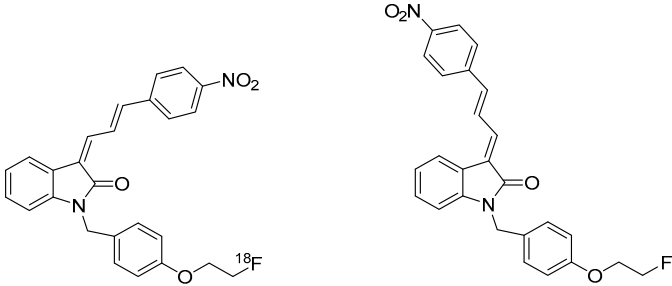
Despite these encouraging results, [^{18}F]**15a** has not been tested on patient-derived tissues, and the compound has not been thoroughly evaluated in preclinical PD animal models. The authors reasoned that **15a** possesses a logP of 4.18, which is outside of the standard range for CNS tracers [80] and furthermore, they were concerned that the nitro-group of **15a** could be reduced in vivo [105]. A limited in vivo evaluation in NHP was nevertheless conducted and [^{18}F]**15a** showed slow clearance [54]. Since **15a** is one of the most selective α -syn ligands ever designed, we believe this compound should have been tested in preclinical PD animal models and in vitro on patient-derived tissues. Why another compound with lower affinity and selectivity, namely compound **10**, was instead evaluated on brain tissue from PD/DLB and PD patients with fluorescence microscopy (Figure 12) remains unclear. Unfortunately, *E,E* and *E,Z* stereoisomers were not isolated, and the compound was applied as a mixture with a 1:1 ratio. **10** was clearly able to stain LB. $A\beta$ plaques from AD patients may also be stained, bringing the α -syn selectivity of **10** into question [105]. Nevertheless, this study showed that radiolabeled derivatives from this structural class are able to detect α -syn fibrils only when the latter are present in high concentrations. Future studies based on **15a** are warranted and should focus first on the in vitro binding profile of patient-derived α -syn tissue at low concentration. If promising, extensive SAR studies should be conducted to develop better compounds with improved pharmacodynamics and α -syn selectivity.

A



General structure 4

B



[¹⁸F]15a
Z, E configuration

15b
E, E configuration

| General structure 4 | | | | | | | | |
|---------------------|------------------|------------------------------------|------------|----------------|--------------------|---------------|--------------------|------------------------------------|
| # | R ₁ | R ₂ | E,E or Z,E | K _i | | | clogP ^a | cLogD _{7.4} ^{**} |
| | | | | [nM] | | | | |
| | | | | α-syn | Aβ ₁₋₄₂ | tau | | |
| 10 | - | - | mixture | 40.7 ± 8.7 | 27.6 ± 4.8 | 53.7 ± 9.7 | 3.85 | 3.6 |
| 11a | H | H | Z,E | 25.0 ± 12.7 | 214.2 ± 52.1 | 121.5 ± 18.8 | 5.4 | 4.6 |
| 12a | H | OCH ₃ | Z,E | 12.9 ± 4.9 | 130.8 ± 64.4 | 72.4 ± 24.1 | 5.3 | 4.3 |
| 13a | OCH ₃ | H | Z,E | 3.8 ± 0.6 | 109.7 ± 0.4 | 228.6 ± 113.7 | 5.3 | 4.3 |
| 14a | OCH ₃ | OCH ₃ | Z,E | 3.5 ± 0.2 | 73.6 ± 27.3 | 151.7 ± 64.7 | 4.8 | 4.4 |
| 15a | H | OCH ₂ CH ₂ F | Z,E | 2.08 ± 0.3 | 142.4 ± 36.9 | 80.1 ± 12.0 | 5.6 | 4.5 |
| 15b | H | OCH ₂ CH ₂ F | E,E | 76.1 ± 41.2 | 125.3 ± 40.1 | 455.7 ± 66.1 | 5.6 | 4.5 |

Figure 11. Chemical structures of indolizone-diene analogues with key properties. (A) General structure of indolizone-dienes and their binding affinity toward recombinant α-syn, tau, and synthetic Aβ₁₋₄₂ fibrils determined by ThT competitive binding assays [105]. ^a clogP were calculated from BioByte software. ^{**} clogD_{7.4} values calculated by ACD/Percepta. (B) Chemical structures of [¹⁸F]15a (Z,E configuration) and 15b (E,E configuration) [105].

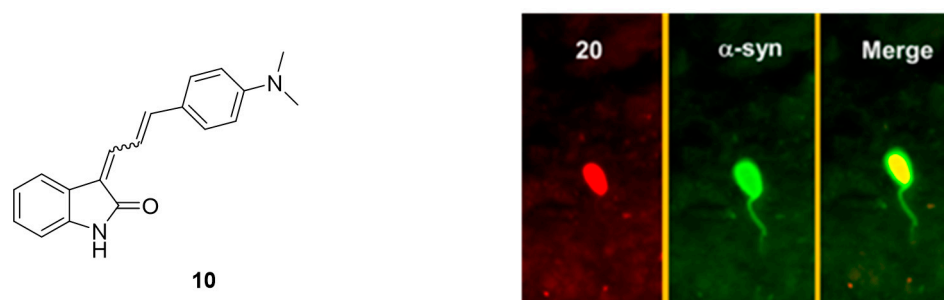


Figure 12. Chemical structure of 10 and fluorescent microscopy studies on brain tissue from PD/DLB and PD patients (reprinted with permission from [105] Copyright 2015 American Chemical Society).

3.4. Thiazole Derivatives

The thiazole moiety is a widely applied scaffold to enhance affinity and selectivity of potential α-syn targeting compounds. For instance, the benzothiazole ring is present in cyanine dyes (T-284 and SH-516, Figure 5) and fluorescent dyes (ThT, Figure 5) that have previously been shown to bind to α-syn fibrils. In previous sections, the thiazole moiety already appeared for example within the ligand BF-227. In this section, we will further discuss its past role in the design of a selective α-syn ligand.

3.4.1. Diphenylthiazole Derivatives

Several diphenylthiazole, diphenyloxazoles and diphenylthiophenes compounds were developed as potential α-syn imaging agents [106]. However, only one diphenylthiazole,

compound **17** (Figure 13) has thus far shown a reasonable affinity ($K_i = 89$ nM) toward α -syn aggregates in affinity measurements conducted using a competition binding assay. Compound **17** also did not show any significant binding for $A\beta$ in AD tissue.

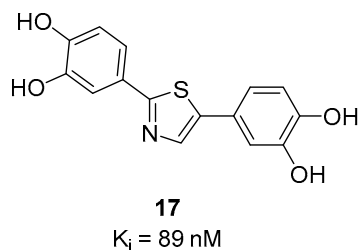


Figure 13. Chemical structure of **17** with binding affinity $K_i = 89$ nM [106].

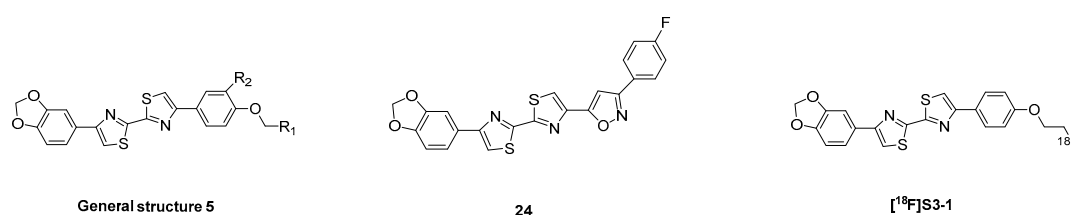
3.4.2. Bithiazole Derivatives

Bithiazole derivatives were reported as promising new ligands for the detection of neuropathological aggregates, including α -syn. Unfortunately, the only available literature source, to date, is patented and no additional articles are available on the subject. Researchers from the Technical University of Munich developed these bithiazoles and among them compounds **18**, **19** and **24** (Figure 14) showed high affinity for α -syn and good selectivity over $A\beta_{1-42}$ and tau fibrils (as determined by saturation binding assays). Several bithiazoles from the same family were identified as potential ligands for targeting $A\beta$ and tau. Potential ligands for α -syn are summarized in Figure 14 with limited binding affinity data. Compound **18** demonstrated the highest affinity ($K_i = 3$ nM) and a selectivity of 127-fold and >300-fold over $A\beta_{1-42}$ and tau, respectively. Additionally, compounds **20**, **21**, **22** and **23** (Figure 14) were also reported to be selective for α -syn, although no binding data was published [107]. Just recently, [^{18}F]S3-1 (Figure 14) a novel structurally related α -syn PET tracer was evaluated in rats, NHPs and humans following a conference abstract [108]. [^{18}F]S3-1 showed binding affinity of 3 nM for α -syn and high selectivity of 120-fold for $A\beta$ and tau. Brain kinetics were investigated in E46K rats demonstrating statistically significant difference between E46K and health controls. Furthermore, in NHPs initial brain uptake was up to 1.4% ID and the SUV was 1.3 at 30 min with rapid clearance (SUV \sim 0.1) but with marginally increases in the later timepoints (SUV = 0.4 at 120 min). Dynamic PET studies showed specific binding of [^{18}F]S3-1 in patients with underlying α -synucleinopathies [108]. In summary, bithiazole derivatives present a class of compounds with excellent affinity and selectivity, however more detailed scientific literature is needed in order to provide more thorough conclusions.

3.4.3. Benzothiazole Derivatives

Benzothiazole analogues have recently attracted attention as potentially selective α -syn PET ligands. Among this class, [^{11}C]PBB-3 was initially developed to image namely tau aggregates [109]. Its binding affinity toward tau was 1.8 nM (neocortex/hippocampus transgenic mice) [110]. During preclinical evaluation, binding toward α -syn was detected. Koga et al. were the first to examine the ability of [^{11}C]PBB-3 (Figure 15A) to bind to brain-derived LB, LN, and glial cytoplasmic inclusions (GCI) from patients with α -synucleinopathies (MSA and DLB). Fluorescence imaging showed that PBB3 can bind to α -synucleinopathies only at high concentrations (32.3 μM). For example, immunofluorescence double-staining clearly demonstrated this binding (Figure 15B). In ARG and at a low concentration (10 nM, $A_m = 133$ GBq/ μmol), [^{11}C]PBB-3 could only bind to the high density GCIs from MSA patients. No specific binding was detected in DLB patients (Figure 15C) [111]. Recently, an additional compound based on the benzothiazole scaffold was identified. PP-BTA-4, a push-pull (PP) benzothiazole derivative, was shown to bind to α -syn. PP-BTA-4 (Figure 15A) strongly increased its fluorescence intensity upon binding to the protein aggregates in solution. A K_d of 48.0 ± 0.6 nM was determined by an in vitro saturation binding assay on α -syn aggregates from human PD brains. PP-BTA-4 also bond

to $A\beta_{1-42}$ (derived from AD patients) with an affinity in the same order of magnitude [112]. Other benzothiazole derivatives of interest are compounds **25**, **26**, and **27** (Figure 15A). In a fluorescence-based assay using amygdala brain sections derived from fully developed PD and AD patients (Braak stage V -VI) selective binding of these compounds to α -syn over $A\beta$ plaques was detected. The compounds were incubated on the brain sections at a high concentration of 100 μ M. Further binding affinity measurements revealed K_d values for compounds **25** and **26** of 50 nM and 14 nM, respectively [113]. Affinities were determined by backscattering interferometry on human PD brain homogenates (cortex). Affinity data for **27** is not reported [113]. Just recently, a novel analogue of PBB3, **C05-01** (Figure 15A), has been discovered showing a K_i of 3.5 nM for brain homogenates and a K_i of 25 nM for α -syn fibrils. **C05-01** was derived from a library of 44 compounds that were structurally similar to PBB3 and was selected based on quantitative evaluation using fluorescence microscopy and a semiquantitative approach using a tissue microarray (TMA).



| General structure 5 | | | | | | | | | | | |
|--------------------------------|--|----------------|-------------------------------------|---------------------|---------------------|---|--------------------|-------------------|--------------------|------------------------------------|--|
| # | R ₁ | R ₂ | K _i [nM] ^a | | | % inhibition of [³ H]PIB ^b | | Lipophilicity | | | |
| | | | α -syn | $A\beta_{1-42}$ | tau | $A\beta_{1-42}$ | clogP ^c | logP ^d | clogP [*] | cLogD _{7.4} ^{**} | |
| 18 | H | F | 3 | 382 | >1000 | 45 ± 2 | 5.47 | n.d. | 5.47 | 4.5 | |
| 19 | CH ₃ | H | 10 | 386 | 558 | 45 ± 2 | 5.95 | n.d. | 5.98 | 4.8 | |
| 20 ([¹⁸ F]S3-1) | CH ₂ F (CH ₂ [¹⁸ F]) | H | 3 ^{***} | >360 ^{***} | >360 ^{***} | n.d. | n.d. | 2.6 | 5.57 | 4.7 | |
| 21 | CH ₂ O(CH ₂) ₂ F | H | n.d. | n.d. | n.d. | n.d. | n.d. | 2.5 | 6.06 | 4.6 | |
| 22 | F | H | n.d. | n.d. | n.d. | n.d. | n.d. | 2.6 | 5.62 | 4.4 | |
| 23 | CH ₂ (OCH ₂ CH ₂) ₂ F | H | n.d. | n.d. | n.d. | n.d. | n.d. | 2.3 | 5.28 | 4.5 | |
| 24 | - | - | 6 | 492 | >1000 | 35 ± 2 | n.d. | 3.2 | 6.00 | 4.7 | |

Figure 14. Chemical structures of bithiazole derivatives with key properties. Chemical structure of potential α -syn ligands with binding properties toward recombinant α -syn, $A\beta_{1-42}$, and tau fibrils. ^a Affinity toward α -syn fibrils, synthetic amyloid peptides ($A\beta_{1-42}$) and human recombinant tau-441 determined by saturation binding assay [107]. ^b % inhibition of [³H]PIB determined by competition binding assay [107]. ^c calculated clogP according to the reference [107]. ^d Measured logP from octanol/PBS study according to the reference [107]. n.d.: not determined. * clogP values were calculated by BioByte. ** clogD_{7.4} values calculated by ACD/Percepta. *** Literature source [108].

TMA is an effective approach for high-throughput molecular analysis of pathological tissues, as it makes use of paraffin blocks, which allow one to measure several tissue cores without consuming the tissue block. A further advantage of TMA is that it can be used to examine tissue from multiple patients. TMA also allows multiplexing of histological analysis including immunohistochemistry, immunofluorescence, histological staining. The binding profile of **C05-01** was determined on recombinant α -syn fibrils using saturation and competition binding assay with [³H]**C05-01** and **C05-01** and an affinity in the range 25–30 nM was determined. Further studies using brain homogenates from DLB (amygdala) revealed different affinities to those previously reported by Koga et al. [111]. [¹¹C]**PBB3** showed a moderate affinity (K_d of 58 nM) while non-labeled **C05-01** demonstrated a high affinity (K_i of 3.5 nM). These data once again showed that the tertiary structure of fibrils and brain homogenates can be different. Another reason for the observed discrepancy may

be the variance of experiments. Further characterization of selectivity using PD, MSA, AD and Pick's disease TMA sections and fresh frozen tissue confirmed the binding of **C05-01** to α -syn, however, binding to other amyloids was also shown [114]. Recently, new ThT analogues, namely **RB1** and **RB2** (Figure 15A), were developed in order to achieve stronger selectivity for α -syn over amyloid fibrils. Key structural features include introduction of a double bond and cyclic nitrogen donors (either piperidine or piperazine). Binding affinities were tested using α -syn fibrils (concentration < 30 μ M) and revealed K_d values of 30 nM and \sim 4.4 μ M for **RB1** and **RB2**, respectively. The authors hypothesize that the piperidine moiety fits better in the hydrophobic pocket of α -syn fibrils and therefore **RB1** shows higher affinity for α -syn than the lead compound. No selectivity data over A β or tau have been reported. Encouraged by these results the authors studied **RB1** and its applicability for live-cell imaging using the SH-SY5Y human neuroblastoma cell line. Cultured cells were incubated with short α -syn fibrils. Then, these cells were incubated with **RB1** at concentration 500 nM and demonstrated selective staining of α -syn fibrils in the cytosol. This study showed an approach to implement the design and development of new compounds. However, binding affinity and selectivity profile need to be further improved and investigated [115].

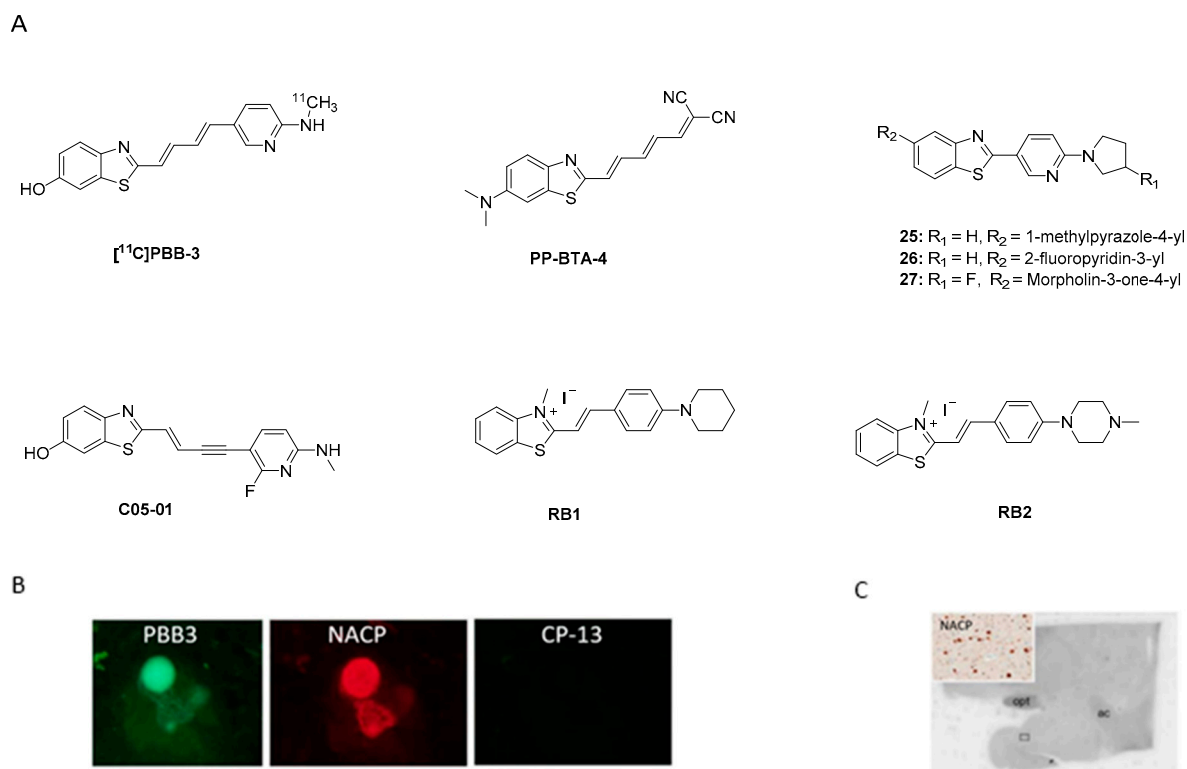
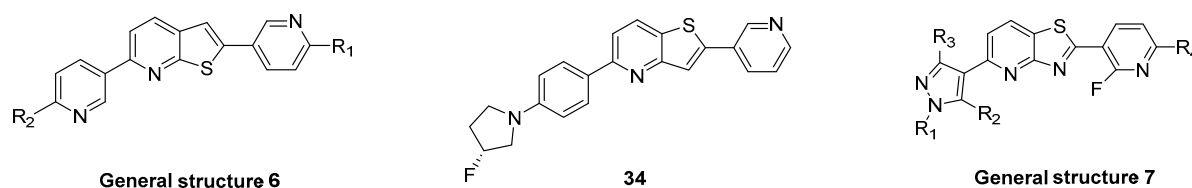


Figure 15. Chemical structures and examples of fluorescence and ARG. (A) Chemical structures of [¹¹C]PBB-3, PP-BTA-4, compounds 25, 26, 27, and RB1, RB2. (B) PBB-3 fluorescence labeling and immunofluorescence double staining for α -syn (NACP) and phosphor-tau (CP13) in DLB from brainstem type LB (reprinted with permission from [111]. Copyright 2017 International Parkinson and Movement Disorder Society). (C) Autoradiographic labeling using [¹¹C]PBB-3 in amygdala of DLB patients (reprinted with permission from [111]. Copyright 2017 International Parkinson and Movement Disorder Society).

In conclusion, benzothiazole derivatives appear to be structural leads which may help in the development of an α -syn selective compound. Extensive SAR studies are still needed to learn more about how binding and selectivity can be improved.

3.4.4. Thienopyridine, Thiazolo Pyridine Derivatives

Recently, a new heterogeneous class of compounds was discovered, which may stain α -syn aggregates as well as A β plaques. Fibrils were derived from fully developed PD and AD patients (Braak stage V-VI) and a library of 130 compounds were incubated at 100 μ M and their neuropathological staining was confirmed by staining with primary antibodies. Of the 130 tested compounds, only several (28–34) showed selectivity for α -syn aggregates over A β plaques (Figure 16, determine with fluorescence staining). The only compound that was tested for affinity was compound 34, although it only shows weak staining of α -syn aggregates. This decision was most likely taken since 34 did not stain A β plaques. An affinity (K_d) of 9 nM was determined by backscattering interferometry on human derived tissue (PD brain homogenates) [113]. To further evaluate this class of compounds, a comprehensive in vivo evaluation, in vitro ARG at lower concentrations and radiolabeling studies should be performed.



| # | R ₁ | R ₂ | R ₃ | R ₄ | K_d [nM] ^a α -Syn | Staining α -Syn aggregates ^b | Staining A β plaques ^c | Staining A β plaques ^d |
|----------------------------|----------------------------------|-------------------|-----------------|------------------------|---|---|--|--|
| General structure 6 | | | | | | | | |
| 28 | N(CH ₃) ₂ | NHCH ₃ | - | - | n.d. | Strong | Weak | n.d. |
| 29 | H | 4-morpholine | - | - | n.d. | Strong | Weak | n.d. |
| General structure 7 | | | | | | | | |
| 30 | H | H | H | 3-fluoropiperidin-1-yl | n.d. | Strong | n.d. | No |
| 31 | H | H | H | pyrrolidin-1-yl | n.d. | Strong | n.d. | No |
| 32 | H | CH ₃ | CH ₃ | pyrrolidin-1-yl | n.d. | Strong | n.d. | No |
| 33 | CH ₃ | H | H | pyrrolidin-1-yl | n.d. | Strong | n.d. | No |
| 34 | - | - | - | - | 9 | Weak | No | n.d. |

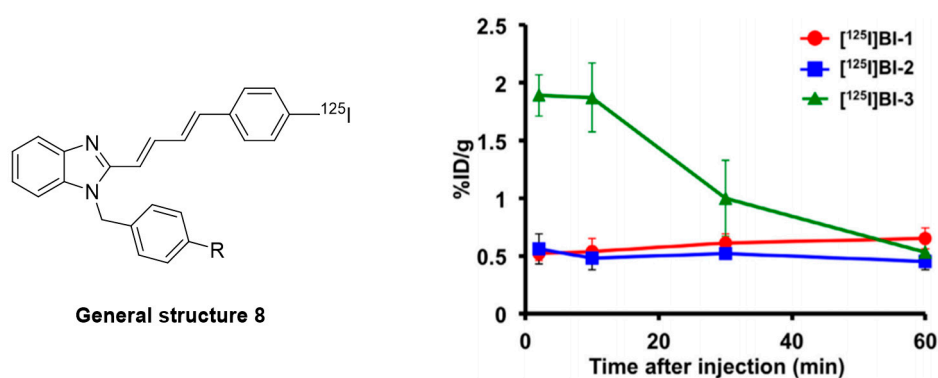
Figure 16. Chemical structures of thienopyridine, thiazolo pyridine derivatives with key properties. Chemical structures of compounds 28–34 and general structures with key binding properties. ^a Affinity toward α -syn fibrils aggregates determined by backscattering interferometry on PD brain homogenates. ^b Staining of α -syn aggregates on PD sections. ^c Staining of A β plaques on AD sections. ^d Staining of A β plaques on PD sections with mixed pathology. n.d.: not determined. Literature source [113].

3.5. Benzoimidazole Derivatives

3.5.1. Styryl Benzodiazole Derivatives

Styryl benzazole derivatives have been shown to interact with different amyloid fibrils [116]. This inspired Watanabe et al. to test if this structural class of compounds can be used to develop an α -syn selective compound [117,118]. Three novel probes were synthesized and subsequently labeled with iodine-125 (Figure 17). Watanabe et al. speculated that incorporation of dienes in the linker would enhance the affinity toward α -syn aggregates and that bulky substituents like benzyl groups might increase selectivity toward α -syn over A β aggregates. These considerations followed the theory developed by Chu et al. during the development of compound 15a [105]. Saturation binding assays based on fluorescence intensity measurements on recombinant α -syn and A β _{1–42} aggregates showed that the

developed probes possessed a K_d in the range of 99.5–874 nM. [^{125}I]BI-2 showed the best affinity and selectivity profile (K_d 99.5 ± 20.8 nM and 7-fold selective over $A\beta_{1-42}$). These results suggest that bulky substituents enhance affinity as well as selectivity. Consequently, BI-2 was studied further using fluorescent staining on PD and AD brain sections (at 200 μM). Stained sections were compared with immunohistochemistry and co-localization was observed in the case of α -syn positive tissue, but not for $A\beta$ positive tissue. These results encouraged the research to label two additional derivatives of BI-2 and evaluate the in vivo biological behavior of all three compounds. Only [^{125}I]BI-3 showed a moderate brain uptake of 2.0% ID/g at 10 min post injection and moderate clearance within 60 min resulting in 0.5% ID/g (Figure 17) [117]. Further improvements regarding affinity, selectivity and lipophilicity are needed to develop an α -syn selective ligand based on this scaffold.



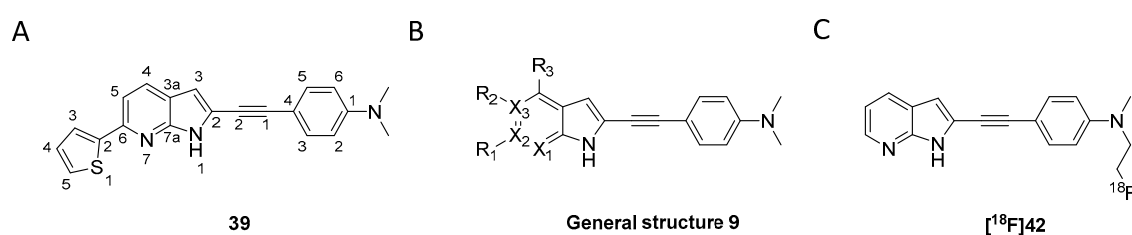
| General structure 8 | | | | | |
|--------------------------|--|-------------------|-----------------|---------|-------------------------|
| # | R_1 | K_i | | clogP * | cLogD _{7.4} ** |
| | | [nM] ^a | | | |
| | | α -Syn | $A\beta_{1-42}$ | | |
| [^{125}I]BI-1 | $\text{CH}_2\text{C}_6\text{H}_5$ | 485 ± 160 | 179 ± 59.1 | 6.28 | 7.12 |
| [^{125}I]BI-2 | p- $\text{CH}_2\text{C}_6\text{H}_4\text{OCH}_3$ | 99.5 ± 20.8 | 727 ± 227 | 6.23 | 7.04 |
| [^{125}I]BI-3 | CH_3 | 874 ± 169 | 271 ± 67.3 | 4.14 | 5.6 |

Figure 17. General structure of radio-iodinated benzoimidazole derivatives and their brain uptake after intravenous injection. Binding affinities were determined on recombinant α -syn and $A\beta_{1-42}$ aggregates. (Reprinted with permission from [117]. Copyright 2017 Elsevier). * clogP values were calculated by BioByte. ** clogD_{7.4} values calculated by ACD/Percepta.

3.5.2. Azaindole Derivatives

A recently published study by Routier et al. reported on a new set of compounds featuring an azaindole moiety and a phenyl ring linked via a triple bond. The process leading to the discovery of these structures was not discussed. Their binding affinity and selectivity were measured by ThT fluorescence assays using synthetic α -syn, $A\beta_{1-42}$, and tau fibrils. Of the nine tested compounds, compound 39 was the most promising ligand (Figure 18A), with a > 22-fold selectivity over $A\beta_{1-42}$ fibrils but only limited selectivity over tau fibrils. SAR studies conducted on the heteroaromatic substituents at the 5-, 6- and 7-position (35 vs. 36 vs. 37, Figure 18) of the indole scaffold revealed that the 7-azaindole structure (Figure 18A) resulted in the best selectivity profile. The influence of 2-thienyl, 3-thienyl, p-F-pyridyl, fluoride substitution on the 6-position were also studied (38 vs. 39 vs. 40 vs. 41, Figure 18). In particular, substitution with 2-thienyl gave the best affinity but also resulted in limited selectivity. The only compound radiolabeled and evaluated in vivo was [^{18}F]42 (Figure 18C). The in vivo study confirmed it to can cross the BBB despite its relatively high clogD [119]. Notwithstanding the limited amount of peer reviewed literature on this class of compounds, its structural similarities with C05-01 make it a lead compound for α -syn PET tracer development [114]. Although it is challenging

to draw solid conclusions from two different classes of compounds and without any knowledge on their binding profile, we are speculating that the triple bond linker and its induced planarity can enhance the binding of ligands to β -sheets. A similar hypothesis was drawn by Kaide and colleagues [120]. However, due to the structural similarity between different amyloids and their frequent colocalization, high planarity compounds will not be able to discriminate between abnormal aggregates; thus, leading to a moderate to low selectivity profile which is the case for azaindole derivatives. Interestingly, this compound class showed moderate selectivity over A β but no selectivity over tau. As such, further SAR studies, in vivo evaluation and ex vivo ARG on postmortem tissue are needed to conclusively determine if azaindole derivatives are promising scaffolds for the future development of α -syn selective ligands.



| General structure 9 | | | | | | | | | | | |
|---------------------|----------------|----------------|----------------|----------------|----------------|----------------|----------------------------------|---------------------------|------------|--------------------|------------------------------------|
| # | X ₁ | X ₂ | X ₃ | R ₁ | R ₂ | R ₃ | K _i [nM] ^a | | | cLogP [*] | cLogD _{7.4} ^{**} |
| | | | | | | | α -Syn | A β ₁₋₄₂ | tau | | |
| 35 | N | C | C | H | H | H | 0.53 ± 0.2 | 11.8 ± 3 | 0.44 ± 0.1 | 3.98 | 4.1 |
| 36 | C | N | C | H | H | H | 1.4 ± 1 | 5.2 ± 3 | 0.49 ± 0.2 | 3.98 | 3.5 |
| 37 | C | C | N | H | H | H | 1.0 ± 0.5 | 3.6 ± 2 | 2.4 ± 0.9 | 3.98 | 3.3 |
| 38 | N | C | C | F | H | H | 0.79 ± 0.4 | 16.8 ± 2 | n.d. | 4.61 | 4.0 |
| 39 | N | C | C | 2-thienyl | H | H | 0.49 ± 0.2 | 4.9 ± 0.6 | 1.67 ± 0.5 | 6.37 | 5.1 |
| 40 | N | C | C | 3-thienyl | H | H | 0.73 ± 0.3 | 4.27 ± 0.6 | n.d. | 6.16 | 5.0 |
| 41 | N | C | C | p-F-pyridyl | H | H | 1.27 ± 0.4 | 3.1 ± 1 | n.d. | 5.28 | 4.4 |
| 42 | - | - | - | - | - | - | 2.4 ± 1 | 1.2 ± 1 | 0.97 ± 0.4 | 4.63 | 4.1 |

Figure 18. Chemical structures of azaindole derivatives with key properties. (A) Chemical structure of compound 39. (B) General structure of azaindole derivatives with identified in vitro K_i and K_d binding properties [119]. (C) Chemical structure of [¹⁸F]42 that was used for in vivo study. * clogP values were calculated by BioByte. ** clogD_{7.4} values calculated by ACD/Percepta.

3.6. Diphenylpyrazole Derivatives

High-throughput screening of more than 20,000 compounds identified 3,5-diphenylpyrazole (DPP) as a promising small molecule scaffold to detect aggregated α -syn inclusions. DPP based compounds inhibited pathological aggregation of α -syn in vivo by binding to α -syn fibrils as demonstrated by fluorescence spectroscopy. The most promising drug candidate, **anle138b** (Figure 19A) was identified to be an oligomer modulator [121]. Interestingly, Wagner et al. demonstrated that **anle138b** binds only to pathological aggregates of prion protein and α -syn in vivo and not to natural monomers of α -syn [121]. In addition, DPP derivatives were shown to directly bind to α -syn fibrils in vitro [122]. Notably, **anle138b** may inhibit 77% of α -syn oligomer formation, which can be shown in several PD animal models. It also slowed down disease progression. **Anle138b** can be administered orally, crosses the BBB and does not show any significant toxicity after long-term therapeutic application. The intrinsic fluorescence of **anle138b** was used to study its binding properties against α -syn [122]. The fluorescence intensity of **anle138b** increased more than 30-fold after the addition of aggregated α -syn, but did not change after the addition

of monomeric α -syn. This change suggested a strong and specific structure-dependent binding of **anle138b**. A K_d of 190 ± 120 nM to aggregated α -syn was determined [122]. However, **anle138b** also inhibited the aggregation of other common protein aggregates involved in neurodegenerative diseases [121,123–127]. This selectivity challenge prompted the group to conduct a comprehensive study to increase affinity and selectivity. This led to the identification of **anle253b** [121]. In a competition assay with [^3H]**anle138b** using recombinant human α -syn fibrils, **anle253b** (Figure 19A) showed a high affinity for α -syn aggregates with an IC_{50} value of 1.6 nM. It also showed preferential binding to α -syn fibrils compared to other α -syn states such as monomers or oligomers. These promising results motivated the carbon-11 labeling of the structure [128]. [^{11}C]**anle253b** was synthesized with a high RCY (47%), but with a low A_m of 15.1 ± 3.4 GBq/ μmol at EOS. Further improvement of the molar activity is most likely needed to optimally image low-density targets such as α -syn aggregates. [^{11}C]**anle253b** was evaluated in healthy rats and showed complete excretion after 75 min from the whole animal and low brain uptake with atypical brain kinetics (Figure 19B). For the latter, the authors hypothesized that the high $\log P$ ($\text{clog}P = 5.61$ calculated by BioByte) could be the reason. No radiometabolites were detected using radio-HPLC [128]. Presently, no DPP derivatives have been evaluated on human pathological tissues for more accurate understanding of their affinity and selectivity. Recently, a new derivative within this compound class has been reported which has a lower lipophilicity, called **MODAG-001** ($\text{clog}P = 3.85$). **MODAG-001** displayed strong binding to α -syn fibrils ($K_d = 0.6 \pm 0.1$ nM), and a moderate affinity to tau ($K_d = 19 \pm 6.4$ nM) and $A\beta$ fibrils ($K_d = 20 \pm 10$ nM). **MODAG-001** could be isolated in 266 ± 113 MBq and with an A_m of 98.6 ± 24.7 GBq/ μmol . [^{11}C]**MODAG-001** (Figure 19C) showed excellent BBB permeability in mice and was able to visualize fibril-inoculations in rat striata using PET imaging. However, [^{11}C]**MODAG-001** was not able to detect aggregated α -syn in human brain sections from DLB patients. Future studies should be designed to reveal the reason for this behavior. Furthermore, no evidence for binding toward tau in AD and PSP brain tissues have been detected by ARG. Authors also questioned binding toward $A\beta$ studied in AD brain tissue, however, additional studies should be conducted [129]. Overall, this compound class is considered promising and may represent a lead compound for future SAR studies.

Furan-2-yl-1H-pyrazoles

Inspired by **anle138b** and in particular by the pyrazole ring interactions with the peptide backbone of α -syn (Figure 20), Ryan et al. proposed a novel class of compounds, namely furan-2-yl-1H-pyrazoles. ThT fluorescence and mass spectrometry (MS) binding assays were performed in order to characterize the inhibitory activity and to understand the binding interactions of this compound class with the protein. As a result, several new compounds were identified. Compound **43** (Figure 20) was identified as a lead pyrazole and compounds **44** and **45** (Figure 20) as lead pyrazolines for further development. These compounds showed the highest ability to inhibit α -syn aggregation. Further in vivo studies are needed to fully characterize them.

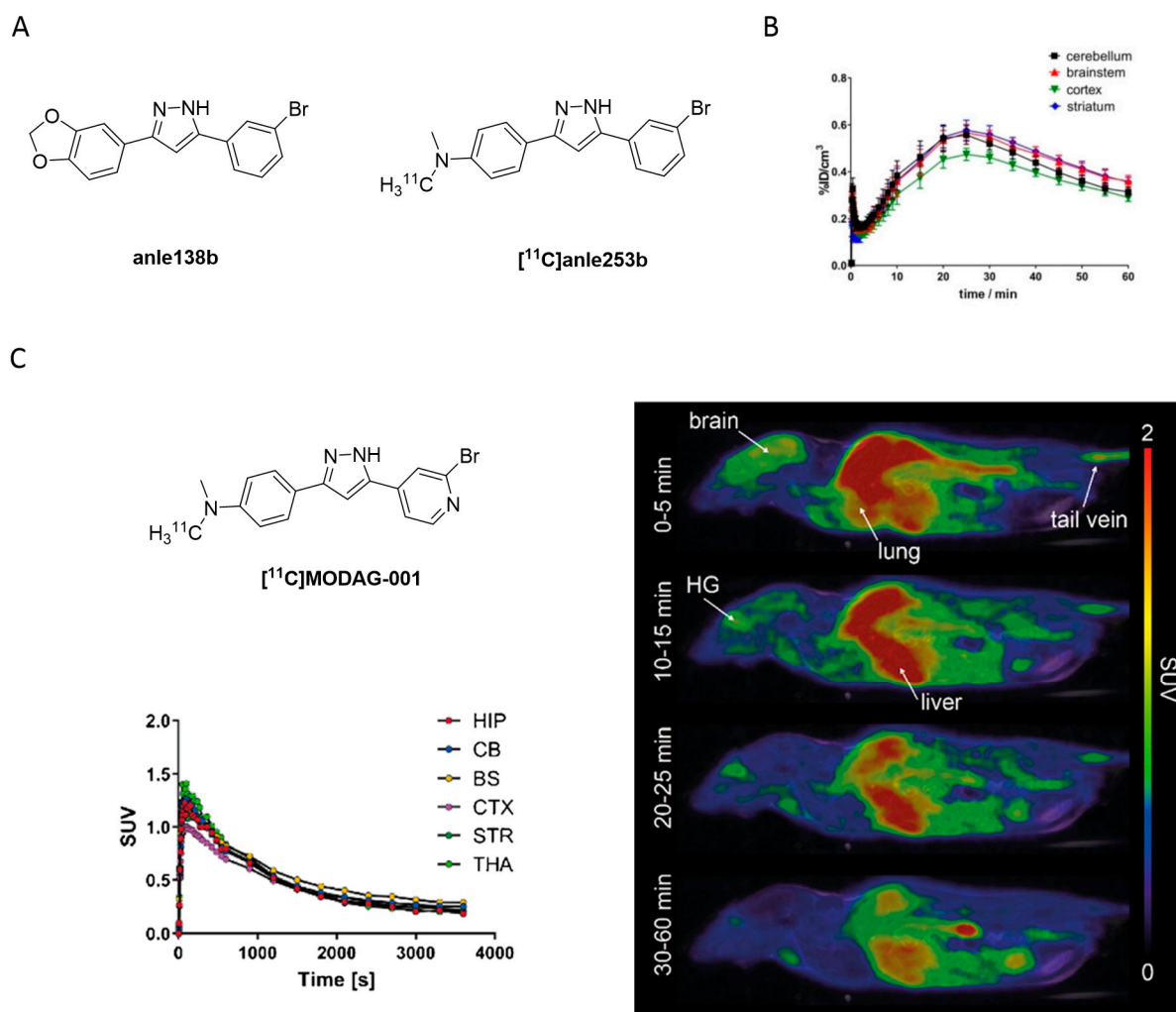


Figure 19. (A) Chemical structures of the 3,5-diphenylpyrazole derivatives **anle138b** and $[^{11}\text{C}]\text{anle253b}$. (B) TACs of the $[^{11}\text{C}]\text{anle253b}$ obtained from the in vivo study in healthy rats (Adapted from [128]). (C) Chemical structure of $[^{11}\text{C}]\text{MODAG-001}$ with TACs and PET images in mouse (Adapted from [129]).

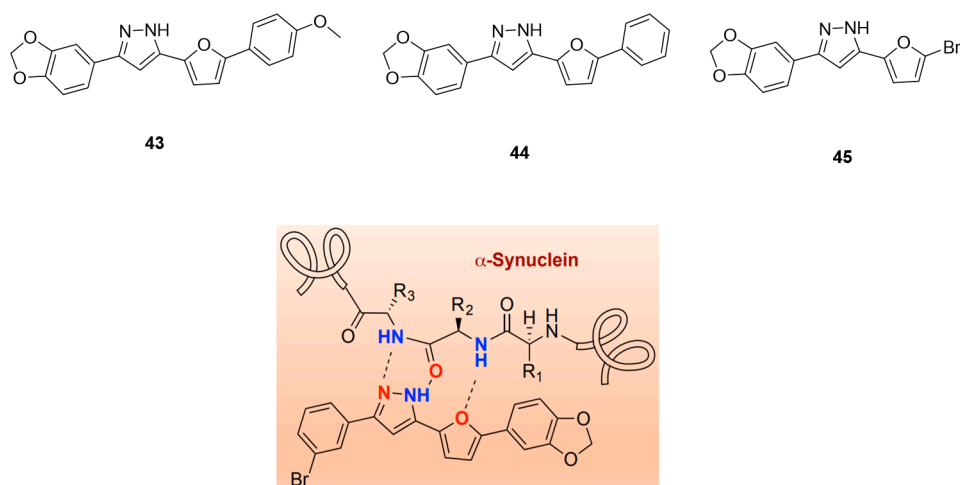


Figure 20. Chemical structures of furan-2-yl-1H-pyrazoles derivatives **43**, **44**, and **45** and proposed binding scheme of a peptide backbone with a furan-2-yl-1H-pyrazole with highlighted HBD and HBA features (reprinted with permission from [130]. Copyright 2020 American Chemical Society).

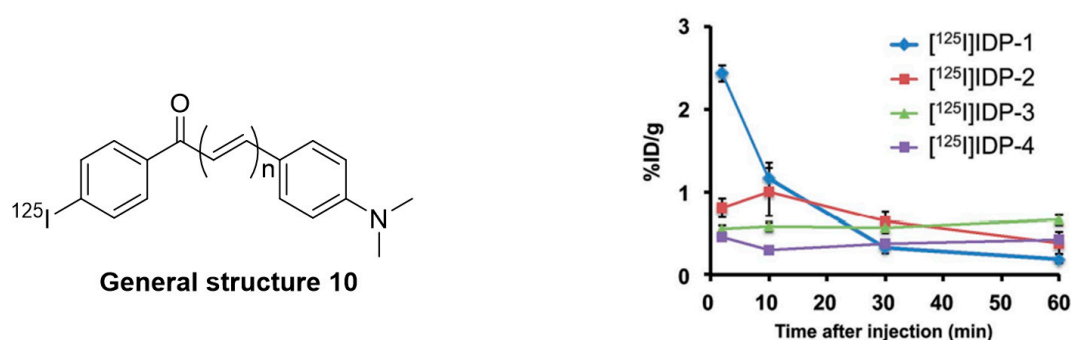
3.7. Chalcone Derivatives

3.7.1. Radioiodinated Diphenyl Derivatives

Chalcone derivatives were originally developed to inhibit the formation of A β aggregates [131]. Four chalcone derivatives (Figure 21) were radiolabeled with iodine-125 ($A_m = 81.4$ GBq/ μmol , RCY range = 19–60%) and subsequently evaluated for their selectivity profile toward α -syn fibrils [132]. Affinities on recombinant α -syn fibrils in the range of 5.4–217 nM were reported, as well as moderate selectivity over recombinant A β fibrils (0.2–3.0-fold). [^{125}I]IDP-4 showed the most promising affinity and selectivity profile with a K_d of 5.4 ± 1.5 nM for α -syn and 3-fold selectivity over A β . Fluorescent and immunohistochemical staining on human brain slices showed that IDP-4 (at 20 μM) was able to visualize α -syn and LBs. IDP-3 and IDP-4 displayed a similar binding pattern. In contrast, IDP-1 and IDP-2 did not show specific α -syn binding on post-mortem brain samples from PD patients. All compounds were evaluated in vivo. [^{125}I]IDP-1 had an initially high brain uptake (2.43% ID/g), while all other derivatives displayed low brain uptake (range 0.45–0.81% ID/g) at 2 min p.i. as exemplified in Figure 21. The reason for the relatively low brain uptake of [^{125}I]IDP-4 is unknown but may be attributed to its high molecular weight [132]. Further improvement with respect to selectivity and affinity are most likely needed to selectively image α -syn depositions.

3.7.2. Chalcone and Five-Membered Heterocyclic Isosteres

Hsieh et al. attempted to diversify the structure of the chalcone core by substituting the phenyl group of the “benzoyl moiety” with a 2-benzothiazolyl and a 2-thiazolyl group (compounds 46, 47, Figure 22) in the development of an α -syn PET tracer. Surprisingly, the five-membered heterocyclic isosteres conferred much higher α -syn selectivity than the benz-fused aromatic constituent. Substitution of the “styrene moiety” at 4-position had a major influence on the affinity and selectivity profile of the compound [133]. Methoxy substitution resulted in the highest affinity and selectivity for α -syn, and further SAR studies were centered around this key structure. For example, replacement of the enone moiety with an isoxazole (48, Figure 22) or a pyrazole structure (50, Figure 22) was investigated. Both of these derivatives were further modified via extension with a styrene moiety which was substituted with a methoxy group at 4-position. A ThT competition binding assay performed with these compounds revealed that the isoxazole and pyrazole derivatives with a double bond (compounds 49, 51 in Figure 22) bind with higher affinity to α -syn fibrils compared to their analogues without the double bond linker. They also displayed a higher affinity for A β fibrils, whereas the affinity toward tau fibrils were not altered [133]. Subsequently, a molecular-modeling approach was conducted to study which properties influenced the binding of these structure toward α -syn, A β or tau fibrils. 3D geometric characteristics such as the shape of the molecule (linearity and flatness), topological diameters or intramolecular distance between hydrogen bond receptors were calculated for various structures. Interestingly, the order of binding affinity ($49b > 47 > 48$) correlated to the order of distance between the isoxazole oxygen and the methoxy group ($9.98 > 8.44 > 7.72$ Å). Moreover, it appeared that compounds with higher degrees of flatness and linearity such as isoxazole and pyrazole analogues showed increased affinity for α -syn [133]. Finally, compounds 49b and 51 displayed a preference for BS2 as indicated by molecular docking [43]. In general, the presented structures display good affinity and selectivity over amyloid fibrils. For example, the two isoxazole derivatives 49a and 49b showed a ~ 50 fold selectivity over tau fibrils and moderate affinity (18.5 ± 9.2 nM) toward α -syn fibrils. Presently, none of these compounds have been radiolabeled and evaluated on human brain tissue or in in vivo animal models. More comprehensive studies on this family of compounds should be conducted.

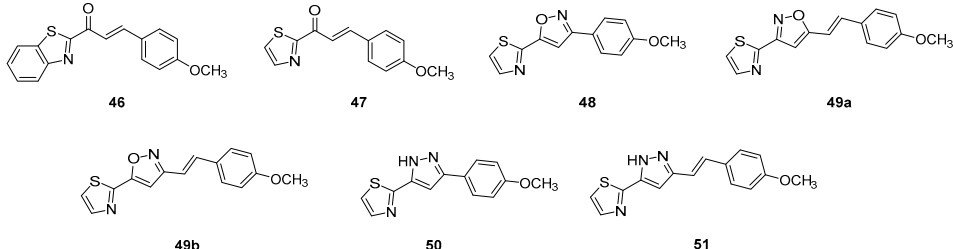


| General structure 10 | | | | | |
|--------------------------|---|-------------------|---------------|---------|-------------------------|
| # | n | K _i | | clogP * | cLogD _{7.4} ** |
| | | [nM] ^a | | | |
| | | α-Syn | Aβ | | |
| [¹²⁵ I]IDP-1 | 1 | n.d. | 12.88 ± 2.02 | 4.45 | 4.8 |
| [¹²⁵ I]IDP-2 | 2 | 217.87 ± 73.87 | 37.14 ± 10.80 | 4.9 | 4.5 |
| [¹²⁵ I]IDP-3 | 3 | 23.28 ± 2.78 | 13.35 ± 5.67 | 5.51 | 5.0 |
| [¹²⁵ I]IDP-4 | 4 | 5.40 ± 1.50 | 16.24 ± 4.78 | 5.51 | 5.5 |

Figure 21. Chemical structure of radioiodinated diphenyl derivatives and brain uptake of radioactivity after intravenous injection. Binding affinity values are determined for recombinant α -syn and A β fibrils. Reprinted with permission from Ono et al. [132]. Copyright 2016 Royal Society of Chemistry. * clogP values were calculated by BioByte. ** clogD_{7.4} values calculated by ACD/Percepta.

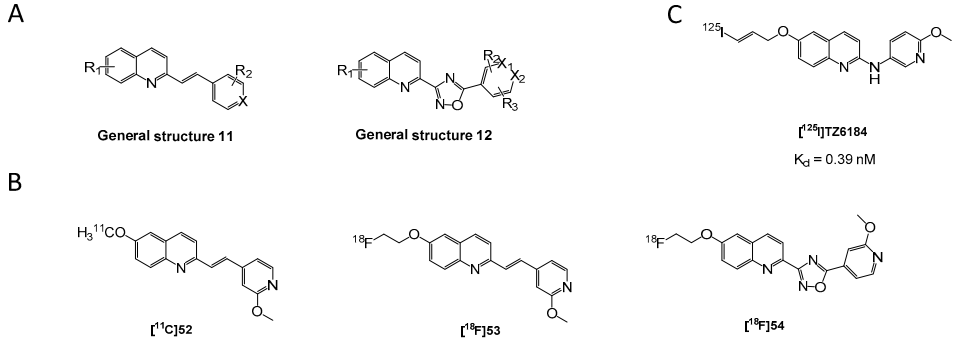
3.8. Quinolinyl Analogues

Several compounds containing a quinolinyl moiety and six-membered aromatic rings linked either by a double bond or an oxadiazole bridge were designed by Yue et al. for α -syn imaging [134]. A rational design approach was applied based on previous findings combining key features of the compounds LDS 798 and 2,6-ANS (Figure 5). In particular, the incorporation of double bonds into the side chain, the addition of heteroatoms on both aromatic rings, the use of secondary amines or oxadiazole fragments to bridge both aromatic rings were explored (Figure 23A). As a result, 25 new quinolinyl analogs were synthesized and tested in vitro. Only three derivatives displayed K_i values < 52 nM. Affinity measurements were conducted using a ThT competitive binding fluorescence assay with recombinant α -syn fibrils. Despite these moderate affinities, all three compounds (52, 53, 54) were radiolabeled with carbon-11 or fluorine-18 (Figure 23B). Using recombinant α -syn fibrils and brain AD tissue homogenates, the affinity of these compounds was determined to be 21, 79, 18 nM for [¹¹C]52, [¹⁸F]53, [¹⁸F]54, respectively. Affinity toward A β fibrils was determined to be in the same order of magnitude [134]. These binding characteristics discouraged the authors from further evaluating the compounds in vivo. Recently, another quinolinyl analogue [¹²⁵I]TZ6184 (Figure 23C) has been reported with limited information. In vitro characterization of this radiotracer on recombinant α -syn fibrils showed that it possesses an extremely good K_d of 0.39 nM [135]. However, no selectivity profile has been reported and thereby no thorough conclusions can be made.



| # | K _i [nM] | | | clogP * | cLogD _{7.4} ** |
|-------|---------------------|--------------------|--------------|---------|-------------------------|
| | α-Syn | Aβ ₁₋₄₂ | Tau | | |
| 46 | 530.5 ± 64.3 | 353.0 ± 29.7 | 716.5 ± 58.7 | 3.72 | 3.7 |
| 47 | 53.0 ± 19.8 | > 500 | >1000 | 2.13 | 2.7 |
| 48 | 133.5 ± 78.5 | > 1000 | >1000 | 3.03 | 2.5 |
| 49a,b | 18.5 ± 9.2 | 91.5 ± 58.7 | >1000 | 3.4 | 2.9 |
| 50 | 162.5 ± 41.7 | >1000 | >1000 | 3.16 | 2.6 |
| 51 | 59.0 ± 11.3 | 327.0 ± 76.4 | >1000 | 3.54 | 3.0 |

Figure 22. Chemical structures of chalcone derivatives and their affinity values expressed as K_i values toward α-syn, Aβ and tau fibrils [133]. * clogP values were calculated by BioByte. ** clogD_{7.4} values calculated by ACD/Percepta.



| # | K _i [nM] | | K _d [nM] | clogP * | cLogD _{7.4} ** |
|----------------------|---------------------|--------------------|--|---------|-------------------------|
| | α-syn ^a | α-syn ^b | Human AD tissue homogenates ^c | | |
| [¹¹ C]52 | 52 ± 21 | 21 | 13 | 4.20 | 3.4 |
| [¹⁸ F]53 | 18 ± 1 | 79 | 55 | 4.45 | 3.5 |
| [¹⁸ F]54 | 15 ± 3 | 18 | 25 | 3.78 | 3.8 |

(C) [125I]TZ6184
K_d = 0.39 nM

Figure 23. Chemical structures of new quinolinyl analogs. (A) General structures 11 and 12 of quinolinyl analogs. (B) Chemical structures of new radiolabeled quinolinyl analogs [¹¹C]52, [¹⁸F]53 and [¹⁸F]54. ^a Binding affinities expressed as K_i values determined by ThT indirect competitive binding using recombinant α-syn fibrils. ^b Binding affinities expressed as K_d values and determined by direct radioligand competitive binding using recombinant α-syn fibrils. ^c Binding affinities expressed as K_d values and determined by direct radioligand competitive binding assay on tissue homogenates from AD patients [134]. * clogP values were calculated by BioByte. ** clogD_{7.4} values calculated by ACD/Percepta. (C) Chemical structure of [¹²⁵I]TZ6184 with binding affinity K_d = 0.39 nM [135].

3.9. N-Substituted Phenyl Amides

3.9.1. N-Phenylbenzamide Analogues

In a series of over 170 compounds, a new class of α-syn binders was identified by Borroni and colleagues [136]. The initial idea about the molecular design of these N-phenylbenzamide derivatives is not disclosed in the patent where these molecules are presented. The binding profile of [³H]55 (Figure 24A) was studied by ARG on A30P transgenic mouse and human PD brain sections, and the results encouraged the authors to use this compound for displacement studies for a set of other N-phenylbenzamides.

Results are expressed as % displacement. Six compounds (56–61) were identified as high affinity ligands with a displacement of >87% (in A30P mice, at 1 μ M), which were tritiated to evaluate their binding profile in ex vivo ARG in A30P mice. High brain accumulation as well as good target engagement in the midbrain, pons and subthalamic brain regions was detected. No significant off-target binding was reported. The selectivity of all tritiated compounds was assessed with an in vitro displacement assay using A β AD human brain tissue. The experiments showed that all compounds also bind to A β (Figure 24B). As such, further structure activity studies are needed to increase the selectivity of these compounds to α -syn [136]. Finally, their binding interactions with α -syn was studied using molecular docking techniques, suggesting that the compounds bind preferentially within BS 9 [43].

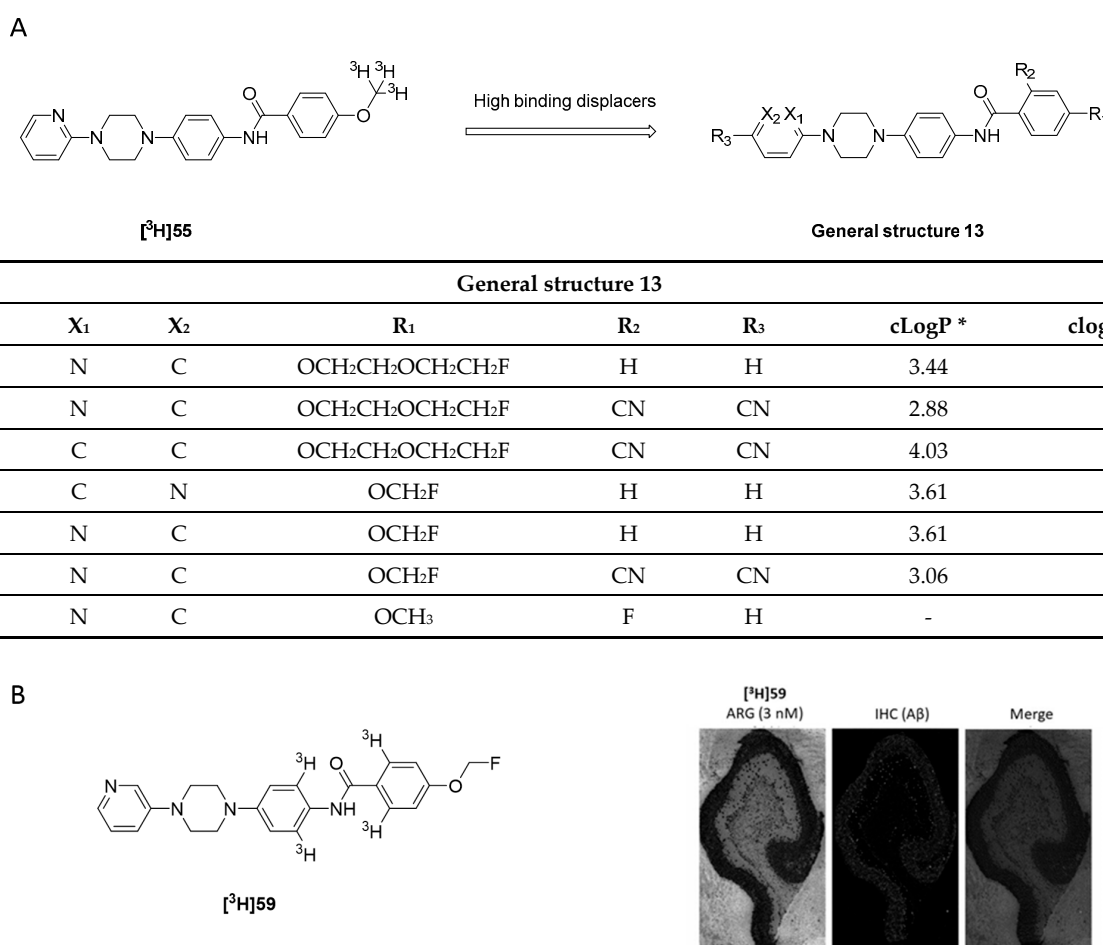


Figure 24. Chemical structures of *N*-phenylbenzamide analogues. **(A)** General structure of *N*-phenylbenzamide analogues (general structure 13) that showed to be high affinity displacers and chemical structure of [³H]55. Key properties are summarized in table below [136]. **(B)** Chemical structure of [³H]59 and its binding to human AD brain tissue (cortical tissue) and comparison with staining of anti-A β mAb (adapted from Borroni et al. [136]). * clogP values were calculated by BioByte. ** clogD_{7.4} values calculated by ACD/Percepta.

3.9.2. *N*-Substituted Phenyl Amides Analogues

Several *N*-substituted phenyl amide derivatives bearing phenothiazine, phenoxazines, quinolinyl, and styryl pyridinyl substituents were also reported to be potential α -syn binders [94]. Moderate binding affinity with K_i values < 100 nM were determined by a ThT competitive assay on α -syn fibrils. *N*-substituted phenyl amides appeared to be most promising (Figure 25) and were studied further. Substitution at the 4-position of the phenyl moiety showed that the binding affinity is reduced in the sequence: Br > OMe > I > OEtF. Compound 63 (Figure 25) showed the highest affinity (ca. 10 nM). No further studies concerning selectivity or in vivo evaluation have been reported up till now [94]. In a

different study, Xu et al. used automated MS as a technique to quickly detect the direct interaction between molecules and proteins. Using this method 2500 compounds were screened for α -binding and resulted in one hit: compound **64** (Figure 25) Furthermore, the increase of fluorescence during aggregation process was evaluated during the ThT assay, showing that compound **64** was able to strongly inhibit α -syn aggregation by 91% [137]. Currently, there are no known PET tracers developed from compound **64** and no binding affinity or selectivity profile are known. Thus, additional studies are needed.

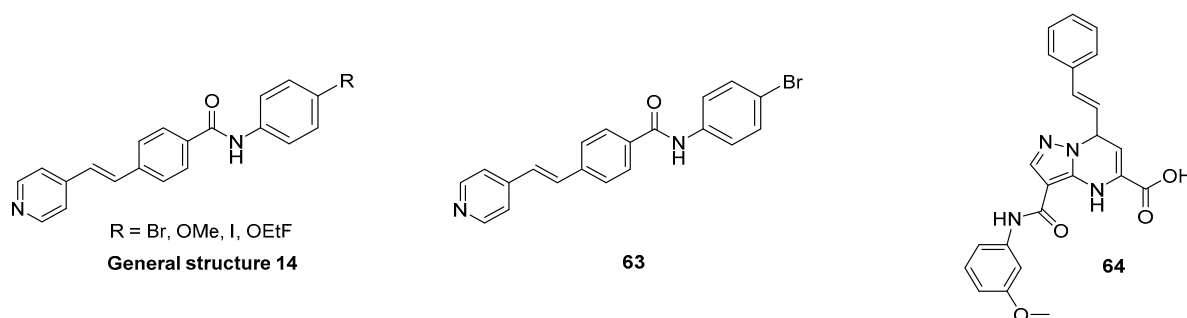


Figure 25. Chemical structures of *N*-substituted phenyl amide analogues. From left to right: general structure 14 of *N*-substituted phenyl amide analogues. Chemical structure of compounds **63** and **64**.

3.9.3. 2-Phenoxy-*N*-(3-phenylisoxazol-5-yl)acetamide Analogues

An exemplar-based in silico screening campaign was used to identify potential ligands for α -syn. An exemplar is defined as an ideal pseudoligand that would optimally fit in the protein surface pocket; therefore, it is exploited as a template for pharmacophore screening [138]. An in silico assay was designed to highlight compounds that bind to two previously identified binding sites—BS2 and BS9—within the α -syn fibrils (2n0a, Figure 2C). Approximately 10 million molecules from the ZINC15 database were screened and led to the identification of 17 chemically diverse potential α -syn binders. Compounds **65** and **66** (Figure 26A,B) were of special interest since they were able to displace [3 H]Tg-190b—a selective ligand for binding site BS2 (Figure 26A)—from α -syn fibrils. Inhibitory concentrations, IC₅₀ values, were 490 nM and 9.49 nM for **65** and **66**, respectively. Compound **66** was used as a lead and the molecule was deconstructed to identify the essential features needed for binding to α -syn. The new resulting scaffold was compound **67**—a 2-phenoxy-*N*-(3-phenylisoxazol-5-yl)acetamide. This template was then used to find structurally similar compounds from the Molecule Library. 39 promising structures were discovered using this approach. All compounds were tested using the aforementioned competition binding assay with [3 H]Tg-190b and [3 H]BF2846 (Figure 26B). More important SAR were obtained when different heterocycles were introduced to the core structure within rings A, B or C (Figure 26B). For example, replacement of the A ring with a pyridine (**68**), furan (**69**) or thiophene (**70**) group did not improve binding. However, we were not able to draw these conclusions since the identical compounds with phenyl moiety as the A ring, for compounds **69** and **70**, were not presented in the publication. Conversely, *para* substitution on the A ring improved binding toward α -syn fibrils in many cases (see for example **76** vs. **66**). Also, the electronic nature of ring A showed to be essential. In particular, a bromo substituted version (**73**) showed to have a higher affinity than **71**, when a methoxy group is present on ring C. Also, comparing compounds **72** and **66** revealed that a bromo substituent has a significant effect on binding affinity. Moreover, the authors studied the influence of additional fluoro substituents (**75**) which showed to have a positive effect on affinity (**75** vs. **76**).

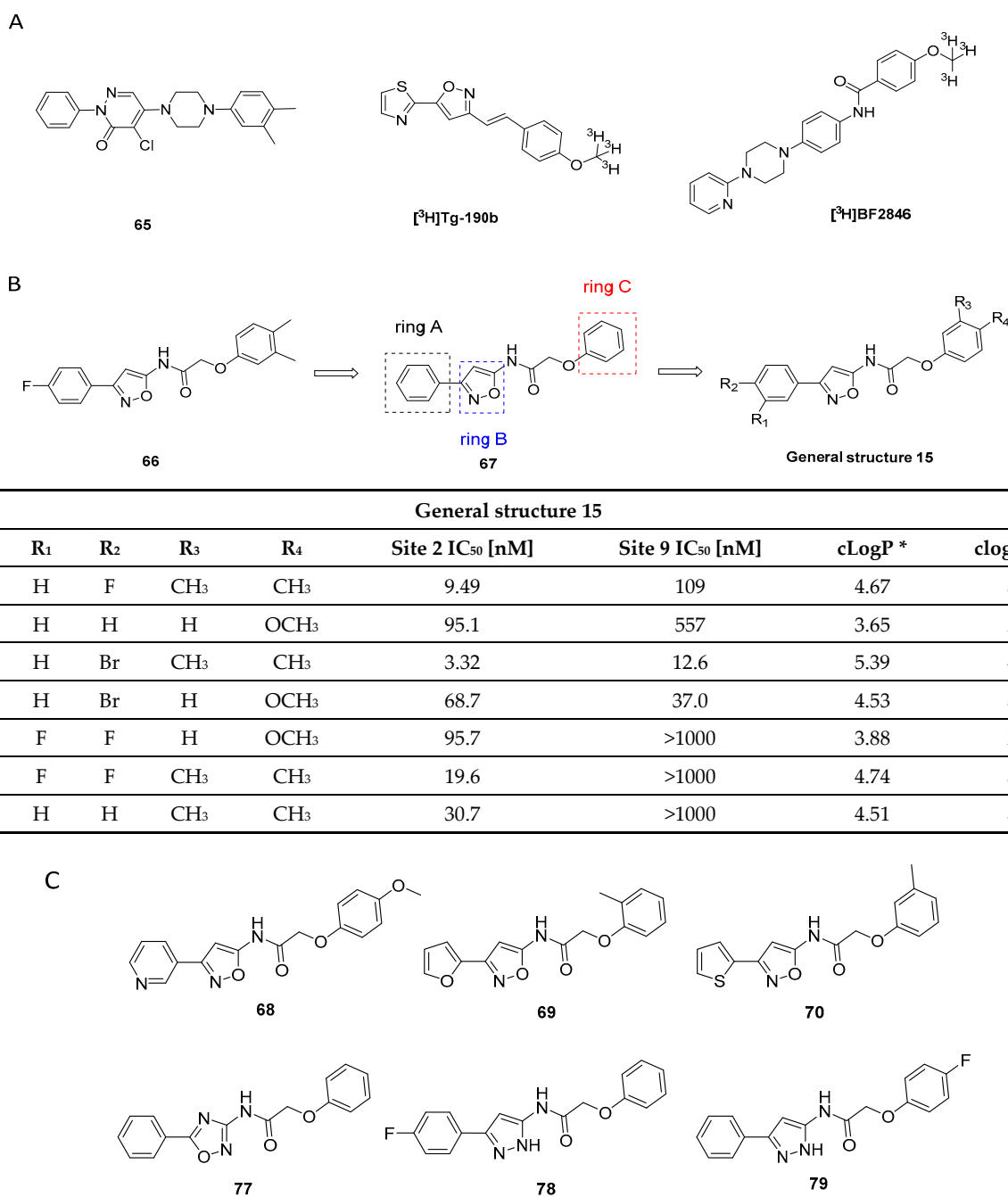


Figure 26. Cont.

General structure 15

| # | R ₁ | R ₂ | R ₃ | R ₄ | Site 2 IC ₅₀ [nM] | Site 9 IC ₅₀ [nM] | cLogP * | clogD _{7.4} ** |
|----|----------------|----------------|-----------------|------------------|------------------------------|------------------------------|---------|-------------------------|
| 66 | H | F | CH ₃ | CH ₃ | 9.49 | 109 | 4.67 | 3.5 |
| 71 | H | H | H | OCH ₃ | 95.1 | 557 | 3.65 | 2.8 |
| 72 | H | Br | CH ₃ | CH ₃ | 3.32 | 12.6 | 5.39 | 4.4 |
| 73 | H | Br | H | OCH ₃ | 68.7 | 37.0 | 4.53 | 3.5 |
| 74 | F | F | H | OCH ₃ | 95.7 | >1000 | 3.88 | 2.4 |
| 75 | F | F | CH ₃ | CH ₃ | 19.6 | >1000 | 4.74 | 3.5 |
| 76 | H | H | CH ₃ | CH ₃ | 30.7 | >1000 | 4.51 | 3.7 |

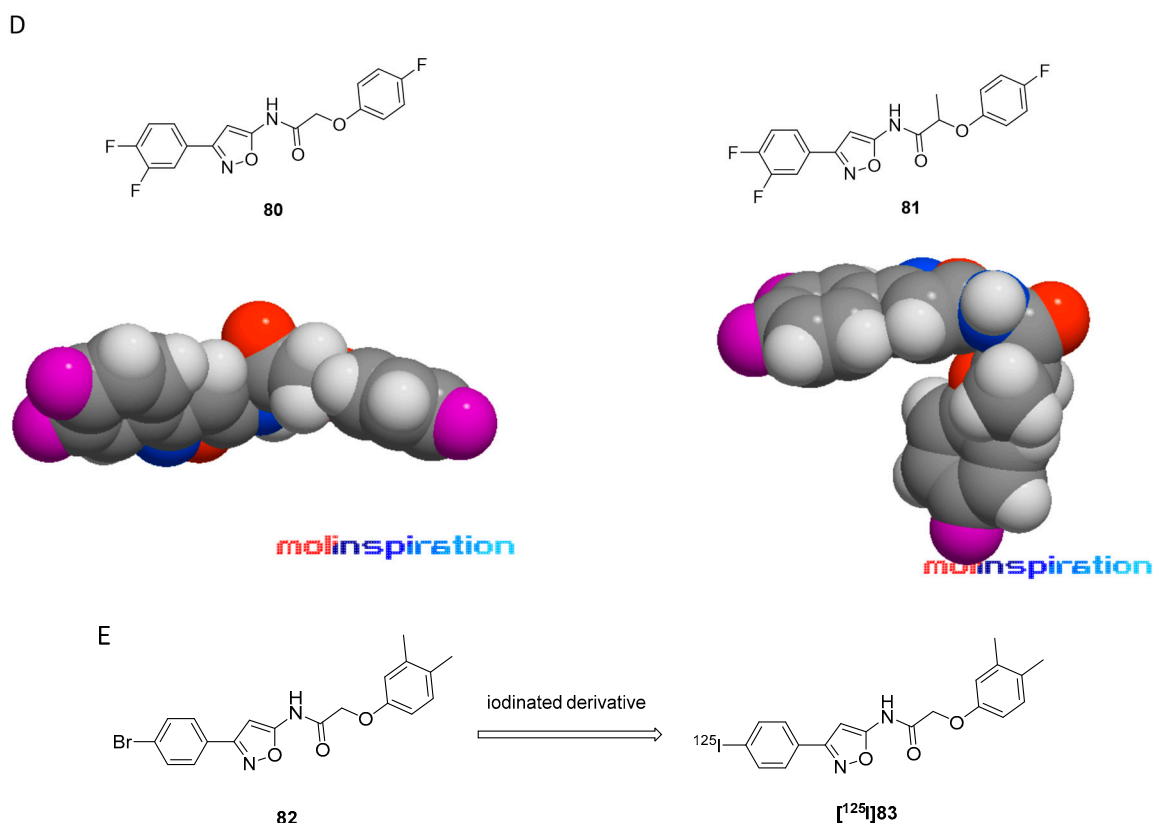


Figure 26. Chemical structures of 2-phenoxy-*N*-(3-phenylisoxazol-5-yl)acetamide analogues. (A) Chemical structure of compounds 65, [³H]Tg-190b and [³H]BF2846. (B) Chemical structure of compounds 66, 67 and general structure of most potent α -syn binders. Table represents IC₅₀ values screened for BS2 and BS9 using [³H]Tg-190b and [³H]BF2846 [139]. * clogP values were calculated by BioByte. ** clogD_{7.4} values calculated by ACD/Percepta. (C) Chemical structures of compounds 68–70, 77–79 (D) Models of likely 3D structures of compounds 80 and 81 (visualized by Molinspiration Galaxys 3D Structure Generator v2018.01 beta). Methyl substituent of compound 81 generates non-planar structure in comparison with compound 80. (E) Chemical structure of compound 82 and [¹²⁵I]83.

Replacement of the B ring with an oxadiazole heterocycle lowered the affinity. All compounds possessing an oxadiazole (for example 77) showed no displacement of [³H]Tg-190b (Figure 26C), no matter the substituents on rings A or C. In contrast, replacement of B with a pyrazole only increased the affinity moderately (compounds 78 and 79 (Figure 26C). In addition, from the comparison of heterocyclic differentiations in the B ring we cannot conclude which of the heterocyclic rings had the best influence on affinity. Substitution on the C ring revealed the following: *ortho* substituents decrease binding, while *meta* and *para* substituents improve binding. In addition, the electronic nature of the C ring for *para* substituents is essential. Since *para* substituents and in particular fluoro substituents show decreased binding, while moderate to strong binding is demonstrated by derivatives bearing electron donating groups such as methyl and methoxy groups. As a general trend, non-planar compounds showed weaker binding than the planar compounds exemplified in Figure 26D (80 and 81) [121,139]. Similar observations were previously drawn for other structural classes. The most promising compound identified in this study was 82 (Figure 26E). It displayed an IC₅₀ of 3.32 nM and of 12.6 nM for BS2 and BS9, respectively. The iodinated derivative 83 (Figure 26E) was selected for labeling with iodine-125. Binding experiments with [¹²⁵I]83 (RCY = 57%, A_m = 81 GBq/μmol) on α -syn fibrils demonstrated excellent binding (K_d = 1.06 nM), but only moderate selectivity over A β _{1–42} fibrils (4-fold, K_d = 4.56 nM). Binding to other proteins in mouse brain lysate was found to be high. In vitro ARG was performed using brain tissue from A53T PD mice (15 months old). Images confirmed binding of [¹²⁵I]83 to α -syn rich brain regions [139]. Further efforts are

needed to decrease unspecific protein binding and increase selectivity. Additional data for human tissue are highly needed to further develop this class of molecules.

3.10. Flavonoids

Flavonoids act as scavenger for free radicals, lowering as such oxidative stress, which has been shown to be relevant in PD pathogenesis due to generation of species such as free radicals and superoxide. For this reason, several flavonoids were assessed for their ability to inhibit α -syn fibrillation in vitro [140]. The assay, based on ThT fluorescence, showed that several of these compounds can inhibit α -syn fibrillation (Figure 27) [140]. Complete α -syn fibrillation inhibition was obtained using 50 μ M of compounds **6-HP** and **Baicalein** (Figure 27). Furthermore, significant inhibition was also detected for 7 additional flavonoids: **Eriodictoyl**, **22-324**, **myricetin**, **EGCG**, **T-415**, **22-340/tricetin**, and **22-341** (Figure 27). The flavonoids have not yet been tested in vivo for their ability to image α -syn fibrils. Hence, more comprehensive studies should be conducted [141].

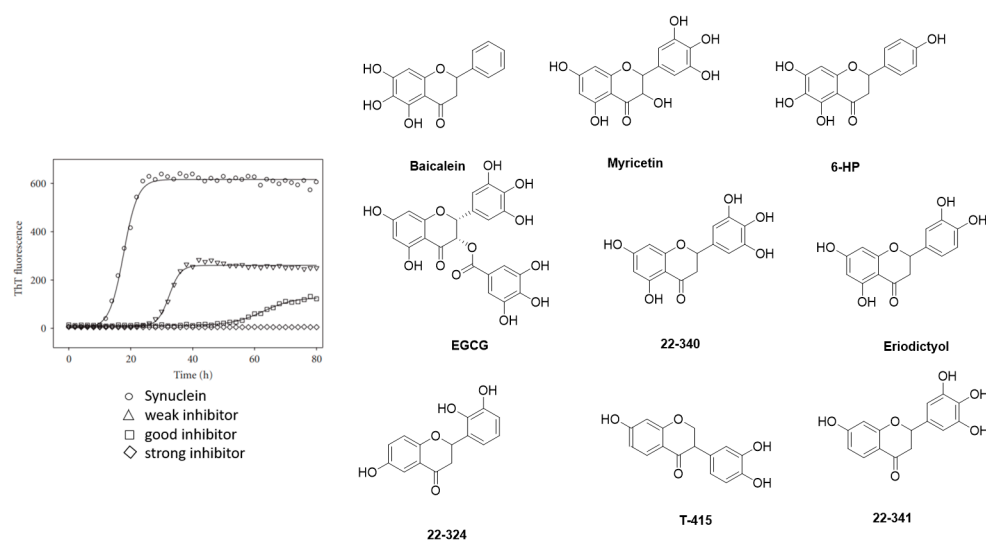


Figure 27. Kinetic profiles of the fibril formation (adapted from Meng et al. [140]) and chemical structures of α -syn fibrillation inhibiting flavonoids.

3.11. Bicyclic Sulfur-Containing 2-Pyridone Analogues

FN075 was initially studied as an antibiotic (Figure 28) as it has been shown to inhibit the formation of bacterial amyloid fibers. Interestingly, and contrary to its behavior in bacteria, **FN075** was also identified as a potent α -syn fibril promoter [142]. Prompted by these results, a limited SAR study on **FN075** was conducted. Derivatives altered the lag time of α -syn aggregation in several animal models. Unfortunately, no affinity studies were conducted making it difficult to rationalize the data obtained [143–145]. However, the carboxylic acid moiety appeared to be an important feature for the activity since the corresponding esters lost their ability to influence the α -syn fibril formation [142]. In 2018, Cairns et al. developed a first PET tracer based on **FN075**. In order to increase the brain accumulation, they exploited a prodrug approach, masking the carboxylic acid as an acetoxymethyl ester, which was designed to be unstable in vivo and release **FN075** within the brain [143,146]. The authors reasoned that the carboxylic acid moiety disabled the compound's ability to enter the brain as it becomes deprotonated at physiological pH. A methoxy derivative was also synthesized and evaluated as possible candidate for radiolabeling. In vitro α -syn fibrillization was also triggered by this methoxy analogue **84**, while the acetoxymethyl analogue was inactive. This promising result prompted the group to radiolabel the compound. They reported an $A_m = > 37$ GBq/ μ mol, an RCP of $>97\%$, but no RCY. [11 C]**84** (Figure 28A) as well as its protected derivative [11 C]**85** (Figure 28A) were evaluated in vivo in healthy NHP by dynamic PET imaging (Figure 28B). [11 C]**85** was able to cross the BBB, showing a slow washed out whereas [11 C]**84** did not enter the brain

(Figure 28B). The authors speculated that [^{11}C]85 was hydrolyzed within the brain however this needs to be proved conclusively [146]. Further studies are needed to determine the potential of FN075 analogues as possible agents for the imaging of α -syn fibrillization. In particular, affinity and selectivity measurements should be conducted.

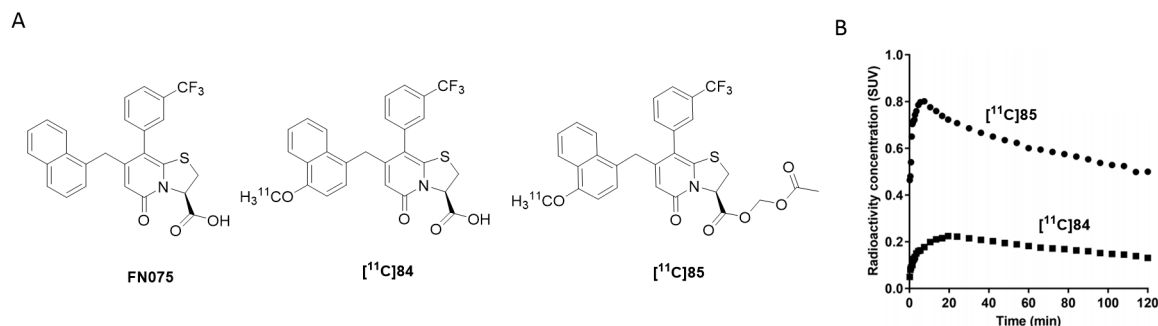


Figure 28. The chemical structures of FN075 and its analogues. (A) The chemical structures of FN075 and radiolabeled acetoxymethyl ester [^{11}C]84 and [^{11}C]85. (B) TACs in the whole brain derived from healthy NHP following the IV injection of [^{11}C]84 and [^{11}C]85 (reprinted with permission from [146]. Copyright 2018 American Chemical Society).

Next, Singh et al. synthesized several structural analogues around a tricyclic skeleton (general structure 16, Figure 29) [147]. ThT displacement assays (expressed as relative fluorescence %) on α -syn and $\text{A}\beta_{1-40}$ fibrils indicated that p-nitrophenyl derivatives (**86b**, **f**, **o**, **p**, **87a**, **i**, **k–o**) displayed affinity toward both fibril types. Other electron-withdrawing groups such as 4-trifluoromethyl and 4-cyanophenyl did not achieve comparable binding results.



General structure 16

| General structure 16 | | |
|----------------------|-----------------|-------------------------|
| # | R | R ₁ |
| 86b | cyclopropyl | Ph |
| 86f | Ph | cyclopropyl |
| 86o | H | Ph |
| 86p | cyclopropyl | 3-trifluoromethylphenyl |
| 87a | cyclopropyl | H |
| 87i | Ph | H |
| 87k | H | H |
| 87l | 3-hydroxyphenyl | H |
| 87m | 3-methylphenyl | H |
| 87n | 3-acetylphenyl | H |
| 87o | 3-thienyl | H |

Figure 29. Chemical structures of novel pyridine-fused 2-pyridones (**86b**, **f**, **o**, **p**, **87a**, **i**, **k–o**).

A non-pyridine-based fused-peptidomimetic scaffold was also synthesized (**88**, Figure 30), but did not show any significant binding toward α -syn fibrils. This indicates that a pyridine-fused tricyclic backbone in this class of compounds is critical for α -syn fibril binding [147].

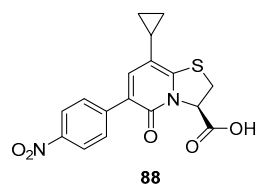
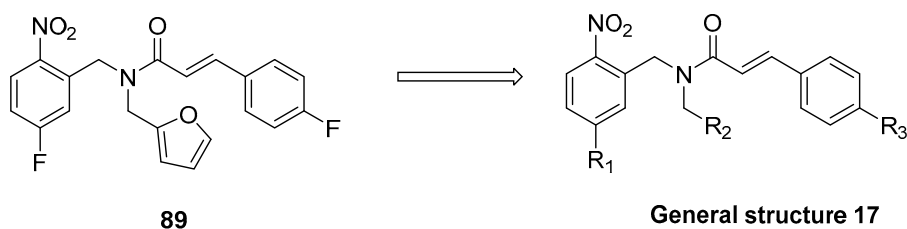


Figure 30. Chemical structure of compound **88**.

3.12. *N,N*-Dibenzylcinnamamide Derivatives

A recently published study by Chen et al. utilized Surface Plasmon Resonance (SPR) screening to identify *N,N*-dibenzylcinnamamide (DBC) derivatives as high affinity α -syn binders [148]. Among 39 compounds, one hit compound was identified with an adequate K_d of 8.21 nM (**89**, Figure 31). Based on these results, eight novel DBC analogues were designed, synthesized, and evaluated against α -syn fibrils. Two compounds (**91** and **93**) showed good binding affinities with K_d values of 1.03 nM and 10.90 nM, respectively. These affinity data lead to three hypotheses. Firstly, fluorine as R_1 substituent appeared to have an essential role for α -syn binding. For example, compound **91** showed significantly better affinity than compound **97**. Secondly, furan-2-yl as the R_2 substituent increased the affinity substantially in comparison to either phenyl or 2-CH₃O-phenyl substituents. Thirdly, fluorine as the R_3 substituent drastically increased binding affinity in comparison to a cyano group [148]. No further evaluation studies have been reported thus far for this compound class, including selectivity and affinity data from post-mortem PD brain tissue on PD. However, this compounds class nonetheless warrants further investigation.



| General structure 17 | | | | | | |
|----------------------|----------------|------------------------|----------------|------------------------|---------|-------------------------|
| # | R ₁ | R ₂ | R ₃ | K _d [nM] | cLogP * | clogD _{7.4} ** |
| 90 | F | Ph | CN | 484.6 | 4.16 | 3.9 |
| 91 | F | furan-2-yl | F | 1.03 | 4.04 | 3.5 |
| 92 | F | furan-2-yl | CN | n.d. | 3.33 | 3.2 |
| 93 | F | Ph | F | 10.90 | 4.87 | 4.1 |
| 94 | H | Ph | F | 47.34 | 4.72 | 4.2 |
| 95 | F | 2-CH ₃ O-Ph | CN | n.d. | 4.07 | 3.7 |
| 96 | F | 2-CH ₃ O-Ph | F | 331.7 | 4.78 | 4.2 |
| 97 | H | furan-2-yl | F | n.d. | 3.9 | 3.6 |

Figure 31. The DBC derivatives tested in SPR assay and structure of DBC compound with binding affinities [148]. * clogP values were calculated by BioByte. ** clogD_{7.4} values calculated by ACD/Percepta.

3.13. Benzofuranone

Due their structural similarity with known α -syn ligands such as **15a** (Figure 11), a small set of benzofuranone derivatives (Figure 32) was synthesized and tested for its ability to bind to α -syn fibrils [149]. Compound **98** was identified to be the most promising structure with a K_i of 2.32 nM for the α -syn fibril BS9 and an IC_{50} value of 1.18 nM for BS2. These affinity data were determined by a competition binding assay using [3H]Tg-190b and [3H]BF-2846 (Figure 26A). Encouraged by these results, the binding properties of **98** were evaluated (at 10 μ M) on human post-mortem PD, AD, and MSA brain sections. Interestingly, **98** was able to distinguish between LB, LN, and GCI pathology. LB from PD brain sections (cortex) and A β plaques from AD brain tissue demonstrated the highest binding. Conversely, a weak binding for of GCI from MSA brain section (cerebellum) and no binding to LN from PD brain sections was obtained (Figure 32) [149]. Presently, no in vivo study has been conducted with these compounds.

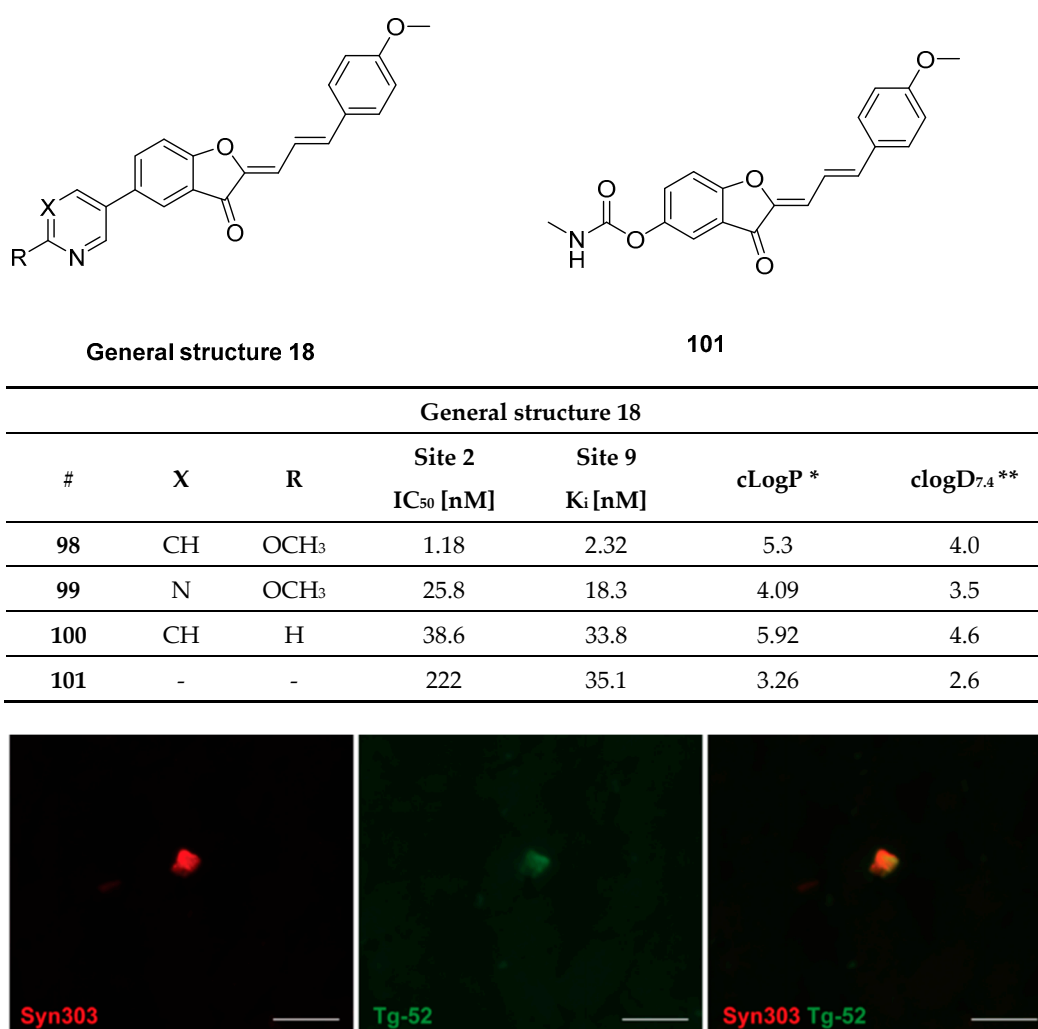
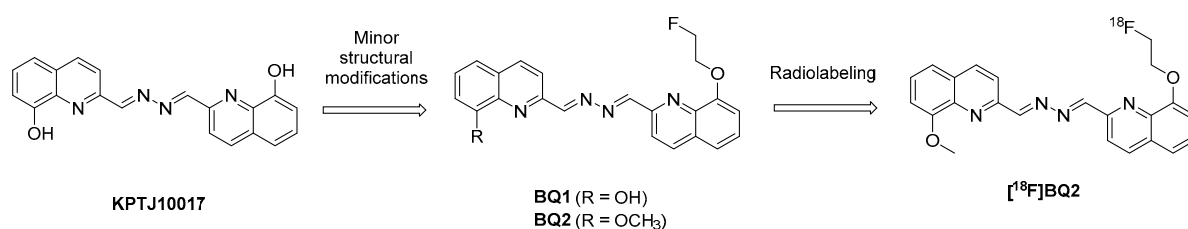


Figure 32. Chemical structure of **99–101** with binding IC_{50} and K_i values. Fluorescence microscopy studies of **98** in postmortem PD tissue. Image shows LB immunostained with syn303 antibody and **98**. Reprinted with permission from [149]. Copyright 2020 The Royal Society of Chemistry. * clogP values were calculated by BioByte. ** clogD_{7.4} values calculated by ACD/Percepta.

3.14. Bisquinolines

Bisquinolines are a new class of compounds that were identified as potential α -syn ligands just recently [120]. A library of 44,000 compounds was screened for structures with high planarity (to recognize β -sheet structures of amyloids), moderate molecular

weight (in order to pass the BBB), and the ability to introduce a radionuclide into the lead structure. Based on these criteria, 150 compounds were selected and further evaluated using an inhibition ThT binding assay. **KPTJ10017** (Figure 33) showed the highest inhibition (62.1%). Next, Kaide and colleagues modified the chemical structure of the lead with the aim of introducing a fluorine atom into the molecule while only minimally changing its physicochemical properties. This led to the identification of **BQ1** and **BQ2** (Figure 33), which showed K_i values of 17.0 and 11.6 nM respectively, in a ThT competition assays using recombinant α -syn aggregates. Selectivity of both compounds for α -syn aggregates over $A\beta$ was not optimal and further SAR studies are needed to reduce the ligands affinity to off-target proteins (Figure 33). However, **BQ1** and **BQ2** can detect α -syn aggregates in human PD brain sections using a fluorescent staining-based experiments. **BQ1** and **BQ2** were also able to detect $A\beta$ fibrils of AD patients in brain tissue whereas no binding to tau fibrils was observed. Finally, compound [^{18}F]**BQ2** (Figure 33) was radiolabeled (RCY = 1.2%, A_m = 8.9 GBq/ μmol) and evaluated in vivo in naïve mice. A moderate brain uptake (1.59% ID/g at 2 min) and slow clearance (1.35% ID/g at 60 min) was detected. This retention could be caused by binding to myelin sheaths, monoamine oxidases, or neuromelanins. Finally, ARG studies were conducted on PD brain sections. A high non-specific binding component in the whole region was detected, suggesting that [^{18}F]**BQ2** as such is not suitable for α -syn PET imaging [120]. Further SAR studies are therefore needed to improve the affinity and selectivity profile of BQ analogues.



| # | K_i [nM] | | clogP * | cLogD _{7.4} ** |
|------------------|---------------|-----------|---------|-------------------------|
| | α -Syn | $A\beta$ | | |
| KPTJ10017 | 3.4 ± 0.1 | 1.1 ± 0.2 | 4.08 | 2.6 |
| BQ1 | 17.0 ± 3.5 | 8.5 ± 3.6 | 4.58 | 3.5 |
| BQ2 | 11.6 ± 2.6 | 7.3 ± 0.7 | 4.83 | 4.4 |

Figure 33. Chemical structure of **KPTJ10017**, **BQ1**, **BQ2**, and [^{18}F]**BQ2** with binding affinities (K_i values) for recombinant α -syn and $A\beta$ aggregates [120]. * clogP values were calculated by BioByte. ** clogD_{7.4} values calculated by ACD/Percepta.

4. Conclusions

Considerable research has been devoted, over the past decades, to the identification of α -syn ligands and a variety of chemically diverse compounds have been evaluated. Approximately 37 different chemical classes have been developed and among them 23 compounds were further radiolabeled and evaluated in preclinical studies (Table S2, Supporting Information). Only two compounds ([^{11}C]**MODAG-001** and [^{125}I]**TZ6184**) showed high affinity (<1 nM) while the rest showed moderate binding toward α -syn fibrils. Four compounds ([^{18}F]**2FBox**, [^{18}F]**15a**, [^{11}C]**MODAG-001** and [^{18}F]**S3-1**) showed high selectivity (30–50-fold) over structurally related amyloid proteins as $A\beta$ and tau fibrils. Most importantly, only 12 were evaluated using human derived brain material and among them six showed binding to α -syn. However, these compounds were either unable to selectively bind to α -syn or its binding was tested only by fluorescent staining and not ARG which is considered to be the “gold standard”. In our opinion, the absence of a valid candidate for α -syn PET imaging is

mainly related to the lack of reliable and reproducible assays. As a matter of fact, the most challenging aspect over the years has been the evaluation process of these compounds.

Thus far, a variety of *in vitro* approaches for the determination of binding affinity on fibrils have been described. However, it is unclear if the specific assays used for compound screening are able to accurately mimic the pathophysiology present in human derived tissue. Recently, Schweighauser et al. [150] found structural discrepancies in MSA α -syn filaments in comparison to *in vitro* “synthetic” filaments (from recombinant wild-type and mutant α -syn). In particular, the size and the packaging of protofilaments seems to differ in human derived tissue compared to “synthetic” fibrils [150]. Moreover, the authors suggested that different strains of α -syn might exist in DLB and MSA patients. Similar hypothesis has been put forward by several other scientists [63,151]. By contrast, Shah-nawaz et al., employing tissues derived from MSA and PD patients, demonstrated with cryo-electron tomography that the structure of α -syn fibrils amplified from human material is consistent with the structure of “synthetic” α -syn fibrils prepared *in vitro* [63]. The discrepancy in results between these two publications is concerning and questions current approaches to design, develop and evaluate α -syn PET tracers. A possible alternative to synthetic fibrils may be sarkosyl-insoluble α -syn material which has been used in more recent studies [150].

Up-to-date, **ThT** competition assays are often used as the only method to evaluate binding, although it has been proved that α -syn fibrils contain multiple binding sites [43]. It might be possible that **ThT** based assays cannot distinguish between compounds that do not bind to the same binding site. Furthermore, many scientists have questioned the reproducibility of these assays, especially given the discrepancies in the reported binding affinities of the studied compounds [67,98,99,114]. The observed discrepancies may be related to several factors, such as, the difference in fibril preparation or practicality of the assay, for example. More reliable and reproducible binding assays are needed in the future to address this challenge. High throughput screening (HTS) may represent an alternative approach to identify α -syn ligands. Until now, only two HTS studies using human derived tissues have been reported [113,114]. Rational drug design is as a matter of fact another alternative development approach. However, this strategy, and in particular structure-based drug design, is hindered as a high resolution crystal structure of α -syn fibril remains elusive. Despite this, several groups have based their research on explorative computational modeling and have identified putative binding sites on α -syn fibrils [43]. We speculate that cryo-electron microscopy (cryo-EM) studies of α -syn from PD, MSA or DLB patients will be a valuable tool in the future that will help to guide the design and development of new imaging probes providing a clearer picture of available binding sites. Finally, a completely different solution to develop α -syn imaging agents is to engineer specific antibodies. A similar approach has been already successfully employed in PET imaging of A β [152–154].

In conclusion, an α -syn selective PET tracer is still missing and no clear pathway is foreseen to develop such a tracer in the near future. Recent findings studying PD revealed that Lewy pathology is complex and consists of a variety of fragmented membranes, organelles and vesicles [151]. This may explain why the development of α -syn PET tracer has faced several challenges. However, the first promising results have been published and hope is on the rise, as outlined in this review.

Supplementary Materials: The following are available online at <https://www.mdpi.com/article/10.3390/ph14090847/s1>, Table S1: Summary of search strategy based on PRISM guidelines, Table S2: Summary table of all radiolabeled compounds with reported results from *in vitro* assays and preclinical studies.

Author Contributions: All the authors contributed to the drafting and other preparation of this manuscript. All authors have read and agreed to the published version of the manuscript.

Funding: This project has received funding from the European Union’s Horizon 2020 research and innovation program under the Marie Skłodowska-Curie grant, agreement no 813528.

Institutional Review Board Statement: Not applicable.

Informed Consent Statement: Not applicable.

Data Availability Statement: Data sharing not applicable.

Conflicts of Interest: The authors declare no conflict of interest.

References

1. McCann, H.; Stevens, C.; Cartwright, H.; Halliday, G. α -Synucleinopathy phenotypes. *Park. Relat. Disord.* **2014**, *20*, S62–S67. [[CrossRef](#)]
2. De Rijk, M.C.; Tzourio, C.; Breteler, M.M.; Dartigues, J.F.; Amaducci, L.; Lopez-Pousa, S.; Manubens-Bertran, J.M.; Alperovitch, A.; Rocca, W.A. Prevalence of parkinsonism and Parkinson's disease in Europe: The EUROPARKINSON Collaborative Study. European Community Concerted Action on the Epidemiology of Parkinson's disease. *J. Neurol. Neurosurg. Psychiatry* **1997**, *62*, 10–15. [[CrossRef](#)]
3. Tanner, C.M.; Goldman, S. EPIDEMIOLOGY OF PARKINSON'S DISEASE. *Neurol. Clin.* **1996**, *14*, 317–335. [[CrossRef](#)]
4. Dorsey, E.R.; Constantinescu, R.; Thompson, J.P.; Biglan, K.M.; Holloway, R.G.; Kiebertz, K.; Marshall, F.J.; Ravina, B.M.; Schifitto, G.; Siderowf, A.; et al. Projected number of people with Parkinson disease in the most populous nations, 2005 through 2030. *Neurology* **2007**, *68*, 384. [[CrossRef](#)] [[PubMed](#)]
5. Statistics. Parkinson's Foundation. Available online: <https://www.parkinson.org/Understanding-Parkinsons/Statistics> (accessed on 1 May 2021).
6. Loane, C.; Politis, M. Positron emission tomography neuroimaging in Parkinson's disease. *Am. J. Transl. Res.* **2011**, *3*, 323–341.
7. Eberling, J.L.; Dave, K.D.; Frasier, M.A. α -synuclein Imaging: A Critical Need for Parkinson's Disease Research. *J. Park. Dis.* **2013**, *3*, 565–567. [[CrossRef](#)]
8. Winge, K.; Friberg, L.; Werdelin, L.; Nielsen, K.K.; Stimpel, H. Relationship between nigrostriatal dopaminergic degeneration, urinary symptoms, and bladder control in Parkinson's disease. *Eur. J. Neurol.* **2005**, *12*, 842–850. [[CrossRef](#)]
9. Parkinson Study Group. Dopamine Transporter Brain Imaging to Assess the Effects of Pramipexole vs Levodopa on Parkinson Disease Progression. *JAMA* **2002**, *287*, 1653–1661. [[CrossRef](#)]
10. Iwai, A.; Masliah, E.; Yoshimoto, M.; Ge, N.; Flanagan, L.; de Silva, H.R.; Kittel, A.; Saitoh, T. The precursor protein of non-A β component of Alzheimer's disease amyloid is a presynaptic protein of the central nervous system. *Neuron* **1995**, *14*, 467–475. [[CrossRef](#)]
11. Yu, S.; Li, X.; Liu, G.; Han, J.; Zhang, C.; Li, Y.; Xu, S.; Liu, C.; Gao, Y.; Yang, H.; et al. Extensive nuclear localization of α -synuclein in normal rat brain neurons revealed by a novel monoclonal antibody. *Neuroscience* **2007**, *145*, 539–555. [[CrossRef](#)]
12. Lee, H.-J.; Choi, C.; Lee, S.-J. Membrane-bound α -Synuclein Has a High Aggregation Propensity and the Ability to Seed the Aggregation of the Cytosolic Form. *J. Biol. Chem.* **2002**, *277*, 671–678. [[CrossRef](#)] [[PubMed](#)]
13. McLean, P.J.; Kawamata, H.; Ribich, S.; Hyman, B.T. Membrane association and protein conformation of alpha-synuclein in intact neurons. Effect of Parkinson's disease-linked mutations. *J. Biol. Chem.* **2000**, *275*, 8812–8816. [[CrossRef](#)] [[PubMed](#)]
14. Bender, J.; Logan, T.P.; Edwards, R.H. The Function of α -Synuclein. *Neuron* **2013**, *79*, 1044–1066. [[CrossRef](#)]
15. George, J.M.; Jin, H.; Woods, W.S.; Clayton, D.F. Characterization of a novel protein regulated during the critical period for song learning in the zebra finch. *Neuron* **1995**, *15*, 361–372. [[CrossRef](#)]
16. Zeniou-Meyer, M.; Zabari, N.; Ashery, U.; Chasserot-Golaz, S.; Haeberlé, A.-M.; Demais, V.; Bailly, Y.; Gottfried, I.; Nakanishi, H.; Neiman, A.; et al. Phospholipase D1 Production of Phosphatidic Acid at the Plasma Membrane Promotes Exocytosis of Large Dense-core Granules at a Late Stage. *J. Biol. Chem.* **2007**, *282*, 21746–21757. [[CrossRef](#)]
17. Lotharius, J.; Brundin, P. Pathogenesis of parkinson's disease: Dopamine, vesicles and α -synuclein. *Nat. Rev. Neurosci.* **2002**, *3*, 932–942. [[CrossRef](#)]
18. Schaser, A.J.; Osterberg, V.R.; Dent, S.E.; Stackhouse, T.L.; Wakeham, C.M.; Boutros, S.W.; Weston, L.J.; Owen, N.; Weissman, T.A.; Luna, E.; et al. Alpha-synuclein is a DNA binding protein that modulates DNA repair with implications for Lewy body disorders. *Sci. Rep.* **2019**, *9*, 1–19. [[CrossRef](#)]
19. Goedert, M.; Jakes, R.; Spillantini, M.G. The Synucleinopathies: Twenty Years On. *J. Park. Dis.* **2017**, *7*, S51–S69. [[CrossRef](#)] [[PubMed](#)]
20. Arima, K.; Ueda, K.; Sunohara, N.; Arakawa, K.; Hirai, S.; Nakamura, M.; Tonzuka-Uehara, H.; Kawai, M. NACP/ α -synuclein immunoreactivity in fibrillary components of neuronal and oligodendroglial cytoplasmic inclusions in the pontine nuclei in multiple system atrophy. *Acta Neuropathol.* **1998**, *96*, 439–444. [[CrossRef](#)] [[PubMed](#)]
21. Crowther, R.A.; Jakes, R.; Spillantini, M.G.; Goedert, M. Synthetic filaments assembled from C-terminally truncated α -synuclein. *FEBS Lett.* **1998**, *436*, 309–312. [[CrossRef](#)]
22. Valera, E.; Masliah, E. The neuropathology of multiple system atrophy and its therapeutic implications. *Auton. Neurosci.* **2018**, *211*, 1–6. [[CrossRef](#)] [[PubMed](#)]
23. Compagnoni, G.M.; Di Fonzo, A. Understanding the pathogenesis of multiple system atrophy: State of the art and future perspectives. *Acta Neuropathol. Commun.* **2019**, *7*, 1–12. [[CrossRef](#)] [[PubMed](#)]

24. Van der Perren, A.; Gelders, G.; Fenyi, A.; Bousset, L.; Brito, F.; Peelaerts, W.; Van den Haute, C.; Gentleman, S.; Melki, R.; Baekelandt, V. The structural differences between patient-derived α -synuclein strains dictate characteristics of Parkinson's disease, multiple system atrophy and dementia with Lewy bodies. *Acta Neuropathol.* **2020**, *139*, 977–1000. [[CrossRef](#)] [[PubMed](#)]
25. Xu, L.; Pu, J. Alpha-Synuclein in Parkinson's Disease: From Pathogenetic Dysfunction to Potential Clinical Application. *Park. Dis.* **2016**, *2016*, 1–10. [[CrossRef](#)]
26. Winner, B.; Jappelli, R.; Maji, S.K.; Desplats, P.; Boyer, L.; Aigner, S.; Hetzer, C.; Loher, T.; Vilar, M.; Campioni, S.; et al. In vivo demonstration that α -synuclein oligomers are toxic. *Proc. Natl. Acad. Sci. USA* **2011**, *108*, 4194–4199. [[CrossRef](#)]
27. Stefanis, L. α -Synuclein in Parkinson's disease. *Cold Spring Harb. Perspect. Med.* **2012**, *2*, a009399. [[CrossRef](#)]
28. Wong, Y.C.; Krainc, D. α -synuclein toxicity in neurodegeneration: Mechanism and therapeutic strategies. *Nat. Med.* **2017**, *23*, 1–13. [[CrossRef](#)]
29. Danzer, K.M.; Haasen, D.; Karow, A.R.; Moussaud, S.; Habeck, M.; Giese, A.; Kretschmar, H.; Hengerer, B.; Kostka, M. Different Species of α -Synuclein Oligomers Induce Calcium Influx and Seeding. *J. Neurosci.* **2007**, *27*, 9220–9232. [[CrossRef](#)]
30. Scott, D.A.; Tabarean, I.; Tang, Y.; Cartier, A.; Masliah, E.; Roy, S. A Pathologic Cascade Leading to Synaptic Dysfunction in α -Synuclein-Induced Neurodegeneration. *J. Neurosci.* **2010**, *30*, 8083–8095. [[CrossRef](#)]
31. Ingelsson, M. Alpha-Synuclein Oligomers—Neurotoxic Molecules in Parkinson's Disease and Other Lewy Body Disorders. *Front. Neurosci.* **2016**, *10*, 408. [[CrossRef](#)]
32. Bengoa-Vergniory, N.; Roberts, R.F.; Wade-Martins, R.; Alegre-Abarrategui, J. Alpha-synuclein oligomers: A new hope. *Acta Neuropathol.* **2017**, *134*, 819–838. [[CrossRef](#)] [[PubMed](#)]
33. Alam, P.; Bousset, L.; Melki, R.; Otzen, D.E. α -synuclein oligomers and fibrils: A spectrum of species, a spectrum of toxicities. *J. Neurochem.* **2019**, *150*, 522–534. [[CrossRef](#)]
34. Fauvet, B.; Mbefo, M.K.; Fares, M.B.; Desobry, C.; Michael, S.; Ardah, M.T.; Tsika, E.; Coune, P.; Prudent, M.; Lion, N.; et al. α -Synuclein in central nervous system and from erythrocytes, mammalian cells, and *Escherichia coli* exists predominantly as disordered monomer. *J. Biol. Chem.* **2012**, *287*, 15345–15364. [[CrossRef](#)]
35. Wang, W.; Perovic, I.; Chittuluru, J.; Kaganovich, A.; Nguyen, L.T.T.; Liao, J.; Auclair, J.R.; Johnson, D.; Landeru, A.; Simorellis, A.K.; et al. A soluble α -synuclein construct forms a dynamic tetramer. *Proc. Natl. Acad. Sci. USA* **2011**, *108*, 17797–17802. [[CrossRef](#)] [[PubMed](#)]
36. Miraglia, F.; Ricci, A.; Rota, L.; Colla, E. Subcellular localization of alpha-synuclein aggregates and their interaction with membranes. *Neural Regen. Res.* **2018**, *13*, 1136–1144. [[CrossRef](#)] [[PubMed](#)]
37. Lashuel, H.A.; Overk, C.R.; Oueslati, A.; Masliah, E. The many faces of α -synuclein: From structure and toxicity to therapeutic target. *Nat. Rev. Neurosci.* **2013**, *14*, 38–48. [[CrossRef](#)] [[PubMed](#)]
38. Lavedan, C. The synuclein family. *Genome Res.* **1998**, *8*, 871–880. [[CrossRef](#)]
39. Beyer, K. α -Synuclein structure, posttranslational modification and alternative splicing as aggregation enhancers. *Acta Neuropathol.* **2006**, *112*, 237–251. [[CrossRef](#)]
40. Zhang, J.; Li, X.; Li, J.-D. The Roles of Post-translational Modifications on α -Synuclein in the Pathogenesis of Parkinson's Diseases. *Front. Neurosci.* **2019**, *13*, 381. [[CrossRef](#)]
41. Menéndez-González, M.; Padilla-Zambrano, H.S.; Tomás-Zapico, C.; García, B.F. Clearing Extracellular Alpha-Synuclein from Cerebrospinal Fluid: A New Therapeutic Strategy in Parkinson's Disease. *Brain Sci.* **2018**, *8*, 52. [[CrossRef](#)]
42. Twohig, D.; Nielsen, H.M. α -synuclein in the pathophysiology of Alzheimer's disease. *Mol. Neurodegener.* **2019**, *14*, 23. [[CrossRef](#)]
43. Hsieh, C.-J.; Ferrie, J.J.; Xu, K.; Lee, I.; Graham, T.J.A.; Tu, Z.; Yu, J.; Dhavale, D.; Kotzbauer, P.; Petersson, E.J.; et al. Alpha Synuclein Fibrils Contain Multiple Binding Sites for Small Molecules. *ACS Chem. Neurosci.* **2018**, *9*, 2521–2527. [[CrossRef](#)]
44. Wassouf, Z.; Schulze-Hentrich, J.M. Alpha-synuclein at the nexus of genes and environment: The impact of environmental enrichment and stress on brain health and disease. *J. Neurochem.* **2019**, *150*, 591–604. [[CrossRef](#)]
45. Conway, K.A.; Lee, S.-J.; Rochet, J.-C.; Ding, T.T.; Harper, J.D.; Williamson, R.E.; Lansbury, P.T. Accelerated Oligomerization by Parkinson's Disease Linked α -Synuclein Mutants. *Ann. N. Y. Acad. Sci.* **2006**, *920*, 42–45. [[CrossRef](#)] [[PubMed](#)]
46. Giasson, B.I.; Murray, I.V.; Trojanowski, J.Q.; Lee, V.M. A hydrophobic stretch of 12 amino acid residues in the middle of alpha-synuclein is essential for filament assembly. *J. Biol. Chem.* **2001**, *276*, 2380–2386. [[CrossRef](#)] [[PubMed](#)]
47. Du, H.-N.; Tang, L.; Luo, X.-Y.; Li, H.-T.; Hu, J.; Zhou, J.-W.; Hu, H.-Y. A Peptide Motif Consisting of Glycine, Alanine, and Valine Is Required for the Fibrillization and Cytotoxicity of Human α -Synuclein. *Biochemistry* **2003**, *42*, 8870–8878. [[CrossRef](#)] [[PubMed](#)]
48. Fujiwara, H.; Hasegawa, M.; Dohmae, N.; Kawashima, A.; Masliah, E.; Goldberg, M.S.; Shen, J.; Takio, K.; Iwatsubo, T. α -Synuclein is phosphorylated in synucleinopathy lesions. *Nat. Cell Biol.* **2002**, *4*, 160–164. [[CrossRef](#)] [[PubMed](#)]
49. Meade, R.M.; Fairlie, D.P.; Mason, J.M. Alpha-synuclein structure and Parkinson's disease—Lessons and emerging principles. *Mol. Neurodegener.* **2019**, *14*, 29. [[CrossRef](#)]
50. Tuttle, M.D.; Comellas, G.; Nieuwkoop, A.J.; Covell, D.J.; Berthold, D.A.; Klopper, K.D.; Courtney, J.M.; Kim, J.K.; Barclay, A.M.; Kendall, A.; et al. Solid-state NMR structure of a pathogenic fibril of full-length human α -synuclein. *Nat. Struct. Mol. Biol.* **2016**, *23*, 409–415. [[CrossRef](#)]
51. Guerrero-Ferreira, R.; Taylor, N.M.I.; Mona, D.; Ringler, P.; Lauer, M.E.; Riek, R.; Britschgi, M.; Stahlberg, H. Cryo-EM structure of alpha-synuclein fibrils. *eLife* **2018**, *7*, e36402. [[CrossRef](#)]
52. Li, B.; Ge, P.; Murray, K.A.; Sheth, P.; Zhang, M.; Nair, G.; Sawaya, M.R.; Shin, W.S.; Boyer, D.R.; Ye, S.; et al. Cryo-EM of full-length α -synuclein reveals fibril polymorphs with a common structural kernel. *Nat. Commun.* **2018**, *9*, 3609. [[CrossRef](#)] [[PubMed](#)]

53. Li, Y.; Zhao, C.; Luo, F.; Liu, Z.; Gui, X.; Luo, Z.; Zhang, X.; Li, D.; Liu, C.; Li, X. Amyloid fibril structure of α -synuclein determined by cryo-electron microscopy. *Cell Res.* **2018**, *28*, 897–903. [[CrossRef](#)]
54. Mathis, C.A.; Lopresti, B.J.; Ikonovic, M.D.; Klunk, W.E. Small-molecule PET Tracers for Imaging Proteinopathies. *Semin. Nucl. Med.* **2017**, *47*, 553–575. [[CrossRef](#)]
55. Bagchi, D.P.; Yu, L.; Perlmutter, J.S.; Xu, J.; Mach, R.H.; Tu, Z.; Kotzbauer, P.T. Binding of the Radioligand SIL23 to α -Synuclein Fibrils in Parkinson Disease Brain Tissue Establishes Feasibility and Screening Approaches for Developing a Parkinson Disease Imaging Agent. *PLoS ONE* **2013**, *8*, e55031. [[CrossRef](#)] [[PubMed](#)]
56. Shah, M.; Seibyl, J.; Cartier, A.; Bhatt, R.; Catafau, A.M. Molecular Imaging Insights into Neurodegeneration: Focus on α -Synuclein Radiotracers. *J. Nucl. Med.* **2014**, *55*, 1397–1400. [[CrossRef](#)]
57. Herth, M.M.; Knudsen, G.M. PET imaging of the 5-HT_{2A} receptor system: A tool to study the receptor's in vivo brain function. In *5-HT_{2A} Receptors in the Central Nervous System*; Guiard, B.P., Di Giovanni, G., Eds.; Springer International Publishing: Cham, Switzerland, 2018; pp. 85–134.
58. L'Estrade, E.T.; Erlandsson, M.; Edgar, F.G.; Ohlsson, T.; Knudsen, G.M.; Herth, M.M. Towards selective CNS PET imaging of the 5-HT₇ receptor system: Past, present and future. *Neuropharmacology* **2020**, *172*, 107830. [[CrossRef](#)]
59. Sun, W.; Ginovart, N.; Ko, F.; Seeman, P.; Kapur, S. In Vivo Evidence for Dopamine-Mediated Internalization of D₂-Receptors after Amphetamine: Differential findings with [³H] raclopride versus [³H] spiperone. *Mol. Pharmacol.* **2003**, *63*, 456–462. [[CrossRef](#)] [[PubMed](#)]
60. Kuang, G.; Murugan, N.A.; Zhou, Y.; Nordberg, A.; Ågren, H. Computational Insight into the Binding Profile of the Second-Generation PET Tracer PI2620 with Tau Fibrils. *ACS Chem. Neurosci.* **2020**, *11*, 900–908. [[CrossRef](#)]
61. Murugan, N.A.; Nordberg, A.; Ågren, H. Different Positron Emission Tomography Tau Tracers Bind to Multiple Binding Sites on the Tau Fibril: Insight from Computational Modeling. *ACS Chem. Neurosci.* **2018**, *9*, 1757–1767. [[CrossRef](#)]
62. Strohäker, T.; Jung, B.C.; Liou, S.-H.; Fernandez, C.O.; Riedel, D.; Becker, S.; Halliday, G.M.; Bennati, M.; Kim, W.S.; Lee, S.-J.; et al. Structural heterogeneity of α -synuclein fibrils amplified from patient brain extracts. *Nat. Commun.* **2019**, *10*, 5535. [[CrossRef](#)] [[PubMed](#)]
63. Shahnawaz, M.; Mukherjee, A.; Pritzkow, S.; Mendez, N.; Rabadia, P.; Liu, X.; Hu, B.; Schmeichel, A.; Singer, W.; Wu, G.; et al. Discriminating α -synuclein strains in Parkinson's disease and multiple system atrophy. *Nature* **2020**, *578*, 273–277. [[CrossRef](#)]
64. Peelaerts, W.; Bousset, L.; Van der Perren, A.; Moskalyuk, A.; Pulizzi, R.; Giugliano, M.; Van den Haute, C.; Melki, R.; Baekelandt, V. α -Synuclein strains cause distinct synucleinopathies after local and systemic administration. *Nature* **2015**, *522*, 340–344. [[CrossRef](#)] [[PubMed](#)]
65. Thakur, P.; Breger, L.S.; Lundblad, M.; Wan, O.W.; Mattsson, B.; Luk, K.C.; Lee, V.M.Y.; Trojanowski, J.Q.; Björklund, A. Modeling Parkinson's disease pathology by combination of fibril seeds and α -synuclein overexpression in the rat brain. *Proc. Natl. Acad. Sci. USA* **2017**, *114*, E8284–E8293. [[CrossRef](#)] [[PubMed](#)]
66. Espa, E.; Clemenson, E.K.H.; Luk, K.C.; Heuer, A.; Björklund, T.; Cenci, M.A. Seeding of protein aggregation causes cognitive impairment in rat model of cortical synucleinopathy. *Mov. Disord.* **2019**, *34*, 1699–1710. [[CrossRef](#)] [[PubMed](#)]
67. Verdurand, M.; Levigoureux, E.; Zeinyeh, W.; Berthier, L.; Mendjel-Herda, M.; Cadarossanesaib, F.; Bouillot, C.; Iecker, T.; Terreux, R.; Lancelot, S.; et al. In Silico, in Vitro, and in Vivo Evaluation of New Candidates for α -Synuclein PET Imaging. *Mol. Pharm.* **2018**, *15*, 3153–3166. [[CrossRef](#)]
68. Recasens, A.; Dehay, B.; Bové, J.; Carballo-Carbajal, I.; Dovero, S.; Pérez-Villalba, A.; Fernagut, P.-O.; Blesa, J.; Parent, A.; Perier, C.; et al. Lewy body extracts from Parkinson disease brains trigger α -synuclein pathology and neurodegeneration in mice and monkeys. *Ann. Neurol.* **2014**, *75*, 351–362. [[CrossRef](#)]
69. Shimoza, A.; Ono, M.; Takahara, D.; Tarutani, A.; Imura, S.; Masuda-Suzukake, M.; Higuchi, M.; Yanai, K.; Hisanaga, S.-I.; Hasegawa, M. Propagation of pathological α -synuclein in marmoset brain. *Acta Neuropathol. Commun.* **2017**, *5*, 12. [[CrossRef](#)] [[PubMed](#)]
70. Kirik, D.; Annett, L.E.; Burger, C.; Muzyczka, N.; Mandel, R.J.; Björklund, A. Nigrostriatal alpha-synucleinopathy induced by viral vector-mediated overexpression of human alpha-synuclein: A new primate model of Parkinson's disease. *Proc. Natl. Acad. Sci. USA* **2003**, *100*, 2884–2889. [[CrossRef](#)] [[PubMed](#)]
71. Holm, I.E.; Alstrup, A.K.O.; Luo, Y. Genetically modified pig models for neurodegenerative disorders. *J. Pathol.* **2016**, *238*, 267–287. [[CrossRef](#)]
72. Lillethorup, T.P.; Glud, A.N.; Landeck, N.; Alstrup, A.K.O.; Jakobsen, S.; Vang, K.; Doudet, D.J.; Brooks, D.J.; Kirik, D.; Hinz, R.; et al. In vivo quantification of glial activation in minipigs overexpressing human α -synuclein. *Synapse* **2018**, *72*, e22060. [[CrossRef](#)] [[PubMed](#)]
73. Kristensen, J.L.; Herth, M.M. In vivo imaging in drug discovery. In *Textbook of Drug Design and Discovery*; Stromgaard, K., Krogsgaard-Larsen, P., Madsen, U., Eds.; CRC Press: Boca Raton, FL, USA, 2017.
74. Pike, V.W. Considerations in the Development of Reversibly Binding PET Radioligands for Brain Imaging. *Curr. Med. Chem.* **2016**, *23*, 1818–1869. [[CrossRef](#)]
75. Herth, M.M.; Ametamey, S.; Antuganov, D.; Bauman, A.; Berndt, M.; Brooks, A.F.; Bormans, G.; Choe, Y.S.; Gillings, N.; Häfeli, U.O.; et al. On the consensus nomenclature rules for radiopharmaceutical chemistry – Reconsideration of radiochemical conversion. *Nucl. Med. Biol.* **2020**, *93*, 19–21. [[CrossRef](#)]

76. McCluskey, S.P.; Plisson, C.; Rabiner, E.A.; Howes, O. Advances in CNS PET: The state-of-the-art for new imaging targets for pathophysiology and drug development. *Eur. J. Nucl. Med. Mol. Imaging* **2019**, *47*, 451–489. [CrossRef] [PubMed]
77. Cai, L.; Lu, S.; Pike, V.W. Chemistry with [18 F]Fluoride Ion. *Eur. J. Org. Chem.* **2008**, *2008*, 2853–2873. [CrossRef]
78. Zhang, L.; Villalobos, A.; Beck, E.M.; Bocan, T.; Chappie, T.A.; Chen, L.; Grimwood, S.; Heck, S.D.; Helal, C.J.; Hou, X.; et al. Design and Selection Parameters to Accelerate the Discovery of Novel Central Nervous System Positron Emission Tomography (PET) Ligands and Their Application in the Development of a Novel Phosphodiesterase 2A PET Ligand. *J. Med. Chem.* **2013**, *56*, 4568–4579. [CrossRef] [PubMed]
79. Alpha-Synuclein Imaging Prize | Parkinson's Disease. Available online: <https://www.michaeljfox.org/news/alpha-synuclein-imaging-prize> (accessed on 16 May 2021).
80. Fridén, M.; Wennerberg, M.; Antonsson, M.; Sandberg-Ställ, M.; Farde, L.; Schou, M. Identification of positron emission tomography (PET) tracer candidates by prediction of the target-bound fraction in the brain. *EJNMMI Res.* **2014**, *4*, 50. [CrossRef]
81. Kotzbauer, P.T.; Tu, Z.; Mach, R.H. Current status of the development of PET radiotracers for imaging alpha synuclein aggregates in Lewy bodies and Lewy neurites. *Clin. Transl. Imaging* **2016**, *5*, 3–14. [CrossRef]
82. Celej, M.S.; Jares-Erijman, E.A.; Jovin, T.M. Fluorescent N-Arylaminothalene Sulfonate Probes for Amyloid Aggregation of α -Synuclein. *Biophys. J.* **2008**, *94*, 4867–4879. [CrossRef]
83. Volkova, K.D.; Kovalska, V.B.; Balanda, A.O.; Losytskyy, M.Y.; Golub, A.G.; Vermeij, R.J.; Subramaniam, V.; Tolmachev, O.I.; Yarmoluk, S.M. Specific fluorescent detection of fibrillar α -synuclein using mono- and trimethine cyanine dyes. *Bioorg. Med. Chem.* **2008**, *16*, 1452–1459. [CrossRef] [PubMed]
84. Krebs, M.R.H.; Bromley, E.H.C.; Donald, A.M. The binding of thioflavin-T to amyloid fibrils: Localisation and implications. *J. Struct. Biol.* **2005**, *149*, 30–37. [CrossRef]
85. Volkova, K.D.; Kovalska, V.B.; Losytskyy, M.Y.; Veldhuis, G.; Segers-Nolten, G.M.J.; Tolmachev, O.I.; Subramaniam, V.; Yarmoluk, S.M. Studies of Interaction Between Cyanine Dye T-284 and Fibrillar Alpha-Synuclein. *J. Fluoresc.* **2010**, *20*, 1267–1274. [CrossRef]
86. Kovalska, V.B.; Losytskyy, M.Y.; Tolmachev, O.I.; Slominskii, Y.L.; Segers-Nolten, G.M.J.; Subramaniam, V.; Yarmoluk, S.M. Tri- and Pentamethine Cyanine Dyes for Fluorescent Detection of α -Synuclein Oligomeric Aggregates. *J. Fluoresc.* **2012**, *22*, 1441–1448. [CrossRef]
87. Neal, K.L.; Shakerdge, N.B.; Hou, S.S.; Klunk, W.E.; Mathis, C.A.; Nesterov, E.E.; Swager, T.M.; McLean, P.J.; Bacsikai, B.J. Development and Screening of Contrast Agents for In Vivo Imaging of Parkinson's Disease. *Mol. Imaging Biol.* **2013**, *15*, 585–595. [CrossRef]
88. Patterson, J.R.; Polinski, N.K.; Duffy, M.F.; Kemp, C.J.; Luk, K.C.; Volpicelli-Daley, L.A.; Kanaan, N.M.; Sortwell, C.E. Generation of Alpha-Synuclein Preformed Fibrils from Monomers and Use In Vivo. *J. Vis. Exp.* **2019**, *148*, e59758. [CrossRef]
89. Hajieva, P.; Mocko, J.B.; Moosmann, B.; Behl, C. Novel imine antioxidants at low nanomolar concentrations protect dopaminergic cells from oxidative neurotoxicity. *J. Neurochem.* **2009**, *110*, 118–132. [CrossRef]
90. Masuda, M.; Suzuki, N.; Taniguchi, S.; Oikawa, T.; Nonaka, T.; Iwatsubo, T.; Hisanaga, S.-i.; Goedert, M.; Hasegawa, M. Small Molecule Inhibitors of α -Synuclein Filament Assembly. *Biochemistry* **2006**, *45*, 6085–6094. [CrossRef]
91. Schwab, K.; Frahm, S.; Horsley, D.; Rickard, J.E.; Melis, V.; Goatman, E.A.; Magbagbeolu, M.; Douglas, M.; Leith, M.G.; Baddeley, T.C.; et al. A Protein Aggregation Inhibitor, Leuco-Methylthionium Bis(Hydromethanesulfonate), Decreases α -Synuclein Inclusions in a Transgenic Mouse Model of Synucleinopathy. *Front. Mol. Neurosci.* **2018**, *10*, 447. [CrossRef]
92. Yu, L.; Cui, J.; Padakanti, P.K.; Engel, L.; Bagchi, D.P.; Kotzbauer, P.T.; Tu, Z. Synthesis and in vitro evaluation of α -synuclein ligands. *Bioorg. Med. Chem.* **2012**, *20*, 4625–4634. [CrossRef]
93. Fisher, E.M. Development of PET Radiotracers for Imaging Neurodegeneration: Targeting Alpha-Synuclein Fibrils and TSPO. Ph.D. Thesis, University of Cambridge, Cambridge, UK, 2017. [CrossRef]
94. Tu, Z.; Li, J.; Yue, X.; Kotzbauer, P. Alpha-Synuclein Ligands. U.S. Patent 2017/0189566 A1, 29 December 2016.
95. Zhang, X.; Jin, H.; Padakanti, P.K.; Li, J.; Yang, H.; Fan, J.; Mach, R.H.; Kotzbauer, P.; Tu, Z. Radiosynthesis and in Vivo Evaluation of Two PET Radioligands for Imaging α -Synuclein. *Appl. Sci.* **2014**, *4*, 66–78. [CrossRef]
96. Pike, V.W. PET radiotracers: Crossing the blood-brain barrier and surviving metabolism. *Trends Pharmacol. Sci.* **2009**, *30*, 431–440. [CrossRef]
97. Tu, Z.; Mach, R.; Yu, L.; Kotzbauer, P. Tricyclic Heteroaromatic Compounds as Alpha-Synuclein Ligands. U.S. Patent Application 2013/0315825 A1, 3 May 2013.
98. Kudo, Y.; Okamura, N.; Furumoto, S.; Tashiro, M.; Furukawa, K.; Maruyama, M.; Itoh, M.; Iwata, R.; Yanai, K.; Arai, H. 2-(2-[2-Dimethylaminothiazol-5-yl]Ethenyl)-6-(2-[Fluoro]Ethoxy)Benzoxazole: A Novel PET Agent for In Vivo Detection of Dense Amyloid Plaques in Alzheimer's Disease Patients. *J. Nucl. Med.* **2007**, *48*, 553–561. [CrossRef]
99. Fodero-Tavoletti, M.T.; Mulligan, R.S.; Okamura, N.; Furumoto, S.; Rowe, C.C.; Kudo, Y.; Masters, C.L.; Cappai, R.; Yanai, K.; Villemagne, V.L. In vitro characterisation of BF227 binding to alpha-synuclein/Lewy bodies. *Eur. J. Pharmacol.* **2009**, *617*, 54–58. [CrossRef]
100. Kikuchi, A.; Takeda, A.; Okamura, N.; Tashiro, M.; Hasegawa, T.; Furumoto, S.; Kobayashi, M.; Sugeno, N.; Baba, T.; Miki, Y.; et al. In vivo visualization of α -synuclein deposition by carbon-11-labelled 2-[2-(2-dimethylaminothiazol-5-yl)ethenyl]-6-(2-(fluoro)ethoxy]benzoxazole positron emission tomography in multiple system atrophy. *Brain* **2010**, *133*, 1772–1778. [CrossRef]

101. Verdurand, M.; Levigoureux, E.; Lancelot, S.; Zeinyeh, W.; Billard, T.; Quadrio, I.; Perret-Liaudet, A.; Zimmer, L.; Chauveau, F. Amyloid-Beta Radiotracer [18F]BF-227 Does Not Bind to Cytoplasmic Glial Inclusions of Postmortem Multiple System Atrophy Brain Tissue. *Contrast Med. Mol. Imaging* **2018**, *2018*, 9165458. [[CrossRef](#)]
102. Levigoureux, E.; Lancelot, S.; Bouillot, C.; Chauveau, F.; Verdurand, M.; Verchère, J.; Billard, T.; Baron, T.; Zimmer, L. 18F]BF227 Does not Reflect the Presence of Alpha-Synuclein Aggregates in Transgenic Mice. *Curr. Alzheimer's Res.* **2014**, *11*, 955–960. [[CrossRef](#)]
103. Josephson, L.; Stratman, N.; Liu, Y.; Qian, F.; Liang, S.H.; Vasdev, N.; Patel, S. The Binding of BF-227-Like Benzoxazoles to Human α -Synuclein and Amyloid β Peptide Fibrils. *Mol. Imaging* **2018**, *17*, 1536012118796297. [[CrossRef](#)]
104. Honson, N.S.; Johnson, R.L.; Huang, W.; Inglese, J.; Austin, C.P.; Kuret, J. Differentiating Alzheimer disease-associated aggregates with small molecules. *Neurobiol. Dis.* **2007**, *28*, 251–260. [[CrossRef](#)]
105. Chu, W.; Zhou, D.; Gaba, V.; Liu, J.; Li, S.; Peng, X.; Xu, J.; Dhavale, D.; Bagchi, D.P.; d'Avignon, A.; et al. Design, Synthesis, and Characterization of 3-(Benzylidene)indolin-2-one Derivatives as Ligands for α -Synuclein Fibrils. *J. Med. Chem.* **2015**, *58*, 6002–6017. [[CrossRef](#)]
106. Hefti Franz, F.; Golding, G.; Li, X.; Choi, S.-R.; Esposito, L.; Yadon, M.-C.; Cummings, J.; Hudson, F.M.; Lake, T.; Snow Alan, D. Compounds for Use in the Detection of Neurodegenerative Diseases. U.S. Patent 2012/0251448 A1, 2 March 2012.
107. Wester, H.-J.; Yousefi Behrooz, H. Compounds Binding to Neuropathological Aggregates. U.S. Patent WO 2016/001422 A1, 3 July 2015.
108. Annual Congress of the European Association of Nuclear Medicine October 12–16, 2019, Barcelona, Spain. *Eur. J. Nucl. Med. Mol. Imaging* **2019**, *46*, 1–952. [[CrossRef](#)]
109. Maruyama, M.; Shimada, H.; Suhara, T.; Shinotoh, H.; Ji, B.; Maeda, J.; Zhang, M.-R.; Trojanowski, J.Q.; Lee, V.M.-Y.; Ono, M.; et al. Imaging of Tau Pathology in a Tauopathy Mouse Model and in Alzheimer Patients Compared to Normal Controls. *Neuron* **2013**, *79*, 1094–1108. [[CrossRef](#)]
110. Ni, R.; Ji, B.; Ono, M.; Sahara, N.; Zhang, M.R.; Aoki, I.; Nordberg, A.; Suhara, T.; Higuchi, M. Comparative In Vitro and In Vivo Quantifications of Pathologic Tau Deposits and Their Association with Neurodegeneration in Tauopathy Mouse Models. *J. Nucl. Med.* **2018**, *59*, 960–966. [[CrossRef](#)]
111. Koga, S.; Ono, M.; Sahara, N.; Higuchi, M.; Dickson, D.W. Fluorescence and autoradiographic evaluation of tau PET ligand PBB3 to α -synuclein pathology. *Mov. Disord.* **2017**, *32*, 884–892. [[CrossRef](#)]
112. Watanabe, H.; Ono, M.; Ariyoshi, T.; Katayanagi, R.; Saji, H. Novel Benzothiazole Derivatives as Fluorescent Probes for Detection of β -Amyloid and α -Synuclein Aggregates. *ACS Chem. Neurosci.* **2017**, *8*, 1656–1662. [[CrossRef](#)]
113. Molette, J.; Gabellieri, E.; Darmency, V. Bicyclic Compounds for Diagnosis and Therapy. U.S. Patent 2019/0071450 A1, 10 March 2017.
114. Miranda-Azpiazu, P.; Svedberg, M.; Higuchi, M.; Ono, M.; Jia, Z.; Sunnemark, D.; Elmore, C.S.; Schou, M.; Varrone, A. Identification and in vitro characterization of C05-01, a PBB3 derivative with improved affinity for alpha-synuclein. *Brain Res.* **2020**, *1749*, 147131. [[CrossRef](#)]
115. Gaur, P.; Galkin, M.; Kurochka, A.; Ghosh, S.; Yushchenko, D.A.; Shvadchak, V.V. Fluorescent Probe for Selective Imaging of α -Synuclein Fibrils in Living Cells. *ACS Chem. Neurosci.* **2021**, *12*, 1293–1298. [[CrossRef](#)]
116. Morais, G.R.; Miranda, H.V.; Santos, I.C.; Outeiro, T.F.; Paulo, A.; Santos, I. Synthesis and in vitro evaluation of fluorinated styryl benzazoles as amyloid-probes. *Bioorg. Med. Chem.* **2011**, *19*, 7698–7710. [[CrossRef](#)]
117. Watanabe, H.; Ariyoshi, T.; Ozaki, A.; Ihara, M.; Ono, M.; Saji, H. Synthesis and biological evaluation of novel radioiodinated benzimidazole derivatives for imaging α -synuclein aggregates. *Bioorg. Med. Chem.* **2017**, *25*, 6398–6403. [[CrossRef](#)]
118. Zhang, S.; Wang, X.; He, Y.; Ding, R.; Liu, H.; Xu, J.; Feng, M.; Li, G.; Wang, M.; Peng, C.; et al. 18F Labeled benzimidazole derivatives as potential radiotracer for positron emission tomography (PET) tumor imaging. *Bioorg. Med. Chem.* **2010**, *18*, 2394–2401. [[CrossRef](#)]
119. Routier, S.; Suzenet, F.; Chalon, S.; Buron, F.; Vercouillie, J.; Melki, R.; Boiaryna, L.; Guilloteau, D.; Pieri, L. Compounds For Using In Imaging And Particularly For The Diagnosis Of Neurodegenerative Diseases. U.S. Patent WO 2018/055316 A1, 26 September 2017.
120. Kaide, S.; Watanabe, H.; Shimizu, Y.; Iikuni, S.; Nakamoto, Y.; Hasegawa, M.; Itoh, K.; Ono, M. Identification and Evaluation of Bisquinoline Scaffold as a New Candidate for α -Synuclein-PET Imaging. *ACS Chem. Neurosci.* **2020**, *11*, 4254–4261. [[CrossRef](#)]
121. Wagner, J.; Ryazanov, S.; Leonov, A.; Levin, J.; Shi, S.; Schmidt, F.; Prix, C.; Pan-Montojo, F.; Bertsch, U.; Mitteregger-Kretzschmar, G.; et al. Anle138b: A novel oligomer modulator for disease-modifying therapy of neurodegenerative diseases such as prion and Parkinson's disease. *Acta Neuropathol.* **2013**, *125*, 795–813. [[CrossRef](#)]
122. Deeg, A.A.; Reiner, A.M.; Schmidt, F.; Schueder, F.; Ryazanov, S.; Ruf, V.C.; Giller, K.; Becker, S.; Leonov, A.; Griesinger, C.; et al. Anle138b and related compounds are aggregation specific fluorescence markers and reveal high affinity binding to α -synuclein aggregates. *Biochim. Biophys. Acta* **2015**, *1850*, 1884–1890. [[CrossRef](#)]
123. Leidel, F.; Eiden, M.; Geissen, M.; Kretzschmar, H.A.; Giese, A.; Hirschberger, T.; Tavan, P.; Schätzl, H.M.; Groschup, M.H. Diphenylpyrazole-derived compounds increase survival time of mice after prion infection. *Antimicrob. Agents Chemother.* **2011**, *55*, 4774–4781. [[CrossRef](#)]
124. Wagner, J.; Krauss, S.; Shi, S.; Ryazanov, S.; Steffen, J.; Miklitz, C.; Leonov, A.; Kleinknecht, A.; Göricke, B.; Weishaupt, J.H.; et al. Reducing tau aggregates with anle138b delays disease progression in a mouse model of tauopathies. *Acta Neuropathol.* **2015**, *130*, 619–631. [[CrossRef](#)]

125. Fellner, L.; Kuzdas-Wood, D.; Levin, J.; Ryazanov, S.; Leonov, A.; Griesinger, C.; Giese, A.; Wenning, G.K.; Stefanova, N. Anle138b Partly Ameliorates Motor Deficits Despite Failure of Neuroprotection in a Model of Advanced Multiple System Atrophy. *Front. Neurosci.* **2016**, *10*, 99. [[CrossRef](#)]
126. Martinez Hernandez, A.; Urbanke, H.; Gillman, A.L.; Lee, J.; Ryazanov, S.; Agbemenyah, H.Y.; Benito, E.; Jain, G.; Kaurani, L.; Grigorian, G.; et al. The diphenylpyrazole compound anle138b blocks A β channels and rescues disease phenotypes in a mouse model for amyloid pathology. *EMBO Mol. Med.* **2018**, *10*, 32–47. [[CrossRef](#)] [[PubMed](#)]
127. Brendel, M.; Deussing, M.; Blume, T.; Kaiser, L.; Probst, F.; Overhoff, F.; Peters, F.; von Ungern-Sternberg, B.; Ryazanov, S.; Leonov, A.; et al. Late-stage Anle138b treatment ameliorates tau pathology and metabolic decline in a mouse model of human Alzheimer's disease tau. *Alzheimer's Res. Ther.* **2019**, *11*, 67. [[CrossRef](#)] [[PubMed](#)]
128. Maurer, A.; Leonov, A.; Ryazanov, S.; Herfert, K.; Kuebler, L.; Buss, S.; Schmidt, F.; Weckbecker, D.; Linder, R.; Bender, D.; et al. ¹¹C Radiolabeling of anle253b: A Putative PET Tracer for Parkinson's Disease That Binds to α -Synuclein Fibrils in vitro and Crosses the Blood-Brain Barrier. *ChemMedChem* **2020**, *15*, 411–415. [[CrossRef](#)] [[PubMed](#)]
129. Kuebler, L.; Buss, S.; Leonov, A.; Ryazanov, S.; Schmidt, F.; Maurer, A.; Weckbecker, D.; Landau, A.M.; Lillethorup, T.P.; Bleher, D.; et al. [¹¹C]MODAG-001—towards a PET tracer targeting α -synuclein aggregates. *Eur. J. Nucl. Med. Mol. Imaging* **2020**, *48*, 1759–1772. [[CrossRef](#)]
130. Ryan, P.; Xu, M.; Jahan, K.; Davey, A.K.; Bharatam, P.V.; Anoopkumar-Dukie, S.; Kassiou, M.; Mellick, G.D.; Rudrawar, S. Novel Furan-2-yl-1H-pyrazoles Possess Inhibitory Activity against α -Synuclein Aggregation. *ACS Chem. Neurosci.* **2020**, *11*, 2303–2315. [[CrossRef](#)]
131. Ono, M.; Haratake, M.; Mori, H.; Nakayama, M. Novel chalcones as probes for in vivo imaging of beta-amyloid plaques in Alzheimer's brains. *Bioorg. Med. Chem.* **2007**, *15*, 6802–6809. [[CrossRef](#)]
132. Ono, M.; Doi, Y.; Watanabe, H.; Ihara, M.; Ozaki, A.; Saji, H. Structure–activity relationships of radioiodinated diphenyl derivatives with different conjugated double bonds as ligands for α -synuclein aggregates. *RSC Adv.* **2016**, *6*, 44305–44312. [[CrossRef](#)]
133. Hsieh, C.-J.; Xu, K.; Lee, I.; Graham, T.J.A.; Tu, Z.; Dhavale, D.; Kotzbauer, P.; Mach, R.H. Chalcones and Five-Membered Heterocyclic Isosteres Bind to Alpha Synuclein Fibrils in Vitro. *ACS Omega* **2018**, *3*, 4486–4493. [[CrossRef](#)] [[PubMed](#)]
134. Yue, X.; Dhavale, D.D.; Li, J.; Luo, Z.; Liu, J.; Yang, H.; Mach, R.H.; Kotzbauer, P.T.; Tu, Z. Design, synthesis, and in vitro evaluation of quinolinyl analogues for α -synuclein aggregation. *Bioorg. Med. Chem. Lett.* **2018**, *28*, 1011–1019. [[CrossRef](#)] [[PubMed](#)]
135. Gao, M.; Wang, M.; Glick-Wilson, B.; Meyer, J.; Peters, J.; Territo, P.; Green, M.; Hutchins, G.; Zarrinmayeh, H.; Zheng, Q.-H. Poster Presentation. Synthesis and initial in vitro characterization of [¹⁸F]fluoroalkyl derivatives of GSK1482160 as new candidate P2X7R radioligands. *J. Label. Compd. Radiopharm.* **2019**, *62*, S123–S588. [[CrossRef](#)]
136. Borroni, E.; Gobbi, L.; Honer, M.; Edelman, M.; Mitchell, D.; Hardick, D.; Schmidt, W.; Steele, C.; Mulla, M. Radiolabeled Compounds. U.S. Patent WO 2019/121661 A1, 18 December 2018.
137. Xu, M.; Loa-Kum-Cheung, W.; Zhang, H.; Quinn, R.J.; Mellick, G.D. Identification of a New α -Synuclein Aggregation Inhibitor via Mass Spectrometry Based Screening. *ACS Chem. Neurosci.* **2019**, *10*, 2683–2691. [[CrossRef](#)]
138. Johnson, D.K.; Karanicolas, J. Ultra-High-Throughput Structure-Based Virtual Screening for Small-Molecule Inhibitors of Protein–Protein Interactions. *J. Chem. Inf. Model.* **2016**, *56*, 399–411. [[CrossRef](#)]
139. Ferrie, J.J.; Lengyel-Zhand, Z.; Janssen, B.; Lougee, M.G.; Giannakoulis, S.; Hsieh, C.-J.; Pagar, V.V.; Weng, C.-C.; Xu, H.; Graham, T.J.A.; et al. Identification of a nanomolar affinity α -synuclein fibril imaging probe by ultra-high throughput in silico screening. *Chem. Sci.* **2020**, *11*, 12746–12754. [[CrossRef](#)]
140. Meng, X.; Munishkina, L.A.; Fink, A.L.; Uversky, V.N. Effects of Various Flavonoids on the α -Synuclein Fibrillation Process. *Park. Dis.* **2010**, *2010*, 650794. [[CrossRef](#)]
141. Snow, A.D.; Castillo, G.M.; Choi, P.Y.; Nguyen, B.P. Proanthocyanidins for the Treatment of Amyloid and Alpha-synuclein Diseases. U.S. Patent WO 2002/076381 A3, 15 February 2002.
142. Horvath, I.; Weise, C.F.; Andersson, E.K.; Chorell, E.; Sellstedt, M.; Bengtsson, C.; Olofsson, A.; Hultgren, S.J.; Chapman, M.; Wolf-Watz, M.; et al. Mechanisms of Protein Oligomerization: Inhibitor of Functional Amyloids Templates α -Synuclein Fibrillation. *J. Am. Chem. Soc.* **2012**, *134*, 3439–3444. [[CrossRef](#)]
143. Åberg, V.; Norman, F.; Chorell, E.; Westermarck, A.; Olofsson, A.; Sauer-Eriksson, A.E.; Almqvist, F. Microwave-assisted decarboxylation of bicyclic 2-pyridone scaffolds and identification of A β -peptide aggregation inhibitors. *Org. Biomol. Chem.* **2005**, *3*, 2817–2823. [[CrossRef](#)]
144. Singh, P.; Chorell, E.; Krishnan, K.S.; Kindahl, T.; Åden, J.; Wittung-Stafshede, P.; Almqvist, F. Synthesis of Multiring Fused 2-Pyridones via a Nitrene Insertion Reaction: Fluorescent Modulators of α -Synuclein Amyloid Formation. *Org. Lett.* **2015**, *17*, 6194–6197. [[CrossRef](#)]
145. Horvath, I.; Sellstedt, M.; Weise, C.; Nordvall, L.-M.; Krishna Prasad, G.; Olofsson, A.; Larsson, G.; Almqvist, F.; Wittung-Stafshede, P. Modulation of α -synuclein fibrillization by ring-fused 2-pyridones: Templatation and inhibition involve oligomers with different structure. *Arch. Biochem. Biophys.* **2013**, *532*, 84–90. [[CrossRef](#)]
146. Cairns, A.G.; Vazquez-Romero, A.; Mahdi Moein, M.; Åden, J.; Elmore, C.S.; Takano, A.; Arakawa, R.; Varrone, A.; Almqvist, F.; Schou, M. Increased Brain Exposure of an Alpha-Synuclein Fibrillization Modulator by Utilization of an Activated Ester Prodrug Strategy. *ACS Chem. Neurosci.* **2018**, *9*, 2542–2547. [[CrossRef](#)]

147. Singh, P.; Adolfsson, D.E.; Ådén, J.; Cairns, A.G.; Bartens, C.; Brännström, K.; Olofsson, A.; Almqvist, F. Pyridine-Fused 2-Pyridones via Povarov and A3 Reactions: Rapid Generation of Highly Functionalized Tricyclic Heterocycles Capable of Amyloid Fibril Binding. *J. Org. Chem.* **2019**, *84*, 3887–3903. [[CrossRef](#)]
148. Chen, Y.-F.; Bian, J.; Zhang, P.; Bu, L.-L.; Shen, Y.; Yu, W.-B.; Lu, X.-H.; Lin, X.; Ye, D.-Y.; Wang, J.; et al. Design, synthesis and identification of N, N-dibenzylcinnamamide (DBC) derivatives as novel ligands for α -synuclein fibrils by SPR evaluation system. *Bioorg. Med. Chem.* **2020**, *28*, 115358. [[CrossRef](#)]
149. Lengyel-Zhand, Z.; Ferrie, J.J.; Janssen, B.; Hsieh, C.-J.; Graham, T.; Xu, K.-y.; Haney, C.M.; Lee, V.M.Y.; Trojanowski, J.Q.; Petersson, E.J.; et al. Synthesis and characterization of high affinity fluorogenic α -synuclein probes. *Chem. Commun.* **2020**, *56*, 3567–3570. [[CrossRef](#)] [[PubMed](#)]
150. Schweighauser, M.; Shi, Y.; Tarutani, A.; Kametani, F.; Murzin, A.G.; Ghetti, B.; Matsubara, T.; Tomita, T.; Ando, T.; Hasegawa, K.; et al. Structures of α -synuclein filaments from multiple system atrophy. *Nature* **2020**, *585*, 464–469. [[CrossRef](#)]
151. Shahmoradian, S.H.; Lewis, A.J.; Genoud, C.; Hench, J.; Moors, T.E.; Navarro, P.P.; Castaño-Díez, D.; Schweighauser, G.; Graff-Meyer, A.; Goldie, K.N.; et al. Lewy pathology in Parkinson's disease consists of crowded organelles and lipid membranes. *Nat. Neurosci.* **2019**, *22*, 1099–1109. [[CrossRef](#)] [[PubMed](#)]
152. Sehlin, D.; Fang, X.T.; Cato, L.; Antoni, G.; Lannfelt, L.; Syvänen, S. Antibody-based PET imaging of amyloid beta in mouse models of Alzheimer's disease. *Nat. Commun.* **2016**, *7*, 10759. [[CrossRef](#)] [[PubMed](#)]
153. Sehlin, D.; Syvänen, S.; Ballanger, B.; Barthel, H.; Bischof, G.N.; Boche, D.; Boecker, H.; Bohn, K.P.; Borghammer, P.; Cross, D.; et al. Engineered antibodies: New possibilities for brain PET? *Eur. J. Nucl. Med. Mol. Imaging* **2019**, *46*, 2848–2858. [[CrossRef](#)]
154. Syvänen, S.; Fang, X.T.; Faresjö, R.; Rokka, J.; Lannfelt, L.; Olberg, D.E.; Eriksson, J.; Sehlin, D. Fluorine-18-Labeled Antibody Ligands for PET Imaging of Amyloid- β in Brain. *ACS Chem. Neurosci.* **2020**, *11*, 4460–4468. [[CrossRef](#)] [[PubMed](#)]